Title
Characterizing Prefrontal Tertiary Sulcal Morphology in Cognition, Development, and Evolution

Author
Voorhies, Willa Ione

Publication Date
2023

Peer reviewed|Thesis/dissertation

Characterizing Prefrontal Tertiary Sulcal Morphology in Cognition, Development, and Evolution

By

Willa Ione Voorhies

A dissertation submitted in partial satisfaction of the

requirements for the degree of

Doctor of Philosophy

in

Psychology

in the

Graduate Division

of the

University of California, Berkeley

Committee in charge:

Professor Kevin S. Weiner, Chair
Professor Silvia A. Bunge
Professor Robert T. Knight
Professor Jason D. Yeatman

Spring 2023

Abstract

Characterizing Prefrontal Tertiary Sulcal Morphology in Cognition, Development, and Evolution

by

Willa Ione Voorhies

Doctor of Philosophy in Psychology

University of California, Berkeley

Professor Kevin S. Weiner, Chair

A major goal of cognitive neuroscience is to understand the link between anatomical brain structure and cognition. In the work that follows, I characterize patterns of cortical folding in the prefrontal cortex and its relation to reasoning skill. A central thread running through this work is that by exploring the relationship between variability in anatomy and cognition, we can establish a link among cortical structure, function, and behavior.

In Chapter 1, I test a classic hypothesis and ask whether small, variable structures known as tertiary sulci have cognitive relevance. By combining precise neuroanatomical techniques with a modern data-driven analysis pipeline, I show that these structures can be reliably identified in individuals across childhood and adolescence and that the depth of a subset of tertiary sulci explains additional variance in reasoning not accounted for by age.

In Chapter 2, I further examine variability in the presence and prominence of cognitively relevant tertiary sulci in prefrontal cortex. I show that the variability in the presence of these structures is associated with variability in behavior and that these sulcal components have discernable functional connectivity profiles that relate to reasoning skill.

Finally, in Chapter 3, I take a modern comparative anatomy approach and show that while these structures exist in chimpanzees, they are notably smaller, shallower, and more variable.

This work lays out a methodological approach to compare structure, function, and behavior across individuals, age groups, and species. I show that sulci, particularly tertiary sulci, can be reliably identified across individuals and that variability in the presence and morphology of these structures can be linked to variability in cognition. The goal of these studies is not to claim that a single sulcus predicts a specific cognitive process, but rather to demonstrate that sulci are useful landmarks that can provide valuable insights into the relationship among cortical structure, function, and cognition.

Dedication

To Papa Chuck, who told me to keep going to school
And to a younger me, who took that very literally

Table of Contents

Acknowledgments

A lot of time and hard work went into these projects and I did not do any part of this alone.

I would like to thank everyone who directly contributed to this work:
My advisors, Dr. Kevin Weiner and Dr. Silvia Bunge, for their endless support and mentorship over the past five years. My committee members, Dr. Robert Knight and Dr. Jason Yeatman for their guidance. All of my collaborators and the current and past members of the Weiner and Bunge labs for their time, skills, thoughtful feedback, and advice. The former members of the Bunge laboratory who performed the data collection and the families who participated in the original study. In particular, thank you, Jacob Miller, for helping me get started and for being an endless source of knowledge, encouragement, and bad puns over the years.

I would also like to thank everyone who does not appear on the author list but without whom I would not be writing this:
Mom, Dad, and Emily, for the love, support, and humor. Sam, for challenging me to think critically, believing in me, and making me go on a walk. Elena, for making me a better teacher, being my favorite person to brainstorm with, and for helping me figure out what I love to do. Madeline, Maddie, and Celia, for always being on my side and generally putting up with me every day. And everyone else in my weird, wonderful grad school family for letting me be myself and making life so fun!

Finally, thank you to Dr. Lucina Uddin and Mrs. Maja Kelly for helping me find my way here in the first place.

This research was supported by a T32 HWNI training grant and an NSF-GRFP fellowship, as well as start-up funds from UC Berkeley (Weiner), NICHDR21HD100858 (Weiner, Bunge) and NSF CAREER Award 2042251 (Weiner). Funding for original human data collection and curation was provided by NINDS R01 NS057156 (Bunge) and NSF BCS1558585 (Bunge). Additional human data were provided by the Human Connectome Project, WU-Minn Consortium (Principal Investigators: David Van Essen and Kamil Ugurbil; 1U54MH091657) funded by the 16 NIH Institutes and Centers that support the NIH Blueprint for Neuroscience Research; and by the McDonnell Center for Systems Neuroscience at Washington University. The National Chimpanzee Brain Resource is supported by NIH grant NS092988.

Main Text

Introduction

Human cognition is unique in that we can easily and flexibly reason about complex and abstract concepts. The emergence of these skills is believed to be tied to the evolution and development of the prefrontal cortex (PFC; Donahue et al., 2018; Miller & Cohen, 2001; Stuss, 2011; Stuss & Alexander, 2000; Stuss & Knight, 2002). The PFC, particularly the dorsolateral PFC (DLPFC), is the last area of the brain to mature and it continues to undergo structural and functional changes well into adulthood (Fry & Hale, 2000; Fuster, 2000; Gogtay et al., 2004; He & Seymour, 2018; Mcardle et al., 2002; Wendelken et al., 2011; Wendelken et al., 2017). There is strong evidence that the PFC is expanded in humans compared to non-human primates (Amiez et al., 2006; Amiez & Petrides, 2009; Croxson et al., 2018; Neubert et al., 2015; Petrides, 2005; Petrides et al., 2012), suggesting its anatomy is unique and essential to complex human cognition. Yet despite its importance, the anatomy of this region remains poorly characterized. In the following chapters, I leverage the structural variability that is intrinsically present across development and evolution to address this gap and show that anatomy can offer insights into the emergence of complex cognition.

Although its precise organization is debated, it is generally accepted that the PFC can be parcellated into subregions (Eickhoff et al., 2018; Glasser et al., 2016; Goulas et al., 2012; Stuss & Knight, 2002; Szczepanski & Knight, 2014). Cytoarchitectonic research, which characterizes the shape, size, and arrangement of cell types, has further shown that the PFC is comprised of distinct cytoarchitectonic areas and various aspects of higher-order cognition have been ascribed to many of these regions (Petrides, 2005; Petrides & Pandya, 1999; Rajkowska & Goldman-Rakic, 1995). Equally as important as its organization, is the PFC's connections. Neuroimaging, post-mortem, and track-tracing studies have revealed that the PFC has a dense network of short-range and long-range connections that allow different parts of the PFC to receive input from, and in turn modulate, cortical and subcortical regions (Catani et al., 2012; Sallet et al., 2013).

Despite what we know about its complexity, in practice, large regions of PFC are often treated as a monolith. The prevailing view in neuroimaging has been that patterns and commonalities in brain function can only be revealed when all brains are aligned to a common anatomical template (Miller et al., 2021a; Miller et al., 2021b; Voorhies et al., 2021). While this approach has provided the field of cognitive neuroscience with many important insights, it has also prevented us from characterizing individual variability in cortical structure-function relationships, which is necessary if we are to understand the biological mechanisms and microstructural properties underlying these functional patterns (Miller et al., 2021a)

A promising approach is to consider individual variability in sulcal morphology. Large, primary sulci in sensory-motor cortices have long been known to be functional and cytoarchitectonic landmarks (Van Essen & Dierker, 2007; Zilles et al., 2013). However, smaller, late-developing tertiary sulci have been largely overlooked in cognitive neuroscience (Weiner, 2018). Hypotheses about the cognitive relevance of tertiary sulci in association cortex date back decades (Sanides, 1964). Yet due to methodological constraints, these remained largely untested (See Chapter 1). While more recent work has shown that smaller, tertiary sulci in association cortices denote functional and structural boundaries (Garrison et al., 2015; Lopez-Persem et al., 2019; Miller et al., 2021a; Miller et al., 2021b; Weiner et al., 2018). Very little work has

characterized these tertiary sulcal patterns in individuals in the lateral prefrontal cortex. In the work that follows I take an individualized anatomical approach and demonstrate that cortical folds, known as sulci, have cognitive relevance and can be used as loci of comparison across individuals, development, and evolution to gain new insight into structure-function-behavior relationships in the lateral prefrontal cortex.

The following studies focus on relational reasoning as the cognitive process of interest. Relational reasoning, simply referred to as "reasoning" moving forward, is the ability to extract common features across objects and conceptualize them in terms of their relation to each other (Wendelken et al., 2017). Reasoning scaffolds learning by allowing us to think logically and solve problems in novel situations (Blair, 2006; Cattell, 1987; Ferrer et al., 2013; Goswami, 1992). Humans excel at this skill in comparison to other primates (Vendetti & Bunge, 2014), suggesting that the human cortex may have undergone specialization to support this process. Psychometric studies show that reasoning increases throughout childhood and adolescence and peaks in adulthood (Mcardle et al., 2002). However, there is notable inter-subject variability that cannot be fully accounted for by chronological age (Ferrer et al., 2013; He & Seymour, 2018). An unanswered question is whether structural variability in LPFC sulci can offer insight into this individual, developmental, and evolutionary variability in reasoning.

In each chapter, I combine knowledge of classic sulcal anatomy with modern techniques to probe questions about cortical function and cognition in development, and evolution. In Chapter 1 I show that tertiary sulci can be reliably identified in individuals and that the morphology of these structures provide insights into cognition. In Chapter 2 I demonstrate the utility of this precise anatomical approach and show that by characterizing the variability in these structures we can better understand variability in behavior and more precisely characterize functional connectivity associated with the development of reasoning skills. Finally, in Chapter 3 I take a comparative anatomy approach and show that tertiary sulci can offer insights into the evolution of the prefrontal cortex, which improves our understanding of the role these structures play in cognition. While the work here focuses on a specific region of the brain and a specific cognitive skill, these findings can, and have been, applied to other questions, cortical regions, and participant groups. The hope is that future work will take these tools and expand our understanding of the mechanisms underlying cortical organization and how these give rise to cognition, function, and behavior.

Chapter 1. Prefrontal tertiary sulci offer insights into cognitive development.

Lateral prefrontal cortex (LPFC) is known to be disproportionately expanded in humans compared to non-human primates. However, the relationship between evolutionarily new LPFC brain structures and uniquely human cognitive skills is largely unknown. In this chapter, I begin to explore the central question of how cortical structure, function, and behavior are related across development by asking whether evoluntionarily new structures, known as tertiary sulci, can provide insight into the acquisition of reasoning skills in children. The methods explored in this work reflect a data-driven approach to a classic theory linking the protracted development of tertiary sulci to complex cognitive processes. These findings also open the door to a novel, mechanistic hypothesis that deeper LPFC tertiary sulci reflect reduced short-range connections in white matter, which in turn, improve the efficiency of local neural signals underlying cognitive skills such as reasoning that are central to human cognitive development.

With permission, this chapter contains previously published material from the following work:
Voorhies WI, Miller JA, Yao JK, et al (2021) Cognitive insights from tertiary sulci in prefrontal cortex. Nat Commun 12:5122

1.2 Introduction

A fundamental question in cognitive neuroscience is how the structure of the brain supports complex cognition. While much progress has been made in answering this question, especially in animal models, human brains differ in both their micro- and macro-structural properties from widely used animals in neuroscience research such as mice, marmosets, and macaques (Zilles et al., 2013). These cross-species differences are especially pronounced in association cortices such as lateral prefrontal cortex (LPFC). LPFC is a late-developing cortical expanse that is enlarged in humans compared to non-human primates (Donahue et al., 2018) and is critical for cognitive control, executive function, reasoning, and goal-directed behavior (Badre & Nee, 2018; Joaquín M. Fuster, 2001; Szczepanski & Knight, 2014; Vendetti & Bunge, 2014). Yet there is still much progress to be made in understanding how the development of evolutionarily new brain structures in the expanded human LPFC support the development of complex, largely human, cognitive skills achieved by neural circuits within LPFC.

Of all the cognitive skills and anatomical features to focus on, we investigate the relationship between relational reasoning and macro-anatomical structures in human cortex known as tertiary sulci. Sulci are commonly classified as primary, secondary, or tertiary based on their time of emergence in gestation (Armstrong et al., 1995; Bailey & Bonin, 1950; Bailey, 1951; Chi et al., 1977; 1964; Turner, 1948; Weiner et al., 2014; Welker, 1990). Tertiary sulci are the last to emerge *in utero*, and subsequently are often the shallowest and smallest class of cortical folds (Bailey & Bonin 1950; Bailey, 1951; Chi et al., 1977; Connolly, 1940, 1950; Cunningham, 1892; Miller et al., 2021; Petrides, 2019; F Sanides, 1962; Friedrich Sanides, 1964; Turner, 1948; Weiner et al., 2014; Weiner & Zilles, 2016; Weiner, 2018; Welker, 1990). They are largely overlooked due to methodological difficulties in their identification (which we expand on further below; Miller et al., 2021; Weiner et al., 2018). Due to these difficulties, very little is known regarding the role of tertiary sulci in human cognition, despite the fact that many tertiary sulci are evolutionarily new structures. We refer to tertiary sulci as evolutionarily new because they are identifiable in humans and non-human hominoids (great apes), but not in other non-human[1] primates (Amiez et al., 2019, 2021; Garrison et al., 2015; Miller et al., 2021a; Miller et al., 2020; Sanides, 1964; Weiner, 2018).

Here, we tested whether tertiary sulci in LPFC are behaviorally significant: that is, whether they relate to higher cognitive functioning. We focus on relational reasoning, which is the ability to extract common features across objects and conceptualize them in terms of their relation to each other (Vendetti & Bunge, 2014; Wendelken et al., 2017). Humans consistently outperform other species in tests of relational reasoning (Mcardle et al., 2002; Vendetti & Bunge, 2014), which relies on a distributed network involving LPFC that has expanded through primate evolution and that develops slowly over childhood and adolescence (Buckner, 2012; Ferrer et al., 2013; Fry & Hale, 2000; Mcardle et al., 2002; Rakic et al., 2009; Vendetti & Bunge, 2014; Wendelken et al., 2016). LPFC is considered critical to reasoning (Badre & D'Esposito, 2009; Christoff et al., 2001; Crone et al., 2006; He & Seymour, 2018; Krawczyk et al., 2011; Wendelken et al., 2016) and developmental improvements in reasoning are correlated with, and predicted by, structural [1]

[1] Non-human primates (NHPs) have shallow dimples, some of which are proposed to be homologous to LPFC tertiary sulci; it is hypothesized that dimples in NHPs have deepened through the course of evolution[21,106].

and functional connectivity between LPFC and lateral parietal cortex (He & Seymour, 2018; Penn et al., 2008; Wendelken et al., 2011; Wendelken et al., 2016).

As both reasoning skills and the LPFC exhibit protracted developmental trajectories in childhood, they serve as ideal targets to test a classic, yet largely unconsidered theory. Specifically, Sanides (1964) proposed that morphological changes in tertiary sulci would likely be associated with the slow development of higher-order thinking and cognitive skills (Sanides, 1962; Sanides, 1964). Fitting these criteria, relational reasoning skills continue to develop throughout childhood, while tertiary sulci emerge late in gestation and continue to develop after birth for a still undetermined period of time (Armstrong et al., 1995; Sanides, 1964; Van Essen & Dierker, 2007; Weiner, 2018; Welker, 1990). A relationship between relational reasoning and tertiary sulcal morphology would build on previous findings relating the development of relational reasoning to changes in LPFC cortical thickness and structural connectivity (Dumontheil, 2014; Dumontheil et al., 2010). Furthermore, relational reasoning supports complex problem-solving and scaffolds the acquisition of additional cognitive skills in children (Blair, 2006; Cattell, 1987). Thus, exploring if or how tertiary sulci contribute to the development of this cognitive skill may not only provide insight into a classic theory but also advance understanding of the anatomical features underlying variability in the development of a wide range of other cognitive skills.

While recent studies suggest a link between the morphology of tertiary sulci in association cortices and cognitive functions (Brun et al., 2016; Garrison et al., 2015; Lopez-Persem et al., 2019; Miller, 2021; Miller et al., 2021b; Weiner, 2018), no study to date (to our knowledge) has tested the role of tertiary LPFC sulci in cognitive development. This gap likely persists for three key reasons. First, previous studies examining individual differences in the development of reasoning and anatomical variability in human LPFC implemented analyses that were averaged across individuals on standard neuroanatomical templates (eg. He & Seymour, 2018), which obscure tertiary sulci in LPFC (Miller et al., 2021a,b; Appendix Figure 1.2). Therefore, to precisely characterize the relationship between tertiary sulcal morphology in LPFC and reasoning performance, it is necessary to consider cortical anatomy at the level of the individual. Second, the shallowness of tertiary sulci makes them hard to reliably identify in post-mortem tissue—typically considered the gold standard for neuroanatomical analyses—because they are easily confused with shallow indentations produced by veins and arteries on the outer surface of the cerebrum (Weiner, 2018a; Weiner et al., 2018b). Researchers interested in the function and structure of tertiary sulci have overcome this latter issue by 1) using T1 magnetic resonance images (MRI) and cortical surface reconstructions—either in-vivo or post-mortem—to visualize tertiary sulci, and 2) manually tracing/defining tertiary sulci on either T1 MRI images or cortical surface reconstructions (Online Methods) (Amiez et al., 2013; Amiez & Petrides, 2007, 2018; Borne et al., 2020; Garrison et al., 2015; Lopez-Persem et al., 2019; Mangin et al., 2015; Miller et al., 2021b; Petrides, 2019; Weiner, 2018a). Third, as detailed below, the patterning of LPFC tertiary sulci has classically remained contentious until recent studies (Amiez & Petrides, 2007; Petrides, 2019; Petrides et al., 2012).

Earlier studies of LPFC sulcal patterning (Ariens-Kappers, 1929; Connolly, 1940; Cunningham, 1892; Eberstaller, 1890; Ono & Kubik, 1990; Rajkowska & Goldman-Rakic, 1995; Shellshear, 1937) left tertiary LPFC sulci undefined or conflated with surrounding structures (Miller et al, 2021) (Online Methods). For example, sulci consistent with the location of the modern definition of the posterior middle frontal sulcus (*pmfs*) were often considered the posterior end of the *intermediate frontal sulcus* (*imfs*; Ono & Kubik, 1990). Functional and

anatomical work by Petrides and colleagues (Amiez & Petrides, 2007; Petrides, 2012) has resolved these contentions by considering three components of the *pmfs* that are distinct from the *imfs* – a definition that additional recent work also supports[25]. The contention in classical definitions of tertiary sulci means that neuroanatomical atlases and neuroimaging software packages largely exclude tertiary sulci. In turn, tertiary sulci in LPFC have been excluded from most developmental cognitive neuroscience studies until the present study (Brun et al., 2016; Lopez-Persem et al., 2019; Miller et al., 2021a; Miller et al., 2021b; Weiner, 2018a). Nevertheless, there is increasing evidence that some tertiary sulci are functionally relevant in association cortices such as ventral temporal cortex (VTC; Weiner 2018a,b), medial PFC (Lopez-Persem et al., 2019), and LPFC (Miller et al., 2021b) in adults, as well as behaviorally and clinically meaningful in medial PFC (Amiez et al., 2013; Amiez et al., 2019; Cachia et al., 2015; Garrison et al., 2015). Irrespective of this mounting evidence that tertiary sulci are functionally and behaviorally relevant in association cortices within adults, it is largely unknown whether morphological features of tertiary sulci will predict individual differences in behavior and cognition in a developmental cohort.

To address this gap in knowledge, we characterized LPFC tertiary sulci for the first time in a developmental sample. We studied a broad age range—children and adolescents between 6 and 18 years old—as we sought to leverage the neuroanatomical and cognitive variability intrinsically present in the sample to explore whether variability in tertiary sulcal morphology predicts individual and developmental differences in relational reasoning. As sulcal depth is a characteristic feature of tertiary sulci, which are shallower than primary and secondary sulci (Armstrong et al., 1995; Caspers et al., 2013; Chi et al., 1977; Van Essen, 2007; Petrides, 2019; Sanides, 1964; Welker, 1990), we hypothesized a relationship between the depth of tertiary sulci and reasoning skills.

To characterize this relationship, we developed a novel pipeline that combines the most recent anatomical definition of LPFC tertiary sulci (Petrides, 2019) with data-driven analyses to model sulcal morphological features and reasoning performance. Our approach addresses four main questions:1) Can LPFC tertiary sulci be reliably identified - and if so, are they smaller, shallower, and more variable compared to primary LPFC sulci as in adults (Miller et al., 2021a,b)? 2) Is there a relationship between the depth of LPFC tertiary sulci and reasoning performance across individuals? 3) If so, can we construct a neuroanatomical-behavioral model to predict an individual's reasoning score from tertiary sulcal depth and age in an independent sample? 4) If successful, does this neuroanatomical-behavioral model generalize to other sulcal features or cognitive tasks? Answering these questions offers the first link between tertiary LPFC sulcal morphology and reasoning, as well as provides novel cognitive insights from evolutionary new brain structures in LPFC.

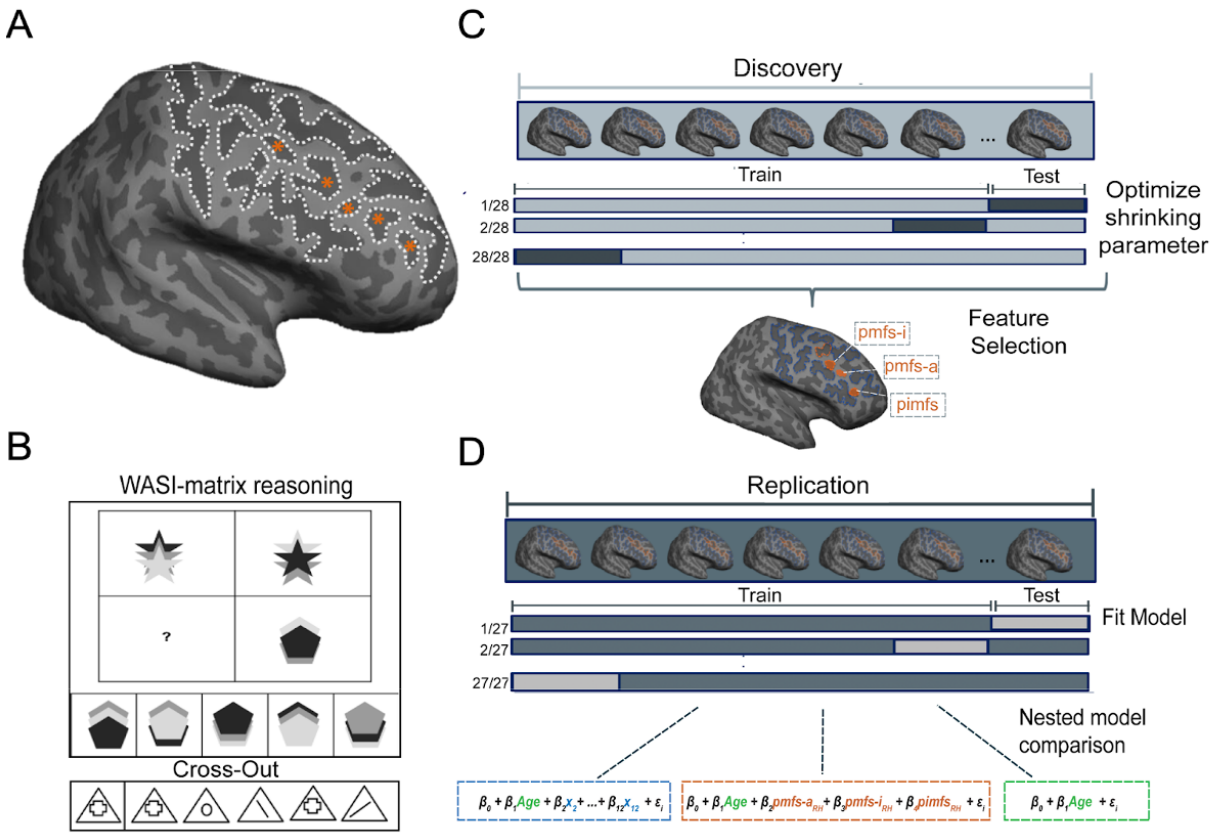

Figure 1.1. ***A novel, data-driven analysis pipeline with Discovery and Replication samples that models the relationship between LPFC sulcal morphological features and reasoning performance.*** **A.** An inflated cortical surface reconstruction of a right hemisphere from one example participant. Dotted white outlines show manually labeled sulci. Asterisks indicate the frequently omitted or misclassified tertiary sulci (Appendix Figure. 1.1 for all participants). **B.** *Top:* Example from the standardized test used to assess relational reasoning in this study (WISC-IV, Matrix reasoning task). In this task, participants are instructed to complete the matrix so that the relation between the two bottom shapes mirrors the relation between the two top shapes. In this example, option 4 completes the pattern. *Bottom:* Example from the processing speed task (WJ-R, Cross Out test), which serves as a behavioral control. In this task, participants are instructed to cross out all objects that match the object on the left as quickly as possible. **C.** *Feature selection – Discovery sample.* A LASSO regression was performed in the *Discovery* sample to determine which sulci, if any, were associated with Matrix reasoning performance. The model parameters were fit iteratively using a leave-one-out cross-validation procedure (Methods). **D.** *Model evaluation – Replication sample.* The sulci selected from the LASSO regression (orange; *pmfs-i*$_{RH}$, *pmfs-a*$_{RH}$, and *pimfs*$_{RH}$) were included along with age in a model to predict task performance in the *Replication* sample. In order to assess the unique contribution of the selected sulci to task performance, this model *(orange)* was compared to two nested alternate models: (1) age alone *(green)* and (2) age in addition to all 12 LPFC sulci *(blue)*. All models were fit with a leave-one-out cross-validation procedure.

1.3 Methods

Participants

The present study consisted of *Discovery* (N=33; 16 males and 17 females) and *Replication* (N=28; 20 males and 8 females) samples. For the *Discovery* sample, 33 typically developing individuals between the ages of 6-18 were randomly selected from the Neurodevelopment of Reasoning Ability (NORA) dataset (Ferrer et al., 2013; Wendelken et al., 2011; Wendelken et al., 2016). Demographic and socioeconomic data are summarized in Appendix Table 1.2. Following the definition of sulci in this sample, we selected an additional 28 age-matched participants for the *Replication* sample. No features other than age were considered in the selection of the *Replication* sample. The terms *male* and *female* are used to denote parent-reported gender identity. All participants were screened for neurological impairments, psychiatric illness, history of learning disability, and developmental delay. All participants and their parents gave their informed assent and/or consent to participate in the study, which was approved by the Committee for the Protection of Human Participants at the University of California, Berkeley.

Data Acquisition

Imaging data: Brain imaging data were collected on a Siemens 3T Trio system at the University of California Berkeley Brain Imaging Center. High-resolution T1-weighted MPRAGE anatomical scans (TR=2300ms, TE=2.98ms, 1×1×1mm voxels) were acquired for cortical morphometric analyses.

Behavioral data: Behavioral metrics are only reported for the participants included in the morphology-behavior analyses (*Discovery*: n = 28, *Replication*: n = 27). Reasoning performance was measured as a total raw score from the WISC-IV Matrix reasoning task (Wechsler, 2003) (Figure 1.1B; *Discovery:* mean(sd) = 24.28 (4.86); *Replication:* mean(sd) = 27.64 (4.52)). Matrix reasoning is an untimed subtest of the WISC-IV in which participants are shown colored matrices with one missing quadrant. The participant is asked to "complete" the matrix by selecting the appropriate quadrant from an array of options (Figure 1.1B). Matrix reasoning score was selected as it is a widely used measure of non-verbal reasoning (Ferrer et al., 2013; Wendelken et al., 2016) and it was the most consistently available reasoning measure for the participants in this study. Matrix reasoning has previously been examined in relation to white matter and functional connectivity in a large dataset that included these participants (Wendelken et al., 2016) and a previous factor analysis in this dataset showed that the Matrix reasoning score loaded strongly onto a reasoning factor that included three other standard reasoning assessments (Ferrer et al., 2013).

Processing speed was computed from raw scores on the Cross Out task from the Woodcock-Johnson Psychoeducational Battery-Revised (Woodcock et al., 2001; WJ-R; Figure 1.1B). In this task, the participant is presented with a geometric figure on the left followed by 19 similar figures. The participant places a line through each figure that is identical to the figure on the left of the row (Figure 1.1B). Performance is indexed by the number of rows (out of 30 total rows) completed in 3 minutes (*Replication:* Mean(sd) = 22.19 (6.26)). Cross Out scores are frequently used to estimate processing speed in developmental populations (McBride-Chang et al., 2002; Kail et al., 2007).

As an additional measure, working memory (WM) was assessed from raw Digit Span Forward scores (*Replication:* Mean(sd) = 9.03(1.77)). Digit Span Forward scores measure WM maintenance and attention. For each forward trial, participants were presented with a string of

numbers by the experimenter and were asked to immediately repeat the numbers in the same order. The task consisted of eight questions with two trials per level (16 total trials). Each question (set of two trials) consisted of a longer string of numbers than the question before. Both processing speed and working memory were selected as they are considered related, but separable, measures from reasoning. We report the Spearman correlation coefficient (*rho*) among each of the three behavioral measures in Appendix 1.6.

Morphological Analyses

Cortical surface reconstruction: All T1-weighted images were visually inspected for scanner artifacts. FreeSurfer's automated segmentation tools (Dale et al., 1999; Fischl et al., 2000; FreeSurfer 6.0.0) were used to generate cortical surface reconstructions. Each anatomical T1-weighted image was segmented to separate gray from white matter, and the resulting boundary was used to reconstruct the cortical surface for each participant (Dale et al., 1999; Wandell et al., 2000). Each reconstruction was visually inspected for segmentation errors, and these were manually corrected. Tertiary sulci are easier to identify on T1 images and cortical surface reconstructions compared to post-mortem tissue (Introduction) for two reasons. First, T1 MRI protocols are not ideal for imaging vasculature; thus, the vessels that typically obscure the tertiary sulcal patterning in post-mortem brains are not imaged on T1 MRI scans. Second, cortical surface reconstructions are made from the boundary between gray and white matter; unlike the outer surface, this inner surface is not obstructed by veins and arteries (Weiner et al., 2018).

Manual labeling of LPFC sulci: Sulci were manually defined separately in the *Discovery* and *Replication* samples according to the most recent atlas proposed by Petrides (2019). This atlas offers a comprehensive schematization of sulcal patterns in the cerebral cortex. The LPFC definitions have recently been validated in adults (Miller et al., 2021a), but to our knowledge, these sulci have never been defined in a developmental sample. 12 LPFC sulci were manually defined within each individual hemisphere in tksurfer (Miller et al., 2021a; Figure 1.2; Appendix Figure 1.1 for all manually defined sulci in 122 hemispheres). Sulcal depth values are a feature of FreeSurfer's scale, which can be explored further on their website (https://surfer.nmr.mgh.harvard.edu). Briefly, depth values are calculated based on how far removed a vertex is from what is referred to as a "mid-surface," which is determined computationally so that the mean of the displacements around this "mid-surface" is zero. Thus, generally, gyri have negative values, while sulci have positive values. Given the shallowness and variability in the depth of LPFC tertiary sulci, some mean depth values extend below zero. We emphasize that this just reflects the metric implemented in FreeSurfer. For example, max depth values are above zero for all sulci (Appendix Figure 1.3B). Manual lines were drawn on the inflated cortical surface to define sulci based on the proposal by Petrides (2019) as well as guided by the *pial* and *smoothwm* surfaces of each individual (Miller et al., 2021b). In some cases, the precise start or end point of a sulcus can be difficult to determine on one surface (Borne et al., 2020). Thus, using the *inflated*, *pial*, and *smoothwm* surfaces of each individual to inform our labeling allowed us to form a consensus across surfaces and clearly determine each sulcal boundary. Our cortical expanse of interest was bounded by the following sulci: (1) the *anterior* and *posterior* components of the *superior frontal sulcus* (sfs) served as the superior boundary, (2) the *inferior frontal sulcus* (ifs) served as the inferior boundary, (3) the *central sulcus* served as the posterior boundary, and (4) the *vertical and horizontal* components of the

intermediate fronto-marginal sulcus (imfs) served as the anterior boundary. We also considered the following tertiary sulci: *anterior* (pmfs-a), *intermediate* (pmfs-i), and *posterior* (pmfs-p) components of the *posterior middle frontal sulcus* (pmfs), and the *para-intermediate frontal sulcus* (pimfs; Miller et al., 2021b; Petrides et al., 2019). Please refer to Figure 1.2A for the location of each of these sulci on example hemispheres and Appendix Figure 1.1 for the location of all 1,320 sulci in all 122 hemispheres. For each hemisphere, the location of each sulcus was confirmed by two trained independent raters (W.V. and J.Y.) and finalized by a neuroanatomist. The surface vertices for each sulcus were then manually selected using tools in *tksurfer* and saved as surface labels for vertex-level analyses of morphological statistics. All anatomical labels for a given hemisphere were fully defined before any morphological or behavioral analyses were performed.

While we could not identify the dorsal and ventral components of the *pimfs* in every hemisphere (Results; Appendix Table 1.1), we could identify at least one component of the *pimfs* in each hemisphere in nearly all participants in the *Discovery* (28/33) and *Replication* (27/28) samples. Thus, our inclusion criteria for all subsequent analyses was to include participants who had at least one *pimfs* component in each hemisphere, which assures that all repeated measures statistics are balanced for effects of sulcus and hemisphere. For those participants who had identifiable dorsal and ventral *pimfs* components, we merged the components into one label, using the FreeSurfer function *mris_mergelabels,* and all findings are reported for the merged label (Dale et al., 1999).

Characterization of sulcal morphology: As the most salient morphological feature of tertiary sulci is their shallowness compared to primary and secondary sulci (Armstrong et al., 1995; Chi et al., 1977; Lopez-Persem et al., 2019; Petrides, 2019; Sanides, 1964; Weiner, 2018a; Weiner 2018b; Welker, 1990), we focused morphological analyses on measures of sulcal depth. Raw depth metrics (standard FreeSurfer units) were computed in native space from the .sulc file generated in FreeSurfer 6.0.0 (Dale et al., 1999). We normalized sulcal depth to the maximum depth value within each individual hemisphere in order to account for differences in brain size across individuals and hemispheres. All depth analyses were conducted for normalized mean sulcal depth. As cortical thickness is a commonly used metric in developmental studies, we also considered the mean cortical thickness (mm) for each sulcus. Mean cortical thickness for each sulcal label was extracted using the *mris_anatomical_stats* function that is included in FreeSurfer (Fischl et al., 2000).

Distinction among primary, secondary, and tertiary sulci: As described in our previous work, as well as classic studies, tertiary sulci are defined as the last sulci to emerge in gestation after the larger and deeper primary and secondary sulci (Bailey & Bonin, 1950; Bailey, 1951; Sanides, 1964; Turner, 1948; Weiner, 2018a; Welker, 1990; Figure 1.2A). Specifically, previous studies specify that a) primary sulci emerge prior to 32 weeks in gestation, b) secondary sulci emerge between 32-36 weeks in gestation, and c) tertiary sulci emerge during and after 36 weeks (Chen et al., 2012; see the following footnotes for direct quotations describing the developmental timeline for primary, secondary, and tertiary sulci). Previous research identifies the *cs, prs, sfs, and ifs* as primary sulci. As such, we apply these definitions to the subcomponents of the sfs (*sfs-a and sfs-p*) and prs (*sprs and iprs*) considered here.

Apart from these sulci, the question of whether or not other LPFC sulci should be considered secondary or tertiary is still unresolved. For example, the *imfs-v* and *imfs-h* are contemporary

labels for classic definitions of sulci commonly labeled as either the *frontomarginal* and/or *middle frontal sulci* (Miller et al., 2021a; Miller et al., 2021b; Petrides, 2019). When considering classic papers and atlases (Connolly, 1940; Cunningham, 1892; O. A. Turner, 1948), both the *imfs-h* and *imfs-v* appear to be prevalent prior to 32 weeks, which would define them as primary sulci. Yet, additional studies define sulci in this cortical expanse as secondary (Tamraz et al., 2006). For the present study, we consider the *imfs-h* and *imfs-v* as primary sulci, but it is possible that future studies will establish them as secondary sulci. Critically, our data-driven approach—and in turn, our findings—are agnostic to these distinctions. That is, the model-based approach adopted here quantitatively determines which sulci best predict reasoning skills, regardless of their classification. Finally, while historical analyses have not considered modern definitions of *pmfs* and *pimfs* sulcal components, more recent studies from Petrides and colleagues do. Moreover, these studies show a correspondence between LPFC tertiary sulcal definitions and brain activation profiles. For example, Amiez and Petrides (2007) showed that the *pimfs* and *pmfs-a* co-localize with clusters of fMRI activation with distinct functional profiles on a serial order memory task. Consistent with this work, Champod and Petrides (2007) also show a direct relationship between activation profiles and tertiary sulcal patterning within LPFC. Considering these data, we refer to *pmfs* and *pimfs* sulcal components as tertiary sulci – for two main reasons. First, from our historical analyses, sulci within the middle frontal gyrus emerge during late stages in gestation, consistent with definitions of tertiary sulci[21]. Second, from our previous analyses in adults (Miller et al., 2021b), *pmfs* sulcal components are small and shallow relative to other primary and secondary LPFC sulci, which is consistent with the morphological features of tertiary sulci. Taken together, our distinction between primary and tertiary sulci is based on classic and modern data. Future studies with larger sample sizes using non-invasive fetal imaging will re-visit the timestamps for the documented sulci, as well as provide new timestamps for those sulci that were not included in these classic studies. For example, based on these classic definitions of sulcal types, the present study did not include any secondary sulci in LPFC. Nevertheless, we also highlight that our data-driven approach is blind to these definitions and identifies sulci that are small in surface area and shallow in depth, which is consistent with the definition of tertiary sulci.

Characterization of tertiary sulcal patterning: For each tertiary sulcus, we characterized sulcal patterns, or types, based on intersections with surrounding sulci. We report the number of intersections for a given sulcus with every other sulcal pair (except the central sulcus as no tertiary sulcus intersected with the central sulcus), relative to the total frequency of occurrence of that sulcus in the hemisphere (Figure 1.2B). We report correlations between left and right hemispheres in each sample, as well as the correlation between samples.

Comparison between tertiary and primary sulci: We compared sulcal depth of tertiary and primary sulci with a 2-way (hemisphere x sulcal type) repeated measures analysis of variance (rm-ANOVA; Figure 1.3). To assess the variability in depth between hemispheres and groups, we conducted the same rm-ANOVA, but replaced mean sulcal depth with the standard deviation. We conducted the same repeated measures analyses with cortical thickness between tertiary and primary sulci in both samples (Appendix Figure 1.3; see Appendix 1). All ANOVAs were computed in R with the *aov* function, imported in python via *rpy2*. Effect sizes are reported with the *generalized* eta-squared (η^2) metric.

Sulcal probability maps: Sulcal probability maps were calculated to describe the vertices with the highest and lowest correspondence across participants (Miller et al., 2021b). These maps were generated across all participants with at least one *pimfs* component in each hemisphere. To generate the maps, each label was transformed from each individual to the common *fsaverage* space. We chose to use the standard *fsaverage* template to increase accessibility for future studies. Then, for each vertex, we calculated the proportion of participants for whom that vertex is labeled as the given sulcus. In the case of multiple labels, labels were assigned to each vertex with a "winner-take-all" approach. That is, the sulcus with the highest overlap across participants was assigned to a given vertex. Consistent with Miller et al. (2021b) in addition to providing unthresholded maps, we also constrained these maps to be maximum probability maps (MPMs) which helps avoid overlapping sulci and can increase interpretability (Figure 1.6A; Miller et al., 2021b). We provide thresholded maps at 33% and 20% spatial overlap for each label. This allows the user to assess both the spatial variability between participants as well as the stable features shared across participants. Finally, since this is the first developmental dataset of tertiary sulci in the frontal lobe, we make these maps publicly available for download at the following link: https://github.com/cnl-berkeley/stable_projects/tree/main/CognitiveInsights_SulcalMorphology.

Assessing the relationship between sulcal depth and reasoning performance

Four-pronged analytic approach: Based on current recommendations (Ghojogh et al., 2019), we implement a four-pronged approach to assess and improve the generalizability of our findings at each stage of analysis.

1. Regularization: In the Discovery sample, we use L1-regularization (LASSO regression) as part of our model selection approach. Not only does this provide a data-driven method for model selection, but regularization techniques are recommended to improve the generalizability of a model (Ghojogh et al., 2019; Heinze et al., 2018). Unlike many techniques that only *assess* generalizability, L1 regularization actually *increases* the generalizability of a model by providing a sparse solution that reduces coefficient values and decreases variance in the model without increasing bias. This technique guards against overfitting and increases the likelihood that a model will generalize to other datasets.
2. Cross-validation: In addition to using regularization techniques to improve generalizability, all models were fit with cross-validation. The purpose of cross-validation is to *test* the generalizability of a model within a sample. We report a very strong fit for our cross-validated models.
3. Replication in an additional sample: We *demonstrate* the generalizability of our findings by showing that the depths of sulci that are predictive of reasoning in the *Discovery* sample generalize to the *Replication* sample. Our regularized regression reveals that the depths of a subset of RH tertiary sulci are relevant for reasoning performance in the *Discovery sample* (Figure 1.4). We then show that these same sulci can be used to predict reasoning with high accuracy in the *Replication sample* (Figure 1.5).
4. Bootstrapped error estimates: We used bootstrapping as a diagnostic tool to assess the generalizability of our models to out-of-sample data. Using 10,000 iterations, we show our chosen models have low variance in estimated error (Figure 1.5C), suggesting that they are not over-fit to the data, and the findings will likely generalize to other samples.

Model selection - Discovery sample: We applied a least absolute shrinkage and selection operator (LASSO) regression model to determine which sulci, if any, were associated with Matrix reasoning. The depth of all 12 LPFC sulci were included as predictors in the regression model. LASSO performs L1-regularization by applying a penalty, or shrinking parameter(α), to the absolute magnitude of the coefficients such that:

$$\min_{\beta \in \mathbb{R}^p} (||\boldsymbol{y} - \boldsymbol{x\beta}||_2^2 + \boldsymbol{\alpha}||\boldsymbol{\beta}||_1)$$

In a LASSO regression, low coefficients are set to zero and eliminated from the model. In this way, LASSO can facilitate variable selection, leading to simplified models with increased interpretability and prediction accuracy (Heinze et al., 2018). In our case, the LASSO regression algorithm shrinks the coefficients of each of the sulci until only the sulci most predictive of reasoning remain in the model. The LASSO regression model was conducted separately for left and right hemispheres. By convention, we used cross-validation to select the shrinking parameter (α). We used the SciKit- learn GridSearchCV package (Pedregosa et al., 2011) to perform an exhaustive search across a range of α-values (0.01- 10.0), and selected the value that minimized cross-validated Mean Squared Error (MSE_{CV}).

Model evaluation - Replication sample: To further characterize the relationship between sulcal depth and reasoning performance, we used the predictors identified by the LASSO regression in the *Discovery* sample to predict Matrix reasoning score in the *Replication* Sample. As age is correlated with Matrix reasoning score, we included age as an additional covariate in the model [1a]. We fit this model as well as alternate nested models with leave-one-out cross-validation (looCV). We used nested model comparison to assess the unique variance explained by sulcal depth, while accounting for age-related effects on reasoning:

$$y_i = \beta_0 + \beta_1 Age + \beta_2 pmfs\text{-}i + \beta_3 pmfs\text{-}a + \beta_4 pimfs + \epsilon_{I.} \quad [1a]$$

Additionally, we conducted this analysis with only the two most predictive sulci (*pmfs-i, pimfs*) from the *Discovery* sample:

$$y_i = \beta_0 + \beta_1 Age + \beta_2 pmfs\text{-}i + \beta_3 pimfs + \epsilon_{I.} \quad [1b]$$

To assess the unique variance explained by tertiary sulcal depth, we compared the MSE_{CV} of this model to the MSE_{CV} of a model with age as the sole predictor [2]:

$$y_i = \beta_0 + \beta_1 Age + \epsilon_{i.} \quad [2]$$

As these models are nested (all predictors in the smaller model [2] are also included in the larger models [1a-b]), we are able to directly compare the prediction error in these two models. Finally, to assess the specificity of the relationship to tertiary sulci in our *Replication* sample, we assessed the fit of model [1] to a full model that included all identified LPFC sulci within a hemisphere [3]. The full model is as follows:

$$y_i = \beta_0 + \beta_1 Age + \beta_2 x_{2\ldots} + \beta_{12} x_{12} + \epsilon_i \quad [3]$$

where $x_2 \ldots x_{12}$ represent the sulcal depth of each identified sulcus within a hemisphere.

Empirical MSE confidence intervals: The size (n = 27) of the *Replication* sample makes looCV suitable. However, models that are fit with looCV can have high variance. Thus, to assess the potential variance in our estimations, we performed a bootstrapping procedure to empirically estimate the distribution of possible MSE_{cv} predictions for models 1b, 2, and 3. For each model, data were randomly selected with replacement 10,000 times and MSE_{cv} was computed for each iteration. From this process, we estimate Median MSE and 95% confidence intervals for each model (shown in Figure 1.5C). All analyses were conducted with SciKit-Learn package in Python (Pedregosa et al., 2011).

Additional morphological and behavioral characteristics

*Cortical thickness:*To assess whether our findings generalized to other anatomical features, we considered cortical thickness, which is an anatomical feature commonly explored in developmental cognitive neuroscience studies (Brown et al., 2012; Gogtay et al., 2004; Tamnes et al., 2013; Vijayakumar et al., 2016). To do so, we replaced sulcal depth with cortical thickness as the predictive metric in our best-performing model in the *Replication* sample [Model 1b]. As with depth, the model was fit to the data with looCV. To compare the thickness model to the depth model, we used the Akaike Information Critertion (AIC), which provides an estimate of in-sample prediction error and is suitable for non-nested model comparison. AIC is given by:

$$AIC_i = -2logL_i + 2K_i$$

Where L_i is the likelihood for the model (i) and K_i is the number of parameters. By comparing AIC scores, we are able to assess the relative performance of the two models. If the ΔAIC is greater than 2, it suggests an interpretable difference between models. If the ΔAIC is greater than 10, it suggests a strong difference between models, with the lower AIC value indicating the preferred model (Burnham & Anderson, 2004; Wagenmakers et al., 2004).

Processing Speed and Working Memory: To ascertain whether the relationship between sulcal depth and cognition is specific to reasoning performance, or transferable to other general measures of cognitive processing (Kail & Ferrer, 2007), we investigated the generalizability of the sulcal-behavior relationship to two other widely used measures of cognitive functioning: Processing speed and working memory. Specifically, we used looCV to predict processing speed (as indexed by Cross Out score) and working memory (as indexed by Digit Span Forwards score; Woodcock et al., 2001) instead of Matrix reasoning score. In the cases in which the model was predictive, we used AIC to compare the predictions to Matrix reasoning predictions.

1. 4 Results

Tertiary sulci are consistently identifiable in the LPFC of 6-18 year-olds

Our sample consisted of 61 typically developing children and adolescents ages 6-18 years old. Participants were randomly assigned to *Discovery* (N = 33) and *Replication* (N = 28) samples with comparable age distributions (*Discovery*: mean(sd) = 12.0 (3.70); *Replication*: mean(sd) = 12.32 (3.53); p = 0.81). For each participant, we generated cortical surface reconstructions in FreeSurfer (Dale et al., 1999; Fischl et al., 2000) from high-resolution T1-weighted anatomical scans. As current automated methods do not define LPFC tertiary sulci and often include gyral components in sulcal definitions (Appendix Figure 1.2), all sulci were manually defined on the native cortical surface for each participant according to the most recent and comprehensive atlas of LPFC sulcal definitions[26] (Figure 1.2). LPFC sulci were classified as primary, secondary, or tertiary based on previous studies documenting the temporal emergence of sulci in gestation (Chi et al., 1977; Connolly, 1940, 1950; Cunningham, 1892; Miller et al., 2021a; Miller et al., 2021b; Turner, 1948). While the most modern sulcal parcellation was not included in these classic studies, it is generally accepted that anterior middle frontal LPFC sulci emerge within the gestational window for primary sulci. Meanwhile, posterior LPFC middle frontal sulci emerge late in gestation (Armstrong et al., 1995; Chi et al., 1977; Connolly, 1940). Consequently, we designate posterior middle frontal sulci as tertiary, and all surrounding sulci as primary (see Figure 1.2A for all classifications). We describe the criteria for classification and the correspondence between historical and contemporary sulcal definitions in more detail in the Methods.

We focused our analyses on the region commonly referred to as dorsal LPFC, which is bounded posteriorly by the central sulcus (*cs*), anteriorly by the horizontal (*imfs-h*) and ventral (*imfs-v*) components of the intermediate frontal sulcus, superiorly by the two components of the superior frontal sulcus (*sfs-p* and *sfs-a*), and inferiorly by the inferior frontal sulcus (*ifs*). Throughout the paper, we refer to this region as the LPFC (Figure 1.2A). Studies in adults report as many as five tertiary sulci within these anatomical boundaries (Petrides, 2019): the three components of the posterior middle frontal sulcus (posterior: *pmfs-p*; intermediate: *pmfs-i*; anterior: *pmfs-a*) and the two components of the para-intermediate frontal sulcus (ventral: *pimfs-v*; dorsal: *pimfs-d*). We defined sulci on the inflated and pial cortical surfaces of each hemisphere for each participant (Methods). We emphasize that 1,320 manual labels were created in total to examine the relationship between LPFC sulcal depth and reasoning performance (Appendix Figure 1.1 for sulcal definitions in all 122 hemispheres included in both samples). Sulcal definitions and all subsequent analyses are conducted separately for the *Discovery* and *Replication* samples, in order to assess the reliability and generalizability of our findings.

Discovery sample: All primary sulci—the central sulcus (*cs*), the superior (*sprs*) and inferior (*iprs*) portions of the precentral sulcus, as well as the *sfs-p*, *sfs-a*, *ifs*, *imfs-h*, and *imfs-v*—were identifiable in both hemispheres of each individual participant. For the first time, we demonstrate that tertiary sulci in LPFC are consistently identifiable within the hemispheres of pediatric participants as young as 6 years old (Figure 1.2A). The three components of the posterior middle frontal sulcus (*pmfs-p; pmfs-i; pmfs-a*) were identifiable in all participants in every hemisphere. However, the most anterior LPFC tertiary sulcus, the *para-intermediate frontal sulcus* (*pimfs*), was consistently variable across individuals (Appendix Table 1.1). Specifically, while almost all participants had at least one identifiable component of the *pimfs* (right hemisphere: 30/33; left hemisphere: 31/33), we were only able to identify both dorsal and ventral *pimfs* components in

42.42% of all participants (right hemisphere: 12/33; left hemisphere: 16/33). We further quantify this variability in tertiary sulci by examining the prevalence of sulcal types, based on their rate of intersection with neighboring sulci (Methods; Figure 1.2B). We find that sulcal patterning is very similar across hemispheres, with comparable rates of intersecting and independent sulci ($r = 0.84$, $p<0.0001$).

Replication sample: Consistent with the *Discovery* sample, all primary sulci (numbered 1-8 in Figure 1.2A) could be identified in both hemispheres of each individual participant. In terms of tertiary sulci, the *pmfs-p*, *pmfs-i*, and *pmfs-a* (numbered 9-11 in Figure 1.2A) were also identifiable in each hemisphere of every individual. Once again, the *pimfs* was the most variable across individuals (Appendix Figure 1.1B; Appendix Table 1.1). We were able to identify at least one *pimfs* component in almost every participant (right hemisphere: 28/28; left hemisphere: 27/28). Both the dorsal and ventral *pimfs* components were identifiable in 76.8% of hemispheres (right hemisphere: 19/28 participants; left hemisphere: 24/28; Appendix Table 1.1). In each hemisphere, the rates and types of intersecting sulci were highly similar to those observed in the *Discovery* sample (right hemisphere: $r = 0.70$, left hemisphere: $r = 0.79$, $p<0.0001$) and these were also consistent between hemispheres in this sample ($r = 0.77$; Figure 1.2B).
In sum, we could identify LPFC tertiary sulci in both *Discovery* and *Replication* samples and found that the sulcal patterning was comparable – and highly correlated – between each sample. However, we could not identify both dorsal and ventral *pimfs* components in each hemisphere. Thus, our inclusion criteria for all subsequent analyses was to include participants who had at least one *pimfs* component in each hemisphere (*Discovery*: 28/33, *Replication*: 27/28), which assures that all repeated measures statistics are balanced for effects of sulcus and hemisphere

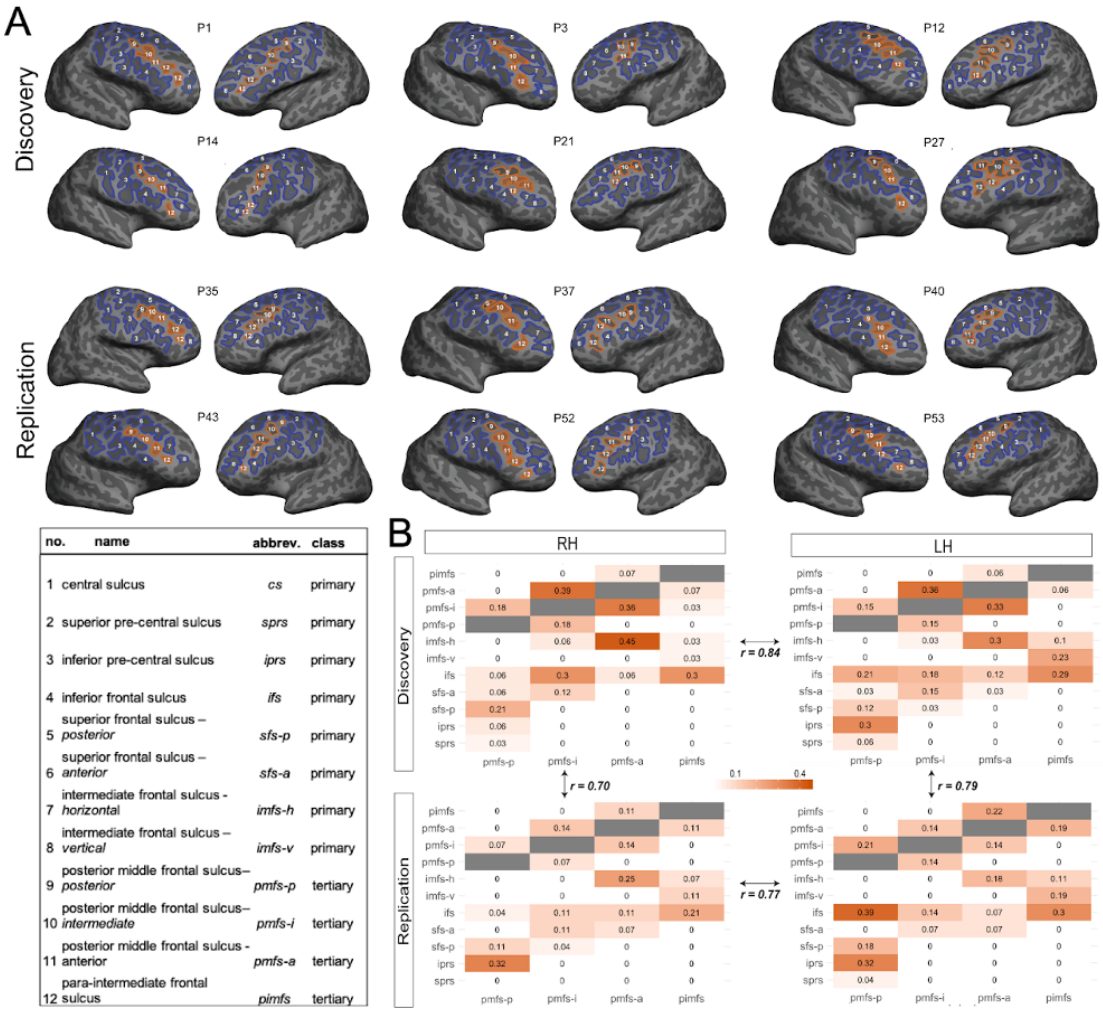

no.	name	abbrev.	class
1	central sulcus	*cs*	primary
2	superior pre-central sulcus	*sprs*	primary
3	inferior pre-central sulcus	*iprs*	primary
4	inferior frontal sulcus	*ifs*	primary
5	superior frontal sulcus – *posterior*	*sfs-p*	primary
6	superior frontal sulcus – *anterior*	*sfs-a*	primary
7	intermediate frontal sulcus - *horizontal*	*imfs-h*	primary
8	intermediate frontal sulcus – *vertical*	*imfs-v*	primary
9	posterior middle frontal sulcus– *posterior*	*pmfs-p*	tertiary
10	posterior middle frontal sulcus– *intermediate*	*pmfs-i*	tertiary
11	posterior middle frontal sulcus - anterior	*pmfs-a*	tertiary
12	para-intermediate frontal sulcus	*pimfs*	tertiary

Figure 1.2 ***LPFC tertiary sulci are identifiable and show comparable patterning across hemispheres and samples in a pediatric cohort.*** **A.** LPFC sulcal definitions on inflated cortical surface reconstructions from six example participants (P1, P3, etc.) in the *Discovery* sample (*top*) and the *Replication* sample (*bottom*). Sulci were identified based on the most recent neuroanatomical atlas to consider a comprehensive definition of tertiary sulci[26]. Primary sulci (1-8) are in blue, while tertiary sulci (9-12) are in orange. The three tertiary sulci (*pmfs-i*$_{RH}$ (*10*)*, pmfs-a*$_{RH}$ (*11*)*,* and *pimfs*$_{RH}$ (*12*)) identified by our model-based approach with cross-validation (Figure 1.4) are filled in. The distinction among primary, secondary, and tertiary sulci is based on classic and recent studies examining the timepoints when sulci emerge in gestation (Methods). Based on these studies, the sulci considered in the present work are either primary or tertiary. **B**. Rates of intersection with surrounding sulci were quantified for each tertiary sulcus in order to identify common sulcal patterns. For each tertiary sulcus (*pmfs-p (9), pmfs-i* (*10*)*, pmfs-a* (*11*)*,* and *pimfs* (*12*)), we report the proportion of intersection (frequency of occurrence/total number of observations) with each LPFC sulcus (see color bar for reference; empty gray cells in the matrix reflect the fact that a sulcus cannot intersect with itself). Calculating the correlation between matrices shows that sulcal patterning is comparable (all *r*s > .70; all ps <0.0001) between hemispheres and samples.

LPFC tertiary sulci are shallower and more variable than primary sulci in children

Classic anatomical studies report a high correspondence between sulcal classification and depth (Armstrong et al., 1995; Chi et al., 1977; Van Essen, 2007; Sanides, 1964; Welker, 1990), and recent *in-vivo* studies in adults show that LPFC tertiary sulci are in fact significantly shallower and more variable than primary sulci (Miller et al., 2021b) . However, this correspondence has not been established for LPFC sulci in children. Thus, we next sought to compare the depth and

variability of LPFC tertiary and primary sulci in children. Sulcal depth was normalized to the maximum depth value within each individual hemisphere to account for differences in brain size across individuals and hemispheres (Methods). From these normalized measures, we conducted a 2-way repeated-measures analysis of variance (rm-ANOVA) to statistically test for differences between sulcal type (*tertiary vs. primary*) and hemisphere (*left vs. right*) in both *Discovery* and *Replication* samples.

Discovery sample: Consistent with findings in adults (Miller et al., 2021b), we observed a main-effect of sulcal type ($F(1,27)= 95.63$, $p<10^{-3}$, $\eta^2G = 0.35$) in which tertiary sulci were significantly more shallow than primary sulci (Mean(sd)Tertiary= 0.04(0.17); Mean(sd)Primary= 0.23(0.07)). We also observed an interaction between sulcal type and hemisphere ($F(1,27) = 5.67$, $p<0.02$, $\eta^2G= 0.01$) in which tertiary sulci were significantly deeper in the right hemisphere than in the left hemisphere (Mean(sd)RH = 0.06(0.17); Mean(sd)LH= 0.02(0.1)). In contrast, the depth of primary sulci did not differ between hemispheres (Mean(sd)RH= 0.21(0.07); Mean(sd)LH = 0.23(0.07)); Figure 1.3A). To explore the morphological variability between sulcal types, we repeated the same analysis replacing mean sulcal depth with the standard deviation of sulcal depth. This analysis quantitatively supports that tertiary sulci are more variable than primary sulci ($F(1,27)= 162.4$, $p<10^{-3}$, $\eta^2G = 0.43$), with no differences between hemispheres ($p = 0.3$).

Replication sample: We observed the same main effect of sulcal type in the *Replication* sample. Tertiary sulci were more shallow than primary sulci ($F(1,26) = 136.5$, $p<10^{-3}$, $\eta^2G = 0.46$; Mean(sd)Tertiary= 0.02(0.16); Mean(sd)Primary = 0.23(0.07)). We did not observe an interaction with hemisphere in this sample ($F(1,26) = 0.26$, $p = 0.62$); Figure 1.3B). Once again, an rm-ANOVA of the standard deviation of sulcal depth revealed that tertiary sulci were more variable than primary sulci across hemispheres ($F(1,26) = 170.4$, $p<10^{-3}$, $\eta^2G = 0.47$).
Additionally, while age was correlated with reasoning performance in both *Discovery* ($r = 0.58$, $p<10^{-3}$) and *Replication* samples ($r = 0.73$, $p<10^{-3}$), there was an inconsistent relationship between sulcal depth and age in either sample (Appendix Figure 1.4). Thus, we next implemented a two-pronged, model-based approach to test if including sulcal depth predicted reasoning skills above and beyond age.

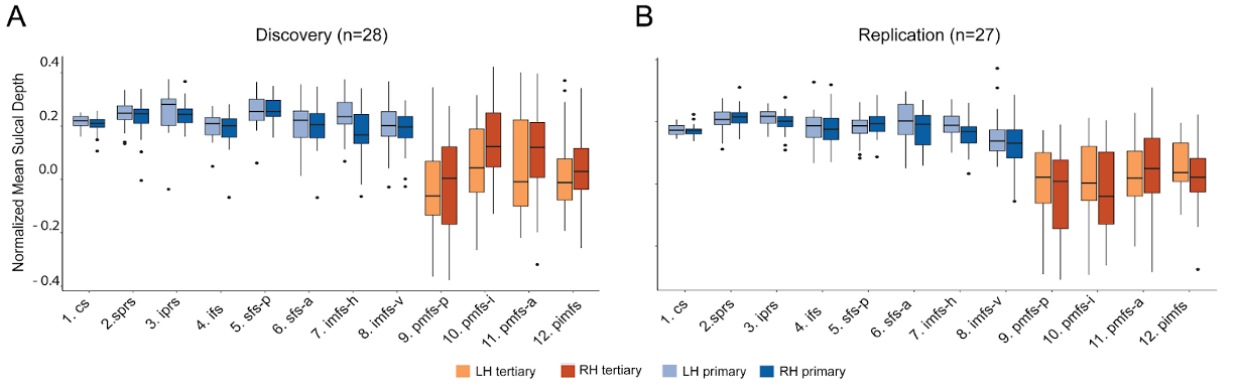

Figure 1.3. ***LPFC tertiary sulci in 6-18 year-olds are more shallow and more variable than primary sulci.*** **A.** Normalized sulcal depth for each of the 12 LPFC sulci in the *Discovery* sample. **B.** Same as in ***A***., but for the *Replication* sample. Tertiary sulci *(orange)* were shallower and more variable than primary sulci *(blue)* in both samples.

A model-based approach with nested cross-validation reveals that including the depth of three LPFC tertiary sulci predicts individual variability in reasoning skills above and beyond age alone.

To examine the relationship between LPFC sulcal depth and reasoning skills, we implemented a data-driven pipeline with an emphasis on producing reliable and generalizable results. Based on current gold-standard recommendations (Ghojogh et al., 2019), we implemented a four-pronged analytic approach to assess and improve the generalizability of our results and each stage of analysis (Methods). First, we implemented a feature selection technique in the *Discovery* sample (Figure 1.1C) to determine if the depths of any LPFC sulci are associated with reasoning performance (to remind the reader, we use depth in the model because this is the main morphological difference between tertiary from primary sulci). To do so, we submitted sulcal depth values for all 12 LPFC sulci in the *Discovery* sample to a LASSO regression model, which provides an automated method for feature selection by shrinking model coefficients and removing sulci with very low coefficients from the model (Figure 1.1C; Methods). This approach allowed us to determine, in a data-driven manner, which sulci are the strongest predictors of reasoning performance. Additionally, this technique guards against overfitting and increases the likelihood that a model will generalize to other datasets, by providing a sparse solution that reduces coefficient values and decreases variance in the model without increasing bias (Ghojogh et al., 2019; Heinze et al., 2018). Also, although we observe a gender imbalance in our samples, gender was not associated with sulcal depth (p = 0.27) or Matrix reasoning (p = 0.51); therefore, we do not consider gender further in our models.

To determine the value of the shrinking parameter (α; Heinze et al., 2018), we iteratively fit the model with a range of α-values using cross-validation. By convention (Heinze et al., 2018), we selected the α that minimized the cross-validated Mean Squared Error (MSE$_{CV}$; Figure 1.4A). Although both tertiary and primary sulci were initially included as predictors, after implementing the LASSO regression, only three tertiary sulci (*pmfs-i, pmfs-a,* and *pimfs*) in the right hemisphere were found to be associated with reasoning performance (MSE$_{CV}$=21.84, α = 0.1; $\beta_{pmfs\text{-}i}$= 4.50, $\beta_{pmfs\text{-}a}$= 1.78, β_{pimfs}= 11.88; Figure 1.4).

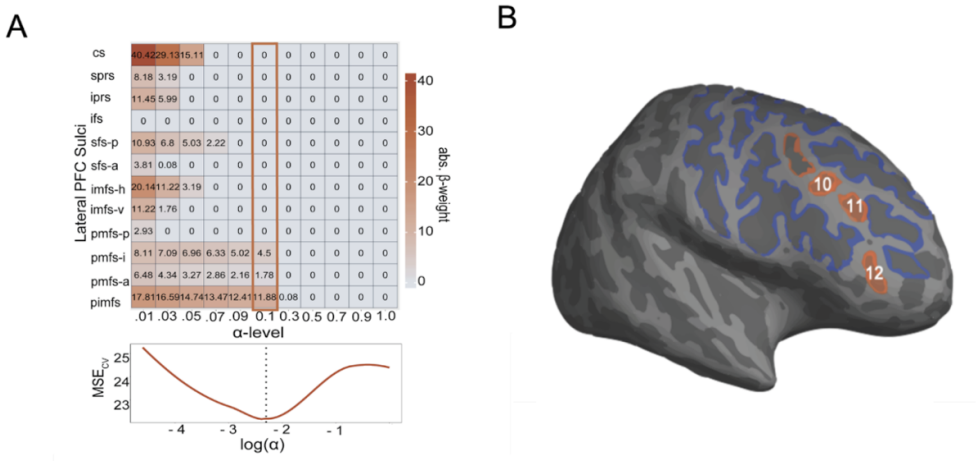

Figure 1.4. ***Data-driven model-selection reveals that the depth of a subset of tertiary sulci is associated with reasoning.*** **A.** Results from the LASSO regression predicting Matrix reasoning score from sulcal depth in the *Discovery* sample. *Top:* Beta-coefficients for each RH sulcus at a range of shrinking parameter (alpha) values.

Highlighted box indicates coefficients at the chosen alpha-level. *Bottom:* Cross-validated MSE at each alpha-level. By convention[67], we selected the α that minimized the cross-validated Mean Squared Error (MSE_{CV}; dotted line).**B**. Inflated cortical surface from an example participant highlighting the three tertiary sulci (*pmfs-i$_{RH}$* (*10*)*, pmfs-a$_{RH}$* (*11*)*,* and *pimfs$_{RH}$* (*12*)) implicated in reasoning performance.

To evaluate the generalizability of the sulcal-behavioral relationship identified in the *Discovery* sample, we constructed a linear model to predict reasoning from sulcal depth and age in our *Replication* sample. The mean depths of the *pmfs-i$_{RH}$*, *pmfs-a$_{RH}$*, and *pimfs$_{RH}$*, as well as age, were included as predictors in the model, as they were the only three sulci identified in the sulcal-behavioral model in the *Discovery* sample. As age was, as expected, highly associated with reasoning (Figure 1.5B), including age in this model allowed us to compare performance of this tertiary sulci + age model to a model with age alone to determine the unique contribution of LPFC tertiary sulcal depth to reasoning performance above and beyond age. This model (and all subsequent models) were fit using a leave-one-out cross-validation (looCV) procedure. While looCV assesses the generalizability of the model within a sample and is appropriate for smaller sample sizes, it can result in models with high variance compared to other cross-validation techniques. To address this concern, we also estimated empirical MSE confidence intervals using a bootstrapping procedure (Methods; Figure 1.5C). High variance in MSE across the bootstrapped iterations would suggest that the model is likely overfit to the original data.

We found that this model (*pmfs-i$_{RH}$* + *pmfs-a$_{RH}$* + *pimfs$_{RH}$* + age) was highly predictive of reasoning score in the *Replication* sample (R^2_{cv}= 0.52, MSE_{CV} = 9.66; Bootstrapped 95% CI_{MSE}: 3.12-13.69, $median_{MSE}$ = 8.14). Additionally, we observed a high correspondence (Spearman's *rho* = 0.70) between predicted and actual measured reasoning scores (Appendix Figure 1.5). Furthermore, if we consider just the two LPFC tertiary sulci that are the strongest predictors of reasoning performance as identified in the *Discovery* sample (*pmfs-i$_{RH}$*: $\beta_{pmfs\text{-}i}$ = 4.50; *pimfs$_{RH}$*: β_{pimfs} = 11.88), the predictions of reasoning performance and model fits improved even further in the *Replication* sample (R^2_{cv}= 0.58; MSE_{CV} = 8.52; Bootstrapped 95% CI_{MSE} = 3.21-12.37, $median_{MSE}$ = 7.47; Spearman's *rho* = 0.73; Figure 1.5).

Once we had determined that the sulci relevant for reasoning in the *Discovery* sample were also predictive of reasoning in the *Replication* sample, we used cross-validation to evaluate the fit of the replication model relative to two alternative models considering either 1) age alone or 2) sulcal depth from all right hemisphere LPFC sulci and age together in the *Replication* sample (Figure 1.1D). This nested model comparison allowed us to determine the unique contribution of the depths of sulci identified by the model while still accounting for the effects of age and the depths of all LPFC sulci considered in the present study on reasoning performance. Removing the *pmfs-i$_{RH}$*, *pmfs-a$_{RH}$*, and *pimfs$_{RH}$* from the model decreased prediction accuracy and increased the MSE_{cv} (R^2_{cv} = 0.48, MSE_{CV} = 10.50; Bootstrapped 95% CI_{MSE} = 4.69-15.67, $median_{MSE}$ = 9.66), indicating that the depths of these right hemisphere tertiary sulci identified by our model-based approach uniquely contribute to the prediction of reasoning scores above and beyond age (Figure 1.5B). Additionally, considering age and the depths of all RH LPFC sulci also weakened the model prediction and increased MSE_{cv} (R^2_{cv} = 0.14, MSE_{CV} = 17.47, Bootstrapped 95% CI_{MSE} = 2.79-306.25, $median_{MSE}$ = 19.70). The bootstrapped CI_{MSE} showed that this model also suffered from very high variance (Figure 1.5C). Taken together, our cross-validated, nested model comparison empirically supports that the depth of only a subset of LPFC tertiary sulci reliably explains unique variance in reasoning performance that is not accounted for by age or the depths of all LPFC sulci considered in the present study.

Finally, while our data demonstrate support for our hypothesis, we wondered whether our findings extended to other neuroanatomical features or related measures of cognitive development. We repeated our procedure with 1) a model in which we replaced sulcal depth with cortical thickness (Burgaleta et al., 2014; Dickerson et al., 2008; Gogtay et al., 2004; Østby et al., 2009) and 2) a model in which we replaced reasoning performance with performance on a behavioral measure that reflects a general cognitive ability: processing speed (Kail et al., 1994). We used the Akaike Information Criterion (AIC) to quantitatively compare models. If the ΔAIC is greater than 2, it suggests an interpretable difference between models. If the ΔAIC is greater than 10, it suggests a strong difference between models, with the lower AIC value indicating the preferred model (Wagenmakers et al., 2004; Burnham et al., 2004; Methods).

With respect to the extension of these findings to another anatomical feature, this approach revealed that a model with cortical thickness and age was predictive of reasoning (R^2_{cv} = 0.33; MSE_{CV} = 13.54), but much less than the model with age alone (R^2_{cv} = 0.48; MSE_{CV} = 10.50). The AIC for the thickness + age model ($AIC_{Thickness}$ = 78.58) was much higher than the AIC for the tertiary sulci + age model ($AIC_{sulcalDepth}$ = 63.85; $\Delta AIC_{Thickness\text{-}Depth}$ = 14.73). This indicates that sulcal depth is strongly preferred as a predictor over cortical thickness (Appendix Figure 1.6A),

To test whether sulcal depth would predict another cognitive measure aside from reasoning, we used a test of processing speed (Cross Out; Figure 1.1B). Processing speed is a general cognitive ability that is correlated with—and theorized to support—reasoning (Ferrer et al., 2013; Fry & Hale, 2000; Kail & Salthouse, 1994; Kail et al., 2016). As predicted based on the prior literature, processing speed was correlated with reasoning performance in our sample (*rho* = 0.54, Appendix Figure 1.6C). Sulcal depth of the three critical LPFC tertiary sulci (*pmfs-*i_{RH}, *pmfs-*a_{RH}, and $pimfs_{RH}$) and age was predictive of processing speed (R^2_{cv}= .45; MSE_{CV} =20.53), but not much more than age alone (R^2 = 0.42; MSE_{CV} = 21.82). The AIC for the processing speed + age model ($AIC_{CrossOut}$ = 89.59) was much higher than the AIC for the tertiary sulci + age model ($AIC_{sulcalDepth}$ = 63.85; $\Delta AIC_{CrossOut\ -\ MatrixReasoning}$ = 25.74), which indicates that reasoning is strongly preferred over processing speed (Appendix Figure 1.6B).

To further probe the relationship between these sulci and reasoning, we performed a follow-up analysis with a measure of phonological working memory (Digit Span Forwards) as another point of comparison. Like processing speed, working memory is a general cognitive ability that is correlated with—and theorized to support—reasoning (Fry & Hale, 2000; Holyoak & Monti, 2021). As predicted based on the literature, our measures of reasoning and working memory were correlated (*rho* = 0.58; Appendix Figure 1.6c). However, the tertiary sulcal model (Model 1a detailed in the Methods) did not predict working memory (R^2_{cv} = 0.10, MSE_{cv} = 2.75).

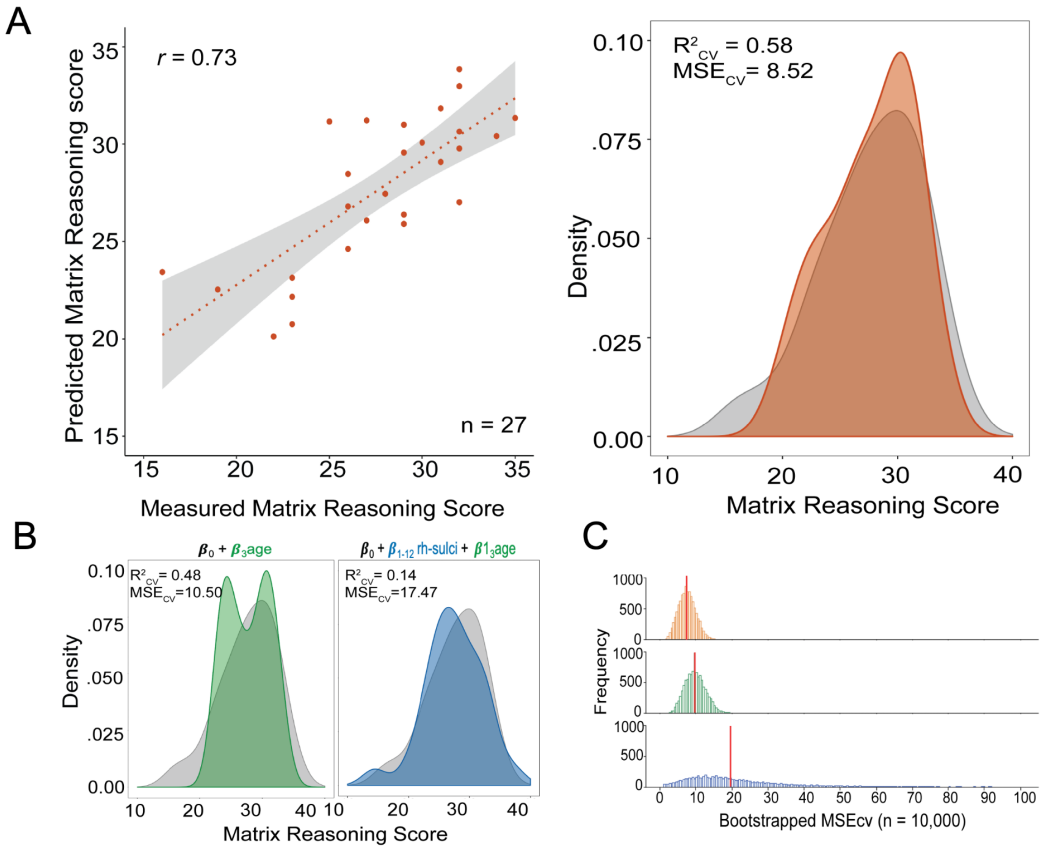

Figure 1.5. ***A model-based approach with nested cross-validation reveals that the depth of a subset of LPFC tertiary sulci predicts individual variability in reasoning above and beyond age.*** **A.** *Left:* Spearman's correlation between measured and predicted Matrix reasoning scores in the *Replication* sample for the best tertiary sulci + age model, which includes the depths of the two most predictive sulci (*pmfs-i*$_{RH}$ + *pimfs*$_{RH}$) from the *Discovery* sample, as well as age (Appendix Figure 1.5 for a model with all three tertiary sulci selected from the *Discovery* sample). *Right*: Density plot of model fit. The predicted scores from the chosen model (*pmfs-i*$_{RH}$ + *pimfs*$_{RH}$ + age) are shown in orange and overlaid on the distribution of measured Matrix reasoning scores (*gray*). **B.** Distribution of predicted scores for the cross-validated nested model comparisons. *Green*: age only. *Blue*: all RH LPFC sulci + age. Each of the model fits are overlaid on the distribution of measured Matrix reasoning scores *(gray*). The *pmfs-i*$_{RH}$ + *pimfs*$_{RH}$ + age model (**a**) produced a better fit than both comparison models. **C.** Empirical MSE for each of the three models estimated with a bootstrapping procedure ($n_{iterations}$ = 10,000) to address the potential for looCV to result in high variance and overfitting. The model including all LPFC RH sulci + age (*blue*) exhibited notably high variance in error estimation. The red vertical line indicates the estimated median MSE.

Probability maps of LPFC sulci in a pediatric cohort

As this is the first developmental dataset of tertiary sulci in LPFC (to our knowledge), we sought to generate spatial probability maps that can be shared with the field. The benefit of such maps is that they capture both the stable and variable features of LPFC sulci across participants. We calculated probability maps (Miller et al., 2021b) across all participants with at least one identifiable *pimfs* component in each hemisphere (N=58). We provide examples of the unthresholded probability maps, which capture the spatial variability across participants, as well as maps thresholded at 20% and 33% overlap across participants (Figure 1.6A). Thresholding captures the shared features across participants and can be applied to increase the interpretability and reduce spatial overlap between sulci (Miller et al., 2021b; Methods). These probability maps

can be projected to cortical surfaces in individual participants across ages (Figure 1.6B) and can guide future research that aims to shed light on how LPFC tertiary sulcal morphology affects the functional organization in LPFC, as well as cognition.

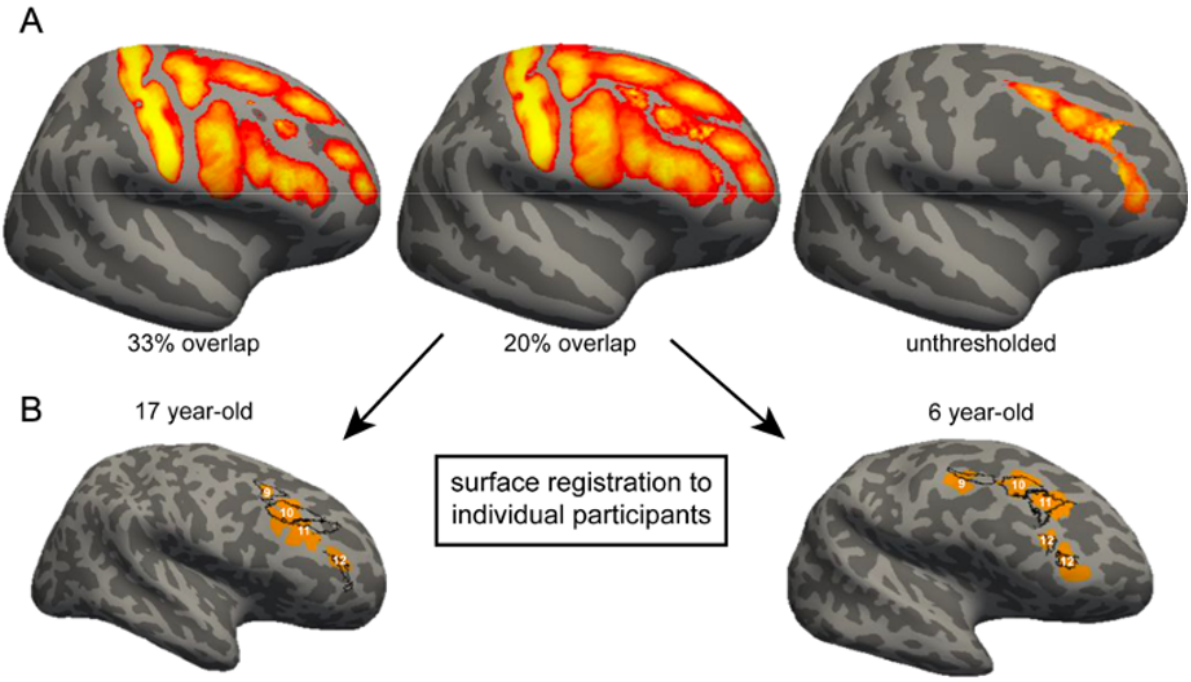

Figure 1.6. ***Probability maps of LPFC tertiary sulci.*** **A.** Maximum probability maps were generated across all participants with an identifiable *pimfs* in both hemispheres (N=58). To generate the maps, each label was transformed from each individual to the common *fsaverage* space. For each vertex, we calculated the proportion of participants for whom that vertex is labeled as the given sulcus (the warmer the color, the higher the overlap in each image). In the case of multiple labels for one vertex, the sulcus with the highest overlap across participants was assigned to a given vertex. To reduce spatial overlap, these maps can be thresholded to only include vertices with a minimum percent overlap across participants (eg. 33% (left) or 20% (middle) overlap). The maps of tertiary sulci within the middle frontal gyrus (MFG) in the present study (right, unthresholded) can be used in future studies to guide the definition of tertiary sulci within the MFG. **B.** Maps can be projected to individual participants to guide the definition of tertiary sulci in LPFC. Here, the thresholded maps (20%) for the tertiary sulci are projected back to example (randomly chosen) hemispheres from a 17 year-old (left) and a 6 year-old (right). The outline of the spatial probability maps (black) are overlaid on the manual sulcal definitions (orange) for visualization purposes. 9: pmfs-p; 10: pmfs-i; 11: pmfs-a; 12: pimfs. While there is not a perfect correspondence between the maps and the tertiary sulci, the maps can guide manual definitions performed by researchers interested in examining LPFC tertiary sulci in future studies. These maps can be applied to other samples and can be downloaded from https://github.com/cnl-berkeley/stable_projects/tree/main/CognitiveInsights_SulcalMorphology.

1.5 Discussion

Recent studies examining sulcal morphology in humans and other species continue to improve our understanding of the development and evolution of association cortices. They also provide anatomical insights into cognitive skills that set humans apart from other species (Amiez et al., 2019; Miller et al., 2021b; Rogers et al., 2010; Zilles et al., 2013). A consistent finding from these previous studies is that developmentally and evolutionarily meaningful changes in sulcal morphology are not homogeneous within association cortices; instead, such changes are focal and related to different aspects of neuroanatomical and functional networks that are behaviorally meaningful (Amiez et al., 2018, 2019; Borst et al., 2014; Brun et al., 2016; Im et al., 2010; Leroy et al., 2015; Liu et al., 2011; Lopez-Persem et al., 2019; Miller et al., 2021b). After manually defining 1,320 sulci in individual participants and implementing a data-driven approach with nested cross-validation in both *Discovery* and *Replication* samples, our results are consistent with and extend these previous findings by showing that the sulcal depth of particular LPFC tertiary sulci predicts behavioral performance on a reasoning task in a developmental cohort, above and beyond age. In the sections below, we discuss 1) the identification of tertiary sulci in future studies, 2) potential underlying mechanisms that likely contribute to the relationship between tertiary sulcal depth and cognitive performance, 3) how the present findings provide a foundation for future studies attempting to link the morphology of brain structures to behavior and functional brain representations, and 4) how our novel, model-based approach can be applied to study other association cortices across the lifespan.

While it may seem surprising that we were able to identify each *pmfs* component in every hemisphere, our findings are consistent with previous work showing that some tertiary sulci are identifiable in every hemisphere and others are not. For example, the mid-fusiform sulcus in ventral temporal cortex (VTC) is identifiable in every hemisphere in humans and non-human primates (Miller et al., 2020; Weiner et al., 2014; Weiner, 2018a), while the paracingulate sulcus is only identifiable in ~70% of hemispheres with a left hemisphere bias in medial prefrontal cortex in humans (Garrison et al., 2015; Lopez-Persem et al., 2019) and only ~30% of the time in chimpanzees with no left hemisphere bias (Amiez et al., 2019; Garrison et al., 2015). Consistent with recent findings in adult LPFC (Miller et al., 2021a; Miller et al., 2021b), we could identify all three *pmfs* sulcal components in each hemisphere across participants in our pediatric cohort. On the other hand, we could identify the *pimfs* components in a majority of participants, but not all. Thus, our findings are consistent with the previous literature regarding the definitions of tertiary sulci in different lobes. For instance, beyond LPFC and VTC, Lopez-Persem and colleagues (2019) found that some ventromedial PFC tertiary sulci are consistently identifiable, while other tertiary sulci are more variable. This is in line with our findings in LPFC - that the *pmfs-p*, *pmfs-i*, and *pmfs-a* are present in all participants, whereas the *pimfs* is variable in its presence and number of components.

An immediate question generated from our findings is: *What underlying mechanisms could explain why the depths of LPFC tertiary sulci and age reliably predict reasoning performance on a complex behavioral task?* We offer one potential explanation that integrates recent anatomical findings (Miller et al., 2021b; Reeley et al., 2015) with a classic theory (Sanides, 1964) and propose a hypothesis linking sulcal depth to short-range anatomical connections, and in turn, to cortical networks and cognitive performance. Specifically, in the 1960s, Sanides (1962; 1964) proposed that morphological changes in tertiary sulci would likely be associated with the development of higher-order processing and cognitive skills. The logic of Sanides' hypothesis extends from the fact that tertiary sulci emerge last in gestation and have a

protracted development after birth, while complex cognitive skills such as reasoning also have a protracted development in childhood. Our findings support this classic hypothesis. However, while the LPFC is considered critical to reasoning (Badre & D'Esposito, 2009; Crone et al., 2006; He & Seymour, 2018; Vendetti & Bunge, 2014; Wendelken et al., 2016), reasoning performance cannot be localized to a single structure (Ehsan et al., 2012; He & Seymour, 2018; Vendetti & Bunge, 2014; Wendelken et al., 2016) and thus, the mechanism behind this relationship still needs to be investigated.

As a starting point toward understanding the underlying mechanism, two recent empirical findings provide underlying anatomical mechanisms that could support this relationship between tertiary sulci and cognition. First, there is a relationship between human LPFC tertiary sulcal morphology and myelination (Miller et al., 2021b; Sanides, 1962; Sanides, 1964), which is critical for short- and long-range connectivity, as well as the efficiency of communicating neural signals among regions within cortical networks (Turner, 2019). Second, anatomical work in non-human primates has shown that long-range white matter fiber tracts have a bias for terminating in gyri, while additional short-range white matter fibers commonly project from the deepest points (*fundi*) of sulci (Reveley et al., 2015), which we refer to as *fundal fibers*. These previous and present findings serve as the foundation for the following novel mechanistic hypothesis linking tertiary sulcal depth to anatomical connections and neural efficiency: deeper tertiary sulci likely reflect shorter fundal fibers, which in turn, reduce the length of short-range anatomical connections between cortical regions, and thus, increase neural efficiency. While speculative, this hypothesis is similar in logic to the tension-based theory of cortical folding (Van Essen, 1997) and also feasible given the fact that short-range structural connectivity increases and sulci deepen during development (Oyefiade et al., 2018; Natu et al., 2021). This increase in neural efficiency could underlie variability in cognitive performance, which can be tested in future studies incorporating anatomical, functional, and behavioral measures, as well as computational modeling.

In addition to this mechanistic hypothesis, our present findings improve the spatial scale of previous studies attempting to link cortical morphology to behavior associated with LPFC. For example, previous studies identified an association between cognitive skills and cortical thickness of LPFC in its entirety (Burgaleta et al., 2014; Dickerson et al., 2008; Gogtay et al., 2004; Østby et al., 2009). While we find an association between reasoning and cortical thickness, when considering individual tertiary sulci, our analyses indicate that the depths of tertiary sulci and age together are much stronger predictors of reasoning than the cortical thickness of these sulci and age together. In fact, when including the cortical thickness of sulci in the model, performance was not better than age alone (Appendix Figure 1.6A). The combination of these findings across studies suggests that neuroanatomical-behavioral relationships can exist at multiple spatial scales in the same macro-anatomical expanse such as LPFC: cortical thickness at the macroanatomical scale and tertiary sulcal depth at the meso-scale.

We also emphasize that, though our model-driven approach identified that the depth of a subset of LPFC tertiary sulci explained a significant amount of variance above and beyond age when predicting reasoning skills in individual participants, it is highly probable that these LPFC tertiary sulci are implicated in other tasks beyond reasoning – and, conversely, that other sulci are also implicated in reasoning. Although we did not observe a relationship between the depths of the identified sulci and two other cognitive measures, this should not be taken as evidence that these sulci show specificity to reasoning; rather, they indicate that these tertiary sulci are relevant for the task at hand.

We also clarify that the present approach of precise anatomical mapping of tertiary sulci does not imply that reasoning can be localized to a single sulcus or even a single cortical region. In fact, our previous work, including previous studies on this dataset, has focused extensively on the distributed nature of reasoning, highlighting patterns of functional and structural connectivity between prefrontal and parietal regions that support this process (He & Seymour, 2018; Vendetti & Bunge, 2014; Wendelken et al., 2016). Additionally, focusing on tertiary sulci in PFC forms a foundation for understanding how these largely overlooked neuroanatomical structures contribute to typical brain function and cognition, especially at the network level (Miller et al., 2021a). Indeed, modern multi-modal neuroimaging research from two recent parallel lines of work shows that meticulously labeling tertiary sulci within individuals uncovers new structural-functional relationships within PFC at the network level (Amiez et al., 2019; Miller et al., 2021b). Interestingly, the former study showed that each component of the *pmfs* participated in more than one network, indicating that these tertiary sulci also have flexible roles as members of different cognitive networks (e.g., ventral attention and cognitive control networks for the *pmfs-a*, for example). Thus, future studies exploring the relationship between sulcal morphology and behavioral performance in additional cognitive tasks at the level of individual participants will begin to generate a more comprehensive sulcal-behavioral map in LPFC with additional insights into cortical networks.

In addition to this sulcal-behavioral map in LPFC, two recent lines of work show feasibility for future studies attempting to link tertiary sulcal morphology to brain function, especially for functional activity related to reasoning: one related to tertiary sulci as a meso-scale link between microstructural and functional properties of LPFC and the other identifying functional representations related to reasoning. In terms of the former, a series of recent studies have shown that tertiary sulci are critical functional landmarks in different association cortices (Cachia et al., 2015; Lopez-Persem et al., 2019; Weiner et al., 2014; Weiner & Zilles, 2016) and variability in sulcal morphology in the medial prefrontal cortex has been associated with changes in cortical morphometry linked to individual differences in cognitive performance and clinical symptom presentation in patients with schizophrenia (Garrison et al., 2015). Additionally, in LPFC, Miller and colleagues (2021b) showed that the different *pmfs* components explored here were functionally distinct in adults with respect to resting-state connectivity profiles. In terms of the latter, numerous functional neuroimaging studies show that LPFC is central for reasoning performance (Crone et al., 2006; Watson & Chatterjee, 2012). More explicitly, several studies also indicate that the middle frontal gyrus, the gyrus in which the three sulci (*pmfs-i, pmfs-a,* and *pimfs*) identified by our model are located, plays an important role in cognitive processes that are integral for reasoning, such as maintaining representations and forming associations (Badre & Nee, 2018; Fuster, 2001). Thus, future investigations of functional connectivity, as well as functional representations, relative to tertiary sulci in future studies in children and adults will likely bring us closer to understanding the complex relationship between the development of LPFC anatomical organization, functional organization, and behavior.

While we limit our focus to the LPFC in the present study, both because of its relevance for reasoning, and also because of the immense manual labor involved in this type of study, the novel, data-driven pipeline introduced here can be applied to any cortical expanse. For example, lateral parietal cortex is also critical for relational reasoning, is expanded in humans compared to non-human primates (Donahue et al., 2018; Van Essen et al., 2018), and contains tertiary sulci (Miller et al., 2020). Additionally, structural connectivity between frontal and parietal regions increases across development (He & Seymour, 2018; Lebel et al., 2017; Lebel & Beaulieu,

2011). Thus, future studies can explore how morphological features of tertiary sulci in a) LPFC and lateral parietal cortex contribute to reasoning performance and b) different association cortices contribute to performance on cognitive tasks, as well as functional representations in each cortical expanse. It will also be important to explore the relationship among tertiary sulci across cortical regions. For example, developmental studies are well suited to explore how the variability in sulcal morphology in one cortical region, such as LPFC, might affect morphology of tertiary sulci in other cortical regions, such as medial frontal or parietal regions. Our modeling approach can also be applied to data across the lifespan – either cross-sectionally or longitudinally. While it is known that tertiary sulci are shallow indentations in cortex that emerge last in gestation (relative to primary and secondary sulci), and have a protracted development after birth (Amiez et al., 2019; Van Essen, 2007; Petrides, 2019; Friedrich Sanides, 1964; Weiner, 2018; Welker, 1990; Zilles et al., 2013), the history of LPFC sulcal definitions, especially within the MFG, has been contentious (Bailey & Bonin, 1950; Bailey, 1951; Sanides, 1964; Turner, 1948; Weiner & Zilles, 2016; Weiner, 2018; Welker, 1990; Chi et al., 1977; Miller et al., 2021a; Miller et al., 2021b; Connolly et al., 1940; Connolly et al., 1950; Cunningham et al., 1892; Petrides et al., 2019). Thus, while we used these classic studies to guide the labeling of each sulcus, the distinctions among primary, secondary, and tertiary sulci should be confirmed by modern studies of cortical folding in gestation. Crucially, our findings are not dependent on this classification. Our data-driven, model-based approach identified that a subset of shallow sulci in LPFC explain the most variance in reasoning skills across participants above and beyond age in both *Discovery* and *Replication* samples. Additionally, the developmental timeline of tertiary sulci relative to the development of functional representations and cognitive skills is unknown. Future studies implementing and improving our model-based approach can begin to fill in these gaps in the developmental timeline of tertiary sulci anatomically, behaviorally, and functionally.

Despite the many positive applications of our model-based approach and the many future studies that will likely build on the foundation of the present novel findings, there are also limitations. The main drawback of the precise approach in individual participants implemented here is that it relies on manual sulcal definitions, which are time-consuming and require anatomical expertise. This limits sample sizes and the expanse of cortex that can be feasibly explored in a given study. Additionally, while there is "no one-size-fits-all sample size for neuroimaging studies" (Marek et al., 2020) and we had a large N (>1000) in terms of sulci explored in the present study, new methods and tools will need to be developed to increase the number of participants in futures studies. Increasing the number of participants will improve the diversity of our sample and reduce imbalances in gender or other demographic features (Methods; Appendix Table 1.2). Ongoing work is already underway to develop deep learning algorithms to accurately define tertiary sulci automatically in individual participants, and initial results are promising (Borne et al., 2020; Lyu et al., 2021). In the interim, our probabilistic sulcal maps can guide manual definitions performed by researchers interested in examining LPFC tertiary sulci in future studies (Figure 1. 6).

In summary, using a data-driven, model-based approach, we provide cognitive insights from evolutionarily new brain structures in human LPFC for the first time. After manually defining 1,320 LPFC sulci, our approach revealed that the depths of a subset of tertiary sulci reliably predicted reasoning skills above and beyond age. Methodologically, our study opens the door for future studies examining these evolutionarily new tertiary sulci in other association cortices, as well as improves the spatial scale of understanding for future studies interested in linking cortical morphology to behavior. Theoretically, the present results support a largely

unconsidered anatomical theory proposed over 55 years ago (Sanides et al., 1964). Mechanistically, we outline a novel hypothesis linking tertiary sulcal depth to short-range white matter fibers, neural efficiency, and cognitive performance. Together, the methodological, theoretical, and mechanistic insights regarding whether, or how, tertiary sulci contribute to the development of higher-level cognition in the present study serve as a foundation for future studies examining the relationship between the development of cognitive skills and the morphology of tertiary sulci in association cortices more broadly.

1.6 References

Zilles, K., Palomero-Gallagher, N. & Amunts, K. Development of cortical folding during evolution and ontogeny. *Trends Neurosci* 36, 275–284 (2013).

Donahue, C. J., Glasser, M. F., Preuss, T. M., Rilling, J. K. & Van Essen, D. C. Quantitative assessment of prefrontal cortex in humans relative to nonhuman primates. *Proc. Natl. Acad. Sci. U. S. A.* 115, E5183–E5192 (2018).

Fuster, J. M. The prefrontal cortex - An update: Time is of the essence. *Neuron* vol. 30 319–333 (2001).

Badre, D. & Nee, D. E. Frontal Cortex and the Hierarchical Control of Behavior. *Trends in Cognitive Sciences* vol. 22 170–188 (2018).

Szczepanski, S. M. & Knight, R. T. Insights into Human Behavior from Lesions to the Prefrontal Cortex. *Neuron* vol. 83 1002–1018 (2014).

Vendetti, M. S. & Bunge, S. A. Evolutionary and Developmental Changes in the Lateral Frontoparietal Network: A Little Goes a Long Way for Higher-Level Cognition. *Neuron* 84, 906–917 (2014).

Bailey P., Bonin, G.V. The isocortex of Man. *Illinois Monogr. mediacal Sci.* V1, (1951).

Bailey P., Bonin G.V., McCulloch, W.S. The isocortex of the chimpanzee. *Urbana, Illinois, Univ. Illinois Press* 292 (1950).

Sanides, F. Structure and function of the human frontal lobe. *Neuropsychologia* 2, 209–219 (1964).

Turner, O. A. Growth and development of the cerebral cortical pattern in man. *Arch. Neurol. Psychiatry* 59, 1–12 (1948).

Weiner, K. S. The Mid‐Fusiform Sulcus (*sulcus sagittalis gyri fusiformis*). *Anat. Rec.* 302, 1491–1503 (2018).

Weiner, K. S. *et al.* The mid-fusiform sulcus: a landmark identifying both cytoarchitectonic and functional divisions of human ventral temporal cortex. *Neuroimage* 84, 453–465 (2014).

Weiner, K. S. & Zilles, K. The anatomical and functional specialization of the fusiform gyrus. *Neuropsychologia* (2016) doi:10.1016/j.neuropsychologia.2015.06.033.

Welker, W. Why does cerebral cortex fissure and fold? A review determinants of gyri and sulci. *Cereb. cortex* 8b, 3--136 (1990).

Tamraz, Jean & Comair, Y. *Atlas of Regional Anatomy of the Brain Using MRI: With Functional*

Correlations. (2006).

Amiez, C. *et al.* Sulcal organization in the medial frontal cortex provides insights into primate brain evolution. *Nat. Commun.* 10, 3437 (2019).

Amiez, C. *et al.* Chimpanzee histology and functional brain imaging show that the paracingulate sulcus is not human-specific. *Commun. Biol.* 4, (2021).

Armstrong, E., Schleicher, A., Omran, H., Curtis, M. & Zilles, K. The ontogeny of human gyrification. *Cereb. Cortex* 5, 56–63 (1995).

Chi, J. G., Dooling, E. C. & Gilles, F. H. Gyral development of the human brain. *Ann. Neurol.* 1, 86–93 (1977).

Garrison, J. R. *et al.* Paracingulate sulcus morphology is associated with hallucinations in the human brain. *Nat. Commun.* 6, 1–6 (2015).

Miller, Jacob A. Mark D'esposito, Weiner, K.S. Using tertiary sulci to map the 'cognitive globe' of prefrontal cortex. *J. Cogn. Neurosci* (2021).

Connolly, C. J. Development of the cerebral sulci. *Am. J. Phys. Anthropol.* 26, 113–149 (1940).

Connolly, C. J. External morphology of the primate brain. *Springf. C. C. Thomas* (1950).

Cunningham, D. Contribution to the surface anatomy of the cerebral hemispheres. *Dublin R. Irish Acad.* (1892).

Miller, J. A., Voorhies, W. I., Lurie, D. J., D'Esposito, M. & Weiner, K. S. Overlooked tertiary sulci serve as a meso-scale link between microstructural and functional properties of human lateral prefrontal cortex. *J. Neurosci.* 41, 2229-2244 (2021).

Petrides, M. *Atlas of the morphology of the human cerebral cortex on the average MNI brain*. (Academic Press, 2019).

Sanides, F. Architectonics of the human frontal lobe of the brain. With a demonstration of the principles of its formation as a reflection of phylogenetic differentiation of the cerebral cortex. *Monogr. Gesamtgeb. Neurol. Psychiatr.* 98, 1–201 (1962).

Weiner, K. S., Natu, V. S. & Grill-Spector, K. On object selectivity and the anatomy of the human fusiform gyrus. (2018) doi:10.1016/j.neuroimage.2018.02.040.

Miller, J. A. *et al.* Sulcal morphology of ventral temporal cortex is shared between humans and other hominoids. *Sci. Rep.* 10, 17132 (2020).

Wendelken, C. *et al.* Frontoparietal structural connectivity in childhood predicts development of functional connectivity and reasoning ability: A large-scale longitudinal investigation. *J. Neurosci.* 37, 8549–8558 (2017).

Penn, D. C., Holyoak, K. J. & Povinelli, D. J. Darwin's mistake: Explaining the discontinuity between human and nonhuman minds. *Behav. Brain Sci.* 31, 109–178 (2008).

Buckner, R. The serendipitous discovery of the brain's default network. *Neuroimage* 62, 1137–1145 (2012).

Rakic, P. Evolution of the neocortex: A perspective from developmental biology. *Nature Reviews Neuroscience* 10, 724–735 (2009).

Fry, A. F. & Hale, S. Relationships among processing speed, working memory, and fluid intelligence in children. *Biol. Psychol.* 54, 1–34 (2000).

Mcardle, J. J., Ferrer-Caja, E., Hamagami, F. & Woodcock, R. W. Comparative Longitudinal Structural Analyses of the Growth and Decline of Multiple Intellectual Abilities Over the Life Span. *Dev. Psychology* 38, 115-142 (2002) doi:10.1037/0012-1649.38.1.115.

Wendelken, C., Ferrer, E., Whitaker, K. J. & Bunge, S. A. Fronto-Parietal Network Reconfiguration Supports the Development of Reasoning Ability. *Cereb. Cortex* 26, 2178-2190 (2016) doi:10.1093/cercor/bhv050.

Ferrer, E. *et al.* White matter maturation supports the development of reasoning ability through its influence on processing speed. *Dev. Sci.* 16, 941–951 (2013).

He, W. & Seymour, R. A. Commentary: Frontoparietal structural connectivity in childhood predicts development of functional connectivity and reasoning ability: A large-scale longitudinal investigation. *Frontiers in Psychology* 9, 265 (2018) doi:10.3389/fpsyg.2018.00265.

Crone, E. A., Wendelken, C., Donohue, S., Van Leijenhorst, L. & Bunge, S. A. Neurocognitive development of the ability to manipulate information in working memory. *Proc. Natl. Acad. Sci. U. S. A.* 103, 9315–9320 (2006).

Badre, D. & D'Esposito, M. Is the rostro-caudal axis of the frontal lobe hierarchical? *Nature Reviews Neuroscience* 10, 659–669 (2009).

Christoff, K. *et al.* Rostrolateral prefrontal cortex involvement in relational integration during reasoning. *Neuroimage* 14, 1136–1149 (2001).

Krawczyk, D. C., Michelle McClelland, M. & Donovan, C. M. A hierarchy for relational reasoning in the prefrontal cortex. *Cortex* 47, 588-97 (2011) doi:10.1016/j.cortex.2010.04.008.

Wendelken, C., O'Hare, E. D., Whitaker, K. J., Ferrer, E. & Bunge, S. A. Increased functional selectivity over development in rostrolateral prefrontal cortex. *J. Neurosci.* 31, 17260-17268 (2011).

Van Essen, D. C. Cerebral Cortical Folding Patterns in Primates: Why They Vary and What They Signify. *Evol. Nerv. Syst.* 267–276 (2007).

Lopez-Persem, A., Verhagen, L., Amiez, C., Petrides, M. & Sallet, J. The human ventromedial prefrontal cortex: Sulcal morphology and its influence on functional organization. *J. Neurosci.* 39, 3627–3639 (2019).

Dumontheil, I., Houlton, R., Christoff, K. & Blakemore, S. J. Development of relational reasoning during adolescence. *Dev. Sci.* 13, F15-24 (2010).

Dumontheil, I. Development of abstract thinking during childhood and adolescence: The role of rostrolateral prefrontal cortex. *Developmental Cognitive Neuroscience* 10, 57–76 (2014).

Blair, C. How similar are fluid cognition and general intelligence? A developmental neuroscience perspective on fluid cognition as an aspect of human cognitive ability. *Behav Brain Sci* 29, 109-25 (2006).

Cattell, R. B. *Intelligence : its structure, growth, and action*. (North-Holland, 1987).

Brun, L. *et al.* Localized Misfolding Within Broca's Area as a Distinctive Feature of Autistic Disorder. *Biol. Psychiatry Cogn. Neurosci. Neuroimaging* 1, 160–168 (2016).

Amiez, C. & Petrides, M. Functional rostro-caudal gradient in the human posterior lateral frontal cortex. *Brain Struct. Funct.* 223, 1487–1499 (2018).

Borne, L., Rivière, D., Mancip, M. & Mangin, J. F. Automatic labeling of cortical sulci using patch- or CNN-based segmentation techniques combined with bottom-up geometric constraints. *Med. Image Anal.* 62, 101651 (2020).

Mangin, J. F. *et al.* Sulci as landmarks. in *Brain Mapping: An Encyclopedic Reference* (ed. Toga, A. W.) (Academic Press, 2015).

Amiez, C. *et al.* The Location of Feedback-Related Activity in the Midcingulate Cortex Is Predicted by Local Morphology. *J. Neurosci.* 33, 2217-2228 (2013) doi:10.1523/JNEUROSCI.2779-12.2013.

Amiez, C. & Petrides, M. Selective involvement of the mid-dorsolateral prefrontal cortex in the coding of the serial order of visual stimuli in working memory. *Proc. Natl. Acad. Sci. U. S. A.* 104, 13786–13791 (2007).

Petrides, M., Tomaiuolo, F., Yeterian, E. H. & Pandya, D. N. The prefrontal cortex: Comparative architectonic organization in the human and the macaque monkey brains. *Cortex* 48, 46–57 (2012).

Ariens-Kappers, C. . The evolution of the nervous system in invertebrates, vertebrates and man. *Haarlem Erven F. Bohn.* (1929).

Eberstaller, O. Das Stirnhirn; ein Beitrag zur Anatomie der Oberfläche des Grosshirns. *Wien Urban Schwarz.* (1890).

Ono M, Kubik S, A. C. Atlas of the Cerebral Sulci. *New York Thieme Med. Publ. Inc.* (1990).

Rajkowska, G. & Goldman-Rakic, P. S. Cytoarchitectonic Definition of Prefrontal Areas in the Normal Human Cortex: II. Variability in Locations of Areas 9 and 46 and Relationship to the Talairach Coordinate System. *Cereb. Cortex* 5, 323–337 (1995).

Shellshear, J. L. V - The brain of the Aboriginal Australian. A study in cerebral morphology. *Philos. Trans. R. Soc. Lond. B. Biol. Sci.* 227, 293–409 (1937).

Petrides, M. *The Human Cerebral Cortex*. (Academic Press, 2012).

Cachia, A. *et al.* How interindividual differences in brain anatomy shape reading accuracy. *Brain Struct. Funct.* 223, 701–712 (2018).

Cachia, A. *et al.* Deviations in cortex sulcation associated with visual hallucinations in schizophrenia. *Mol. Psychiatry* 20, 1101–1107 (2015).

Ghojogh, B., Ca & Crowley, M. The Theory Behind Overfitting, Cross Validation, Regularization, Bagging, and Boosting: Tutorial. *arXiv* (2019).

Heinze, G., Wallisch, C. & Dunkler, D. Variable selection – A review and recommendations for the practicing statistician. *Biometrical Journal* vol. 60 431–449 (2018).

Burgaleta, M., Johnson, W., Waber, D. P., Colom, R. & Karama, S. Cognitive ability changes and dynamics of cortical thickness development in healthy children and adolescents. *Neuroimage* 84, 810–819 (2014).

Dickerson, B. C. *et al.* Detection of cortical thickness correlates of cognitive performance: Reliability across MRI scan sessions, scanners, and field strengths. *Neuroimage* 39, 10–18 (2008).

Østby, Y. *et al.* Heterogeneity in subcortical brain development: A structural magnetic resonance imaging study of brain maturation from 8 to 30 years. *J. Neurosci.* 29, 11772–11782 (2009).

Gogtay, N. *et al.* Dynamic mapping of human cortical development during childhood through early adulthood. *Proc. Natl. Acad. Sci. U. S. A.* 101, 8174–8179 (2004).

Kail, R. & Salthouse, T. A. Processing speed as a mental capacity. *Acta Psychol. (Amst).* 86, 199–225 (1994).

Wagenmakers, E.-J., Farrell, S. & Wagenmakers, J. AIC model selection using Akaike weights. *Psychnomic Bulletin & Review* 11, 192-196 (2004).

Burnham, K. P. & Anderson, D. R. Multimodel Inference: Understanding AIC and BIC in Model Selection *Sociological Methods & Research* 33, 261-304 (2004).

Kail, R. V., Lervåg, A. & Hulme, C. Longitudinal evidence linking processing speed to the development of reasoning. *Dev. Sci.* 19, 1067–1074 (2016).

Holyoak, K. J. & Monti, M. M. Relational Integration in the Human Brain: A Review and Synthesis. *J. Cogn. Neurosci.* 33, 341–356 (2021).

Rogers, J. *et al.* On the genetic architecture of cortical folding and brain volume in primates. *Neuroimage* 53, 1103–1108 (2010).

Leroy, F. *et al.* New human-specific brain landmark: The depth asymmetry of superior temporal sulcus. *Proc. Natl. Acad. Sci. U. S. A.* 112, 1208–1213 (2015).

Im, K. *et al.* Spatial distribution of deep sulcal landmarks and hemispherical asymmetry on the cortical surface. *Cereb. Cortex* 20, 602–611 (2010).

Liu, T. *et al.* The relationship between cortical sulcal variability and cognitive performance in the elderly. *Neuroimage* 56, 865–873 (2011).

Borst, G. *et al.* Folding of the anterior cingulate cortex partially explains inhibitory control during childhood: A longitudinal study. *Dev. Cogn. Neurosci.* 9, 126–135 (2014).

Reveley, C. *et al.* Superficial white matter fiber systems impede detection of long-range cortical connections in diffusion MR tractography. *Proc. Natl. Acad. Sci. U. S. A.* 112, E2820–E2828 (2015).

Ehsan, S. K., Motes, M. A., Rypma, B. & Krawczyk, D. C. The network architecture of cortical processing in visuo-spatial reasoning. *Sci. Rep.* 2, 1–7 (2012).

Turner, R. Myelin and modeling: Bootstrapping cortical microcircuits. *Frontiers in Neural Circuits* 13, 34 (2019).

Van Essen, D. C. A tension-based theory of morphogenesis and compact wiring in the central nervous system. *Nature* 385, 313–318 (1997).

Oyefiade, A. A. *et al.* Development of short-range white matter in healthy children and adolescents. *Hum. Brain Mapp.* 39, 204–217 (2018).

Natu, V. S. *et al.* Sulcal depth in medial ventral temporal cortex predicts the location of a place-selective region in macaques, children, and adults. *Cereb. Cortex* 31, 48-61(2021).

Watson, C. E. & Chatterjee, A. A bilateral frontoparietal network underlies visuospatial analogical reasoning. *Neuroimage* 59, 2831–2838 (2012).

Van Essen, D. C., Donahue, C. J. & Glasser, M. F. Development and evolution of cerebral and cerebellar cortex. *Brain. Behav. Evol.* 91, 158–169 (2018).

Lebel, C. & Beaulieu, C. Longitudinal Development of Human Brain Wiring Continues from Childhood into Adulthood. *J. Neurosci.* 31, 10937–10947 (2011).

Lebel, C., Treit, S. & Beaulieu, C. A review of diffusion MRI of typical white matter development from early childhood to young adulthood. *NMR Biomed.* 32, e3778 (2017) doi:10.1002/nbm.3778.

Lyu, I. *et al.* Labeling lateral prefrontal sulci using spherical data augmentation and context-aware training. *Neuroimage* 229, 117758 (2021).

McBride-Chang, C. & Kail, R. V. Cross-cultural similarities in the predictors of reading acquisition. *Child Dev.* 73, 1392–1407 (2002).

Kail, R. V. & Ferrer, E. Processing speed in childhood and adolescence: Longitudinal models for examining developmental change. *Child Dev.* 78, 1760–1770 (2007).

Dale, A. M., Fischl, B. & Sereno, M. I. Cortical Surface-Based Analysis I. Segmentation and Surface Reconstruction. *NeuroImage* 9, 179-194 (1999).

Fischl, B., Dale, A. M. & Raichle, M. E. Measuring the thickness of the human cerebral cortex from magnetic resonance images. *PNAS* 97, 11050-11055 (2000).

Wandell, B. A., Chial, S. & Backus, B. T. Visualization and measurement of the cortical surface. *J. Cogn. Neurosci.* 12, 739–752 (2000).

Chen, C. H. *et al.* Hierarchical genetic organization of human cortical surface area. *Science* 335, 1634–1636 (2012).

Pedregosa, F. *et al.* Scikit-learn: Machine Learning in Python. *Journal of Machine Learning Research* 12, 2825-2830 (2011).

Tamnes, C. K. *et al.* Longitudinal working memory development is related to structural maturation of frontal and parietal cortices. *J. Cogn. Neurosci.* 25, 1611–1623 (2013).

Brown, T. T. *et al.* Neuroanatomical assessment of biological maturity. *Curr. Biol.* 22, 1693–1698 (2012).

Vijayakumar, N. *et al.* Thinning of the lateral prefrontal cortex during adolescence predicts emotion regulation in females. *Soc. Cogn. Affect. Neurosci.* 9, 1845–1854 (2014).

Woodcock, R., Mather, N., McGrew, K. & Wendling, B. *Woodcock-Johnson III tests of cognitive abilities*. (Riverside Publishing Company, 2001).

Zilles, K., Armstrong, E., Schleicher, A. & Kretschmann, H.-J. The human pattern of gyrification

in the cerebral cortex. *Anat. Embryol. (Berl).* 179, 173–179 (1988).

Destrieux, C., Fischl, B., Dale, A. & Halgren, E. Automatic parcellation of human cortical gyri and sulci using standard anatomical nomenclature. *Neuroimage* 53, 1-15 (2010).

Schall JD, Zinke W, Cosman JD, Schall MS, Pare M, P. P. On the Evolution of the frontal eye field: comparisons of monkeys, apes, and humans. in *Evolutionary Neuroscience, Ed 2* 861–883 (2020).

Champod, A.S. & Petrides, M. Dissociable roles of the posterior parietal and the prefrontal cortex in manipulation and monitoring processes. *PNAS* 104, 14837-14842.

Marek, S. *et al.* Towards Reproducible Brain-Wide Association Studies. *bioRxiv* 2020.08.21.257758 (2020) doi:10.1101/2020.08.21.257758.

Wechsler, D. *Wechsler intelligence scale for children–Fourth Edition (WISC-IV)*. (The Psychological Corporation).

Chapter 2. A role for sulcal variability in behavior and function

Our previous findings showed that the morphology of LPFC sulci predicts reasoning performance. This work also led to the observation of substantial individual variability in the morphology of one of these sulci, the para-intermediate frontal sulcus (pimfs). Building on this observation, I present two studies. In the first, I sought to characterize this variability and assess its behavioral significance. In the second study, I examine how the individual sulcal components related to whole-brain functional connectivity in the same sample. Consistent with the behavioral findings, these differences in component connectivity interacted with reasoning skills. These findings show that the cortex lining the banks of sulci can support the development of complex cognitive skills, and highlight the importance of considering individual differences in local morphology when exploring the neurodevelopmental basis of cognition.

With permission, this chapter contains previously published material from the following work:
Willbrand, E.H., Voorhies, W.I., Yao, J.K. et al. Presence or absence of a prefrontal sulcus is linked to reasoning performance during child development. Brain Struct Funct 227, 2543–2551 (2022). https://doi.org/10.1007/s00429-022-02539-1

2.2 Introduction

Tertiary sulci play an important role in cognition. While tertiary sulcal morphology is related to the development of cognitive skills (Voorhies et al., 2021, Yao et al., 2022), there is still a lot to learn about the role these sulci play in complex cognition. In the previous chapter, we demonstrated that the depth of specific LPFC tertiary sulci was related to abstract reasoning skill. However, we observed pronounced variability in the number of components, and overall prominence in one of the three sulci identified by the model, the para-intermediate frontal sulcus (pimfs). However, this previous study only considered participants with both pimfs components and did not consider the effect of the presence or absence of the dorsal or ventral component of the pimfs on the findings of our model-based approach.

Although the majority of sulci are identifiable across individuals, some late-emerging tertiary sulci, like the pimfs, are not (Chiavaras and Petrides 2000; Lopez-Persem et al. 2019; Amiez et al. 2019; Voorhies et al. 2021; Willbrand et al. 2021). In some cases, the variable presence of sulci has been linked to behavioral and functional variability. For example, the variable presence of the paracingulate sulcus in the anterior cingulate cortex is related to performance on cognitive, motor, and affective tasks in young adults (Fornito et al. 2004, 2006; Whittle et al. 2009; Huster et al. 2009, 2011; Buda et al. 2011; Amiez et al. 2018), inhibitory control in children (Cachia et al. 2014; Borst et al. 2014), and in disorders such as schizophrenia (Yücel et al. 2002, 2003; Le Provost et al. 2003), obsessive-compulsive disorder (Shim et al. 2009), and frontotemporal dementia (Harper et al. 2022). Functionally, the absence of multiple sulci in the ventromedial prefrontal cortex (PFC) affects the functional organization of the default mode network (Lopez-Persem et al. 2019). Viewed within the context of this other literature, our previous findings raise the question of whether the inter-participant variability of the pimfs has implications for reasoning.

There is reason to suspect that anatomical variability may have implications for reasoning skill across development. The pimfs falls in a region that is functionally defined as the rostrolateral prefrontal cortex (Appendix Figure 2.1.5; Christoff et al. 2001; Vendetti and Bunge 2014; Urbanski et al. 2016; Hartogsveld et al. 2018; Assem et al. 2020). Across development, structural connectivity increases between the left rostrolateral prefrontal and inferior lateral parietal cortex (LPC; Wendelken et al., 2017). This increased connectivity is positively associated with future improvements in reasoning skill as well as increased functional connectivity between these two regions (Wendelken et al., 2017). However, it is presently unknown how sulcal variability might relate to behavioral or functional variability in reasoning.

Here, we build on these findings with two studies. In the first study, we characterized the variability in these components in a sample of 72 children and adolescents aged 6-18 and tested the targeted hypothesis that the presence or absence of specific components of the pimfs, and/or the prominence of this sulcus – quantified as the total sulcal surface area – is related to reasoning skill. In the second study, we explored the functional role of these sulci in complex cognition by characterizing sulcal functional connectivity of each component during a relational reasoning task. Paralleling the behavioral study, we also explore how the functional connectivity of each component relates to an individual's reasoning skill.

2.3.1 Study 1 - Materials and Methods

Participants

The present study consisted of 72 typically developing participants between the ages of 6–18 (mean ± std age = 12.11 ± 3.77 years old, including 30 individuals identified by caregivers as female) that were randomly selected from the Neurodevelopment of Reasoning Ability (NORA) dataset (Wendelken et al. 2011, 2016, 2017; Ferrer et al. 2013). These participants largely overlapped with those included in Chapter 1 with a few additional participants. All participants were right-handed; for additional demographic and socioeconomic information see Appendix Table 2.1.1 61 of these participants were also included in prior research on sulcal depth (Voorhies et al. 2021). All participants were screened for neurological impairments, psychiatric illness, history of learning disability, and developmental delay. All participants and their parents gave their informed assent/consent to participate in the study, which was approved by the Committee for the Protection of Human Participants at the University of California, Berkeley.

Data acquisition

Imaging data: MRI data were collected on a Siemens 3T Trio system at the University of California Berkeley Brain Imaging Center. High-resolution T1-weighted MPRAGE anatomical scans (TR = 2300 ms, TE = 2.98 ms, $1 \times 1 \times 1$ mm voxels) were acquired for cortical morphometric analyses.

Behavioral data: All 72 participants completed a matrix reasoning task (WISC-IV), which is a widely used measure of abstract, nonverbal reasoning (Ferrer et al. 2013; Wendelken et al. 2016). Two additional control measures were included when available: processing speed (N = 71) and verbal working memory (N = 64). Reasoning performance was measured as a total raw score from the WISC-IV Matrix reasoning task (Wechsler 1949; mean±std = 25.65±6.01). Matrix reasoning is an untimed subtest of the WISC-IV in which participants are shown colored matrices with one missing quadrant. The participant is asked to "complete" the matrix by selecting the appropriate quadrant from an array of options. Previous factor analysis in this dataset (Ferrer et al. 2013) showed that the Matrix reasoning score loaded strongly onto a reasoning factor that included three other standard reasoning assessments consisting of the *Block Design* subtest of the Wechsler Abbreviated Scale of Intelligence (WASI; Wechsler 1999), as well as the *Analysis Synthesis* and *Concept Formation* subtests of the Woodcock-Johnson Tests of Achievement (Woodcock et al. 2001).

Processing speed was computed from raw scores on the Cross Out task from the Woodcock-Johnson Psychoeducational Battery-Revised (WJ-R; (Brown et al. 2012). In this task, the participant is presented with a geometric figure on the left followed by 19 similar figures. The participant places a line through each figure that is identical to the figure on the left of the row. Performance is indexed by the number of rows (out of 30 total rows) completed in 3 minutes (mean±std = 22.1±6.75). Cross Out scores are frequently used to estimate processing speed in developmental populations (McBride-Chang and Kail 2002; Kail and Ferrer 2007).

Verbal working memory was measured via raw scores of the Digit Span task from the 4th edition of the Wechsler Intelligence Scale for Children (WISC-IV; Wechsler 1949). The Digits Forward condition of the Digit Span task taxes working memory maintenance, whereas the Backward condition taxes both working memory maintenance and manipulation. In Digits Forward, the experimenter reads aloud a sequence of single-digit numbers, and the participant is asked to immediately repeat the numbers in the same order; in Digits Backward, they are asked

to immediately repeat the numbers in the reverse order. The length of the string of numbers increases after every two trials. The Forwards task has eight levels, progressing from 2 to 9 digits. The Backwards task has seven levels, from 2 to 8 digits. Participants are given a score of 1 for a correct answer or a 0 for an incorrect answer. Testing on a given task continues until a participant responds incorrectly to both trials at a given level, after which the experimenter recorded a score out of 16 for Digits Forward (16 total trials; mean±std = 9.03±2.24) and a score out of 14 for Digits Backward (14 total trials; mean±std = 5.84±2.12).

Morphological analyses

*Cortical surface reconstruction:*All T1-weighted images were visually inspected for scanner artifacts. FreeSurfer's automated segmentation tools (Dale et al. 1999; Fischl and Dale 2000; FreeSurfer 6.0.0) were used to generate cortical surface reconstructions. Each anatomical T1-weighted image was segmented to separate gray from white matter, and the resulting boundary was used to reconstruct the cortical surface for each participant (Dale et al. 1999; Wandell et al. 2000). Each reconstruction was visually inspected for segmentation errors, and these were manually corrected when necessary.

Cortical surface reconstructions facilitate the identification of shallow tertiary sulci compared to post-mortem tissue for two main reasons. First, T1 MRI protocols are not ideal for imaging vasculature; thus, the vessels that typically obscure the tertiary sulcal patterning in post-mortem brains are not imaged on standard-resolution T1 MRI scans. In fact, indentations produced by these smaller vessels that obscure the tertiary sulcal patterning are visible in freely available datasets acquired at high field (7T) and micron resolution (100–250 μm; Lüsebrink et al. 2017; Edlow et al. 2019). Thus, the present resolution of our T1s (1 mm isotropic) is sufficient to detect the shallow indentations of tertiary sulci but is not confounded by smaller indentations produced by the vasculature. Second, cortical surface reconstructions are made from the boundary between gray and white matter; unlike the outer surface, this inner surface is not obstructed by blood vessels (Weiner et al. 2018; Weiner 2019).

Defining the presence and prominence of the para-intermediate frontal sulcus: We first manually defined the pimfs within each individual hemisphere in *tksurfer* (Miller et al. 2021b). Manual lines were drawn on the *inflated* cortical surface to define sulci based on the most recent schematics of pimfs and sulcal patterning in LPFC by Petrides (Petrides 2019), as well as by the *pial* and *smoothwm* surfaces of each individual (Miller et al. 2021b). In some cases, the precise start or end point of a sulcus can be difficult to determine on a surface (Borne et al. 2020). Thus, using the *inflated*, *pial*, and *smoothwm* surfaces of each individual to inform our labeling allowed us to form a consensus across surfaces and clearly determine each sulcal boundary. For each hemisphere, the location of the pimfs was confirmed by three trained independent raters (E.H.W., W.I.V., J.K.Y.) and finalized by a neuroanatomist (K.S.W.). Although this project focused on a single sulcus, it took the manual identification of all LPFC sulci (2448 sulcal definitions across all 72 participants) to ensure the most accurate definitions of the pimfs components (for descriptions of these LPFC sulci see: Petrides 2019; Miller et al. 2021a, b; Voorhies et al. 2021; Yao et al. 2022).

Individuals typically have three to five tertiary sulci within the middle frontal gyrus (MFG) of the lateral prefrontal cortex (Miller et al. 2021a, b; Voorhies et al. 2021; Yao et al. 2022). The posterior MFG contains three of these sulci, which are present in all participants: the anterior (pmfs-a), intermediate (pmfs-i), and posterior (pmfs-p) components of the posterior

middle frontal sulcus (pmfs; Miller et al. 2021a, b; Voorhies et al. 2021; Yao et al. 2022). In contrast, the tertiary sulcus within the anterior MFG, the para-intermediate frontal sulcus **(**pimfs), is variably present. A given hemisphere can have zero, one, or two pimfs components (Figure 2.1A; Appendix Figure 2.1.1; Voorhies et al. 2021; Yao et al. 2022).

Drawing from criteria outlined by Petrides (2013, 2019), the dorsal and ventral components of the para-intermediate frontal sulcus (pimfs-d and pimfs-v) were generally defined using the following two-fold criterion: i) the sulci ventrolateral to the horizontal and ventral components of the intermediate frontal sulcus, respectively, and ii) superior and/or anterior to the mid-anterior portion of the inferior frontal sulcus. Note that in this schematic (Petrides, 2019), there is presently an unidentified sulcus located on the MFG between the pmfs-a and pimfs-d, which appears as a posterior branch of the imfs-h (below the star (*) symbol in the schematic). In the present work, we included this unidentified sulcus as the posterior extent of the imfs-h in our definitions of the imfs-h. In our sulcal definitions, our principled criteria always identified the pimfs-d below the imfs-h and the pimfs-v always below the imfs-v. Thus, with this criteria, the posterior component of the imfs-h was not confusable with our definition of the pimfs-d. Future work can seek to clarify the incidence and distinctiveness of this branch from the imfs-h. The location of each indentation was cross-checked using the *inflated*, *pial*, and *smoothwm* surfaces. We first confirmed the accuracy of this criterion by applying it to the individual participants with two identifiable pimfs. Next, we extended this criterion to label the cases in which an individual only had one component. We then compared incidence rates between components and hemispheres with a Chi-Squared and Fischer exact test, respectively.

We quantified the prominence of the pimfs as its surface area (in mm^2). The surface area values for each pimfs label were extracted using the *mris_anatomical_stats* function that is included in FreeSurfer (Fischl and Dale 2000). For those with two pimfs components, the surface area was extracted as a sum of both components together (via a merged label with *mris_mergelabel* function (Dale et al. 1999) and for each individual component separately. We also considered normed values. To normalize pimfs surface area by the surface area of the PFC, we automatically defined the PFC in both hemispheres of each participant with the *mris_annot2label --lobesStrict* function and then extracted surface area values with the *mris_anatomical_stats* function (Fischl and Dale 2000).

Behavioral Analyses

Relating the presence of the pimfs to reasoning performance: To assess whether the presence of the pimfs in each hemisphere is related to reasoning performance, we first conducted an analysis of covariance (ANCOVA) with number of components in the left and right hemispheres (*two or less than two*) as factors, and assessment age as a covariate. There was not a robust relationship between age and the number of pimfs components (*left:* $p = .059$, *right*: $p = .31$; Appendix Figure 2.1.2A). Sex was not associated with either matrix reasoning ($p = .65$) or the number of components (*left*: $p = .27$, *right*: $p = .80$), and including sex as a factor in the ANCOVA did not affect the model results, or result in any effects with sex ($ps > .44$). Therefore, sex was dropped from the final model. Next, to determine if the presence of a specific pimfs component was related to reasoning performance, we ran a second ANCOVA with left and right hemisphere presence of the pimfs-v and pimfs-d (*yes, no*) as factors and age as a covariate. Although age differed as a function of the presence/absence of one of the four pimfs components in one hemisphere (left pimfs-d: $p = .021$; all other $ps > .20$; Appendix Figure 2.1.2B), this collinearity did not, according to the conventional Variance Inflation Factor (VIF) threshold of five (James et

al. 2014), affect the model results (VIF < 2). Further, there were no sex differences in the presence/absence of pimfs components (*p*s > .37), and including sex as a factor in the second ANCOVA did not affect the model results, or result in any effects with sex (*p*s > .75). Therefore, sex was dropped from the final model.

Control behavioral analyses: To ascertain whether the relationship between left pimfs-v presence and cognition is specific to reasoning performance, or generalizable to other general measures of cognitive processing (Kail and Ferrer 2007), we tested this sulcal-behavior relationship with two other widely used measures of cognitive functioning: processing speed and working memory maintenance and manipulation. Specifically, we ran three ANCOVAs with left pimfs-v presence (*yes, no*) as a factor and assessment age as a covariate.

Matching analysis: To confirm that differences in the sample size and age distribution did not drive the effect of left pimfs-v presence on reasoning scores, we conducted variable-ratio matching on age (ratio = 3:1, min = 1, max = 5) with the *MatchIt* package in R (https://cran.r-project.org/web/packages/MatchIt/MatchIt.pdf). The optimal ratio parameter was determined based on the calculation provided by (Ming and Rosenbaum 2000). To accommodate variable-ratio matching, the distance between each member of each group was computed by a logit function:

$$Estimate\ \pi_i = Pr(noPimfs_i = 1|X) = \frac{1}{1+e^{-X_i\beta}}$$

$$Distance(X_i, X_j) = \pi_i - \pi_j$$

where X is participant age in groups without (*i*) and with (*j*) a $pimfs_{lh\_ventral}$. Matches were determined by greedy nearest-neighbor interpolation such that each participant in the smaller group received at least one, and up to five, unique matches from the larger group.

A weighted linear regression was then run in the matched sample with left pimfs-v presence and age as predictors of reasoning to confirm the robustness of our initial finding with the whole sample. We then employed a two-pronged analysis to assess and verify the unique variance explained by left pimfs-v presence, while accounting for age-related effects on reasoning. First, we ran a Chi-Squared test to compare the previously-described weighted-regression model to a weighted-regression model with age only. Second, as described and implemented in prior work (Voorhies et al. 2021; Yao et al. 2022), we fit these two weighted-regression models with leave-one-out cross-validation (looCV), which is suitable for our sample size. Since these are nested models (the largest model contains all elements in the smaller models), the best fit was determined as the model with the lowest cross-validated $RMSE_{cv}$ and the highest R^2_{cv} value.

Relating the size of the pimfs to reasoning performance: To test if the prominence (surface area) of the pimfs was related to reasoning performance, we implemented a multiple linear regression with surface area of pimfs (combined if two were present) in left and right hemispheres as predictors, while controlling for assessment age. Sex was not included, as it was not related to surface area in either hemisphere (*left*: $p = .16$, *right*: $p = .78$), and including sex as a factor in the regression did not affect the model results and did not uncover any effects involving sex (*p*s > .53). Despite there being a significant correlation between age and left pimfs SA ($r = 0.24$, $p = .042$; Appendix Figure 2.1.2 C) and a trending correlation between age and right pimfs SA (r =

.20, p = .087; Appendix Figure 2.1.2C), this collinearity did not affect the model results (VIFs < 5); thus, age and left and right pimfs SA were included in the model. As in the previous analysis, we first compared the pimfs SA model to age alone with a Chi-Squared test, and then further validated with looCV and repeated K-fold (5-fold, 10 repeats) cross-validation methods. Finally, to assess whether prefrontal surface area affected the model, we also ran an exploratory linear regression with normed surface area of the pimfs (by hemispheric PFC surface area) in left and right hemispheres with the covariate assessment age as predictors. See the appendix for an in-depth description of these results.

Statistical tests: All statistical tests were implemented in R v4.1.2 (https://www.r-project.org/). Incidence Chi-Squared tests were carried out with the *chisq.test* function from the R *stats* package. Fisher's exact tests were carried out with the *fisher.test* function from the R *stats* package. All ANCOVAs were implemented using the *lm* and *Anova* functions from the R *stats* and *cars* packages. Effect sizes for the ANCOVA effects are reported with the *generalized* eta-squared (η2G) metric. Linear models were run using the *lm* function from the R *stats* package. Leave-one-out and K-fold cross-validation analyses were carried out with the *train.control* and *train* functions from the R *caret* package. The effect of each pimfs model was compared to the effect of age alone with the *anova* function from the R *stats* package.

2.3.2 Study 2 - Materials and Methods

Participants

Participants came from the NORA dataset (Wendelken et al., 2011; 2016; Ferrer et al., 2013). We considered all participants in the NORA study who had completed one fMRI visit and the matrix reasoning assessment (N = 106). We further screened the dataset for fMRI quality. We required each participant to have three complete runs of data. Participants were further excluded if estimated gross motion (FD) exceeded 0.5mm or if the three runs combined had less than 5 minutes of frames free from motion spikes (FD_{Power} < 0.5 mm or DVARS < 1.5; Behzadi et al., 2007; Buckner et al., 2009). This resulted in a cross-sectional cohort of 49 participants that was a largely overlapping subset of the participants in Study 1. 47 of these participants had frontal and parietal sulci labeled as part of a larger study and were included in these analyses (mean Age (range) = 14.26(7.21 - 18.86) years; mean FD (range) = 0.22 (0.08 - 0.43) mm; mean scan length = 12.67 (5.47-16.20) minutes).

Data Acquisition

MRI acquisition: Brain imaging data were collected on a Siemens 3 T Trio system at the University of California, Berkeley Brain Imaging Center. Participants viewed stimuli back-projected onto a projection screen with a mirror mounted on the head coil and responded using a button box held in their right hand. Stimulus presentation and response acquisition were controlled with Presentation software (Neurobehavioral Systems). Two high-resolution T1-weighted MPRAGE anatomical scans (TR, 2300 ms; TE, 2.98 ms; 1 × 1 × 1 mm voxels) were acquired for cortical morphometric analyses. These two MPRAGE scans were averaged during post-processing to increase the signal-to-noise ratio. Multi-slice echo-planar imaging (EPI) was used to collect functional imaging data (gradient-echo EPI sequence; TR, 2000 ms; TE, 25 ms; 33 axial slices; 2.0 × 1.8 × 3.0 mm voxels; no interslice gap; flip angle, 90°; field of view, 230 mm; 165 volumes per run).

Task design: Participants performed 3 runs of a relational matching task (Wendelken et al., 2011). The experiment was run as a blocked design with three scans of 5 min 25 seconds (165 volumes) each. Each scan consisted of three 90-s blocks, one for each relational condition and two 20-second rest blocks, during which participants fixated on a crosshair, alternated with the task blocks (see Wendelken et al. 2011 for a full task description).

Structural MRI analysis

We generated cortical surface reconstructions from T1 scans using FreeSurfer's recon-all function (Freesurfer v. 7.1.0). All sulcal labels were defined on the surface according to the procedure described in Study 1. For some participants, sulcal labels had been defined on cortical surfaces generated with an earlier version of freesurfer. To ensure consistency, all labels were projected to the freesurfer v.7 surfaces using built-in freesurfer functions. Projected labels were manually checked for accuracy. We considered two prefrontal labels: *pimfs-d and pimfs-v* (Willbrand et al., 2022; Voorhies et al., 2021). In follow-up sulcal-to-sulcal analyses we also considered eight lateral parietal labels that were consistently identifiable in every participant (Fig 2.2.1C).

fMRI preprocessing

Results included in this manuscript come from preprocessing performed using FMRIPREP version 21.0.1 (Esteban et al., 2018), a Nipype (Gorgolewski et al., 2011; Gorgolewski et al., 2017) based tool. Each T1w (T1-weighted) volume was corrected for INU (intensity non-uniformity) using N4BiasFieldCorrection v2.1.0 (Tustison et al., 2010) and skull-stripped using antsBrainExtraction.sh v2.1.0 (using the OASIS template). Brain surfaces were reconstructed using recon-all from FreeSurfer v7.0.1 (Dale et al., 1999), and the brain mask was refined to reconcile ANTs-derived and FreeSurfer-derived segmentations of the cortical gray-matter of Mindboggle (Klein et al., 2017). Spatial normalization to the ICBM 152 Nonlinear Asymmetrical template version 2009c (Fonov et al., 2009) was performed through nonlinear registration with the antsRegistration tool of ANTs v2.1.0 (Avants et al., 2008), using brain-extracted versions of both T1w volume and template. Brain tissue segmentation of cerebrospinal fluid (CSF), white-matter (WM) and gray-matter (GM) was performed on the brain-extracted T1w using fast (Zhang et al., 2001; FSL v5.0.9, RRID:SCR_002823).

After excluding the initial three volumes, functional data were slice time corrected using 3dTshift from AFNI v16.2.07 (Cox et al., 1996) and motion corrected using mcflirt (FSL v5.0.9; Jenkinson et al., 2002). This was followed by co-registration to the corresponding T1w using boundary-based registration (Greve et al., 2009) with six degrees of freedom, using bbregister (FreeSurfer v6.0.1). Motion correcting transformations, BOLD-to-T1w transformation, and T1w-to-template (MNI) warp were concatenated and applied in a single step using antsApplyTransforms (ANTs v2.1.0) using Lanczos interpolation. Results were then sampled to the native mid-thickness surface, the largest spikes truncated, data bandpass filtered (AFNI 3DBandpass, 0.008–0.1 Hz), and linear trends and known (filtered) confounds removed from the timeseries by regression (Nilearn's image.clean_img). Nuisance regressors included the first 5 principal components of mean white matter and CSF signals (Behzadi et al., 2007) and 24 motion parameters (Friston et al., 1996). Given the small effects of task-induced, activation-related, hemodynamic responses on global network organization in the dataset, we focused our analyses on network coupling across the full scan (ie., both task and rest blocks as in

previous work: Buckner et al., 2009; Gratton et al., 2018; Hermosillo et al., 2022; Sun et al., 2022).

Functional connectivity analyses

Sulcal functional connectivity: Each manually defined label was associated with the mean timeseries of the vertices assigned to the label on the mid-grey matter surfaces (full native resolution). Functional connectivity between sulci was measured by Pearson correlation of the timeseries between each label pair, and Fischer's z-transformed for further analysis. Motion censoring was applied to exclude frames associated with large motion spikes (FD < 0.5 or DVARS < 1.5).

Group-level analyses (sulcal-to-whole brain): A General Linear Model (GLM) was used to assess the effects of pimfs component and reasoning skill on functional connectivity. To test the interaction with reasoning skill, we used a median split to classify participants as "higher skill" or "lower skill" based on their matrix reasoning score. The model included contrasts for the main effect of pimfs component (dorsal vs. ventral) and for the component (dorsal vs. ventral) x reasoning (higher vs. lower) interaction. Mean framewise displacement was included as an additional covariate. To perform this analysis, individual sulcal-to-whole brain connectivity maps were projected to standard surface template (fsaverage) space with 3mm surface smoothing on the target surface. Statistical inference was performed with PALM software (Wrinkler et al., 2014). Statistical significance was assessed using 10,000 permutations and the resulting t-stat maps were thresholded for significance at $p<0.05$ (t = 1.96). Cluster correction was performed using cluster mass thresholding.

Sulcal-to-sulcal analyses: To assess the relationship between pimfs and lateral parietal sulci, we calculated the Pearson correlation between each pimfs component and each lateral parietal label (Figure 2.2.1C) in the left hemisphere, as the presence and prominence of pimfs-v was related to reasoning performance in the left, but not right, hemisphere. All connectivity values were computed on the native cortical surface and residualized for mean framewise displacement. To reduce effects of in-scanner head motion, connection strengths were residualized with respect to subject-level gross motion (mean FD).
We then conducted a linear mixed effects (LME) model to test the effect of source label (pimfs component) and target label (lateral parietal labels) on residualized connectivity. Residualizing connectivity values first allowed us to include age, which is heavily correlated with mean FD, as an additional covariate in the model. An interaction term was included for each predictor and random intercepts were modeled for each participant. The model was fit with the nlme package in R (Pinheiro & Bates, 2000). Pairwise post-hoc tests were conducted with the lsmeans package and used a Tukey HSD correction for multiple comparisons.

2.4.1 Study 1 - Results

Sulci were manually identified as component(s) of the pimfs in each hemisphere according to previous work (Figure 2.1A; Appendix Figure 2.1; Amiez and Petrides 2007; Petrides 2019; Voorhies et al. 2021). We confirmed our prior observation that the pimfs was highly variable (Figure 2.1B): in a given hemisphere, there could be zero, (*left* = 2.78% of participants; *right* = 8.33%), one (*left:* 22.22%; *right:* 25%), or two components (*left*: 75%; *right:* 66.67%; *left:* $X^2 = 60.333$, df = 2, $p < .001$; *right:* $X^2 = 39$, df = 2, $p < .001$; no hemispheric asymmetry: $p = .30$). Based on published criteria (Petrides 2013), we further defined pimfs components as either dorsal (pimfs-d) or ventral (pimfs-v) and assessed the prevalence of each component (Figure 2.1.1B). Numerically, a single dorsal component was more frequent than a single ventral one, but statistically, these profiles were equally frequent ($X^2 \geq .89$, $p > .30$ for both hemispheres).

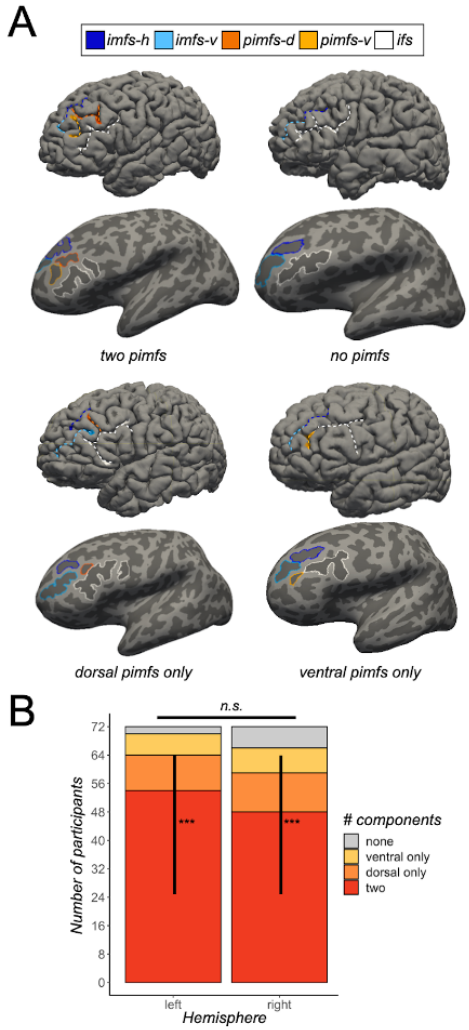

Figure 2.1.1. The para-intermediate frontal sulcus: A tertiary sulcus in lateral prefrontal cortex with pronounced individual differences. A. Pial (top) and inflated (bottom) left hemispheres (sulci: dark gray; gyri: light gray; Cortical surfaces are not to scale) depicting the four types of the para-intermediate frontal sulcus (pimfs): i) both components present, ii) neither present, iii) dorsal component present, iv) ventral component present. The prominent sulci bounding the pimfs are also shown: the horizontal (imfs-h) and ventral (imfs-v) intermediate frontal sulci and inferior frontal sulcus (ifs). These four sulci are colored according to the legend. **B**. Stacked bar plot

depicting the incidence of the pimfs components in both hemispheres across the sample (N = 72 participants). The incidence of the pimfs is highly variable. In each hemisphere, it is more common for participants to have two components than a single component or no component (*** *p*s < .0001); the distribution of incidence does not differ between hemispheres (p = .30). When only one component was present in a given hemisphere, it was equally likely to be a dorsal or ventral component (*p*s > .30).

An analysis of covariance (ANCOVA; including age as a covariate) testing the effect of pimfs incidence rates on reasoning (measured with the WISC-IV matrix reasoning task described in Materials and Methods) revealed that the presence of two pimfs components in the left hemisphere was associated with better reasoning performance relative to one or none ($F(1,67) = 4.18$, $p = .045$, $\eta 2G = 0.059$; Figure 2.2A, left). This result was not obtained for the right hemisphere ($F(1,67) = 2.63$, $p = .11$, $\eta 2G = 0.038$). An ANCOVA testing whether the incidence of a dorsal and/or ventral pimfs component, specifically, was linked to reasoning revealed that the presence of the left hemisphere pimfs-v was associated with higher reasoning scores, controlling for age ($F(1,66) = 5.10$, $p = .027$, $\eta 2G = 0.072$; Appendix Figure 2.1.3). Follow-up analyses with additional behavioral measures revealed that the presence of the left pimfs-v was not related to processing speed or phonological working memory (all *p*s > .50; see Materials and Methods for details on the tasks), suggesting some degree of specificity in this brain-behavior relation.

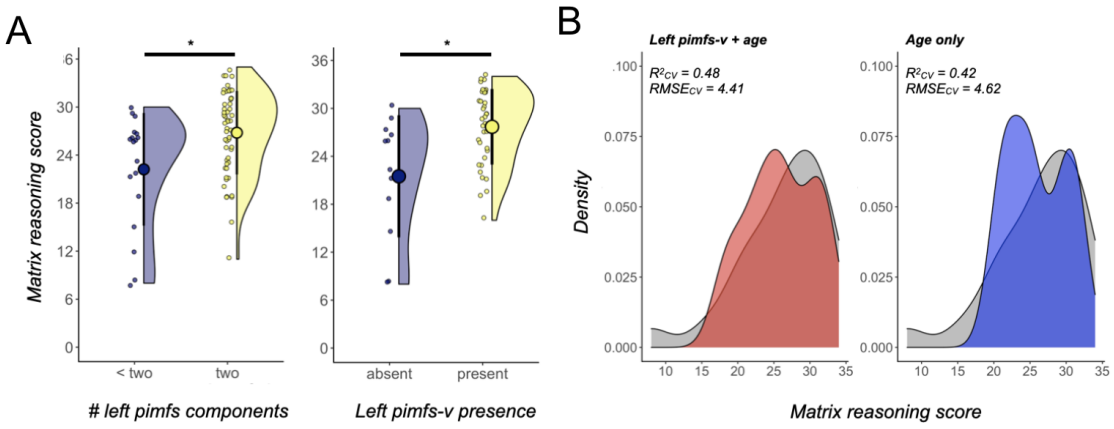

Figure 2.1.2. ***The presence/absence of the para-intermediate frontal sulcus is related to reasoning.*** **A**. Raincloud plots (Allen et al. 2021) depicting reasoning score as a function of (left) the number of para-intermediate frontal sulcus (pimfs) components and (right) the presence of the ventral pimfs component in the left hemisphere only. The large dots and error bars represent the mean±std reasoning score, and the violin plots show the kernel density estimate. The smaller dots indicate individual participants. *Left:* Across the whole sample (N = 72), those with two pimfs components (N = 54) had better reasoning scores than those with only one component (N = 18), controlling for age (*p = .045). *Right*: Matching subsamples for age and sample size (total N = 48), participants with the left pimfs-v component had better reasoning performance than those without, also controlling for age (*p = .012); this group difference was also observed across the full sample (Appendix Figure 2.1.3). **B**. Density plots of cross-validated model fit, using leave-one-out cross-validation. *Left:* The predicted scores from the pimfs-v sulcal-behavioral model (visualized in 2A, right; left pimfs-v presence + age) are shown in red and overlaid on the distribution of measured Matrix reasoning scores (gray). *Right:* The same format as the left, but for the distribution of predicted scores for the cross-validated nested model with age only (blue). Cross-validated model fit (R^2_{CV}) and root-mean-squared error ($RMSE_{CV}$) are reported for each model. The model including left pimfs-v presence as a factor performs better than the nested model with age alone.

Due to differences in the sample size and age distribution of the two groups ($median(sd)_{present}$ = 11.78(3.52), $median(sd)_{absent}$ = 8.81(4.22)), we sought to further confirm the effect of presence/absence of the left pimfs-v on reasoning performance. To this end, we employed variable-ratio matching (Materials and Methods) to create an age-matched sample that consisted of the original 12 participants without a left pimfs-v and the 36 age-matched participants with a left pimfs-v (mean age = 10.66, eCDF). A weighted regression in the matched sample with left pimfs-v presence and age as predictors of reasoning revealed that the presence of the left pimfs-v remained significant (ß = 3.69, t = 2.61, p = .012; Figure 2.1,2A, right). Critically, this model explained significantly more variance than a model with age alone in the same sample (pimfs: R^2_{adj} = 0.51, p < .001; age: R^2_{adj} = 0.45, p < .001; model comparison: p = .012). We also employed leave-one-out cross-validation to further evaluate the fit of the sulcal-behavioral model relative to the alternative model with age alone (Materials and Methods). The model including left pimfs-v presence as a factor showed increased prediction accuracy and decreased $RMSE_{CV}$ (R^2_{CV} = 0.48, $RMSE_{CV}$ = 4.41; Figure 2.1.2B, left) compared to a model with age only (R^2_{CV} = 0.42, $RMSE_{CV}$ = 4.62; Figure 2.1.2B, right), indicating that the presence or absence of the left pimfs-v explained unique variance in reasoning scores above and beyond age.

Finally, in line with previous neuroanatomical analyses (e.g. see Cachia et al. 2018), we examined a continuous metric as a complement to the discrete measure of the presence or absence of a sulcus: total pimfs surface area (mm^2). Left pimfs surface area was correlated with reasoning scores (ß = 0.01, t = 2.35, p = .022; Appendix Figure 2.1.4). However, total surface area varied as a function of number of components; therefore, we sought to pit the discrete and continuous measures against one another to see whether one provided greater explanatory power. In contrast to the discrete model, the model with pimfs surface area explained reasoning scores only marginally better than age alone (p = .071; see Appendix for additional information). Thus, the presence or absence of pimfs-v was more closely linked to reasoning than was total pimfs surface area.

2.4.2 Study 2 - Results

As a complement to the behavioral analyses, we compared the whole-brain functional FC of the pimfs components (dorsal, ventral) during a reasoning task. Of the 47 included participants, 33 had both pimfs components in the right hemisphere, 35 had both components in the left hemisphere, and 24 had both components in both hemispheres. Given our reduced sample size, we lacked sufficient power to accurately assess how FC varies between participants as i) a function of the number of components (1 vs. 2) or ii) the presence/absence of the ventral component. However, we were able to leverage the participants with both components to explore whether pimfs components showed separable patterns of connectivity within subjects and whether these connectivity patterns varied with reasoning skill. We then conducted a follow-up analysis to examine which lateral parietal sulci showed the strongest FC with each component.

Dissociable patterns of pimfs connectivity vary with reasoning skill.

To examine how FC varied for each pimfs component, we considered participants with both pimfs components in both hemispheres (N = 24). The same pattern of results held when we broadened the analysis to include all participants with both components in a given hemisphere (RH: N = 33, LH: N = 35; Appendix). We performed a seed-to-whole-brain connectivity analysis in each hemisphere to generate whole-brain connectivity maps for the pimfs-v and pimfs-d in

every participant in individual participant space (Methods; Appendix 2.2.1). We then used a GLM to assess how connectivity varied by component (pimfs-v vs. pimfs-d) and reasoning skill (higher vs. lower).

Contrast maps suggested differences between pimfs-v and pimfs-d FC, although they did not survive cluster correction. At an uncorrected threshold of $p<0.05$ (two-tailed), the left pimfs-v component showed notably stronger connectivity with the left lateral parietal cortex than did pimfs-d (Figure 2.2.1A). The interaction contrast also showed trending differences between the two components that varied as a function of reasoning skill. In particular, stronger connectivity between the left pimfs-v component and left lateral parietal cortex was present in participants with higher reasoning skill but not those with lower reasoning skills (Figure 2.2.1B; $p<0.05$ uncorrected).

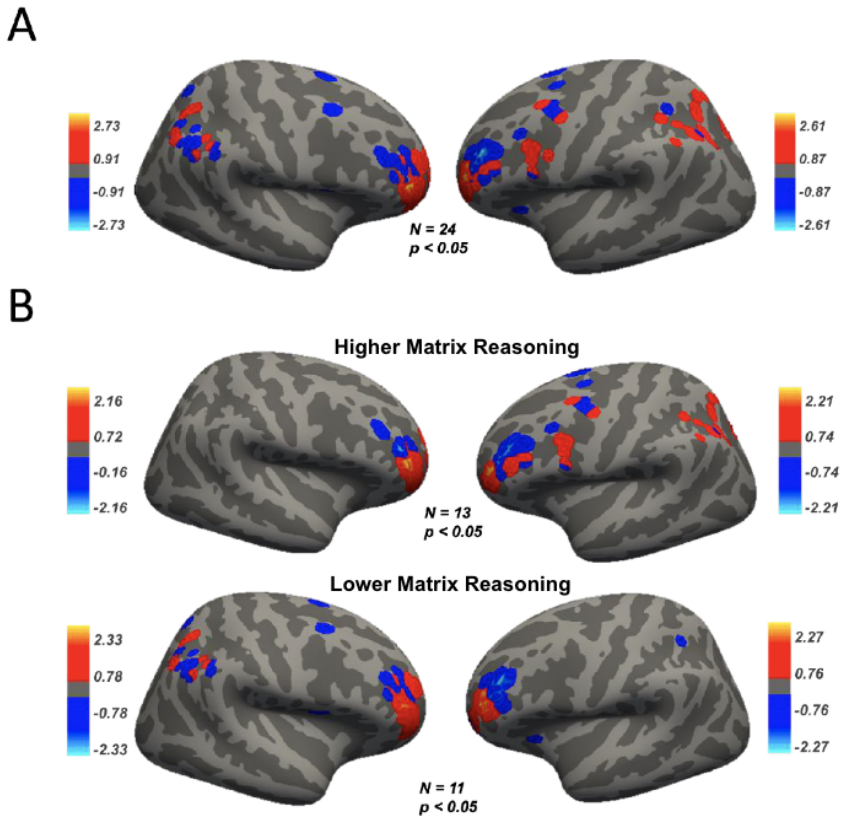

Figure 2.2.1 The *pimfs components were associated with spatially separable patterns of functional connectivity with lateral parietal cortex which varied with reasoning skill.* A. A group-level analysis compared the difference in functional connectivity between pimfs components. Reasoning skill (median split) was included as an interaction term. A t-statistic map shows differences in connectivity for the ventral (*red*) and dorsal (*blue*) components ($p>0.05$, uncorrected). Consistent with behavioral results, the left ventral pimfs component shows greater functional connectivity with lateral parietal cortex compared to the dorsal component. Results did not, however, survive cluster correction. **B.** A significant interaction between pimfs component and reasoning skill revealed separable patterns of connectivity for those with lower and higher reasoning skills. t-stat maps show patterns of functional connectivity for the ventral (*red*) and dorsal (*blue*) components in higher (*top*) and lower (*bottom*) reasoning groups. Those with higher matrix reasoning show increased left hemisphere connectivity between the pimf-v and the lateral parietal cortex.

Pimfs components show the strongest connectivity with a subset of inferior lateral parietal sulci.

As a follow-up analysis, we asked which of the left hemisphere lateral parietal sulci showed the strongest connectivity with the left hemisphere pimfs components. Based on the behavioral findings from Study 1 that implicated the left, but not the right, pimfs-v in reasoning and the whole-brain results showing notable differences between pimfs component connectivity in the left hemisphere, we restricted our follow-up analyses to the left hemisphere. To assess sulcal-to-sulcal connectivity we performed a seed-to-seed connectivity analysis on the cortical surface in native subject space (see Methods). As in the PFC, we only considered the lateral parietal sulci that could be consistently identified in every participant. We used a GLM to compare how connectivity varied as a function of source sulcus (left pimfs-v vs. left pimfs-d), target sulcus (left lateral parietal sulci), and Age. All functional connectivity values were residualized for head motion. There were no significant differences between the pimfs-v and pimfs-d ($p > 0.05$). However, there was a significant main effect of lateral parietal sulcus ($F(7, 300) = 7.99$, $p < .0001$). Post-hoc analyses revealed that the left intraparietal sulcus was strongly coupled with both pimfs components (Figure 2.2.2A). When collapsing across components, post-hoc analyses further revealed that two smaller surrounding sulci, the pips and aipsJ, were more strongly connected to the pimfs than were neighboring parietal sulci (Figure 2.2.2). There was also a significant interaction between parietal sulci and age ($F, (7,300) = 3.67$, $p < 0.001$), reflecting stronger pimfs-parietal connectivity in older participants. When residualized for head motion, pimfs connectivity with IPS and pips – but not with surrounding parietal sulci – increased with age (Figure 2.2.2B).

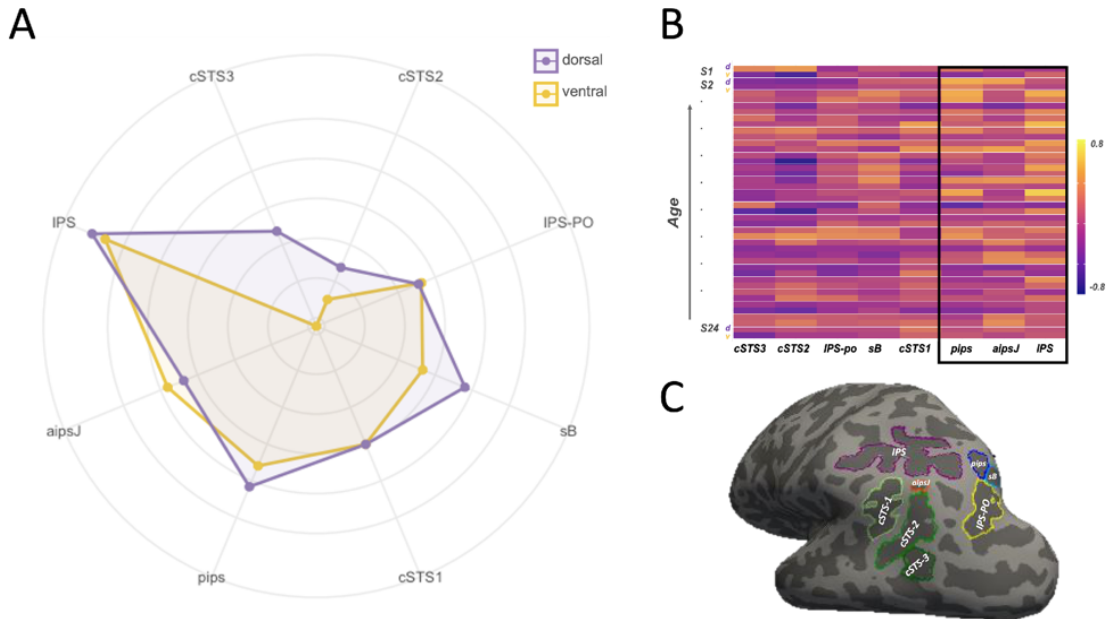

Figure 2.2.2 ***pimfs components are most strongly connected to a subset of inferior lateral parietal sulci.*** **A.** A group-level polar plot showing mean connectivity between the left hemisphere pimfs-d (*purple*) and pimfs-v (*yellow*) and left hemisphere lateral parietal sulci. Follow-up analyses investigating left hemisphere sulcal-to-sulcal connectivity for both components with the lateral parietal sulci revealed a main effect of lateral parietal sulci. Across components, the strongest connectivity was with the IPS. The pips and aipsJ also showed significantly stronger connectivity with left hemisphere pimfs components than did the neighboring cSTS and IPS-PO. **B.** A heat map showing mean connectivity between the pimfs components and left hemisphere lateral parietal sulci for each participant. Participants are ordered from oldest to youngest. All connectivity values are residualized by mean frame-wise displacement. **C.** Lateral parietal labels visualized on an example participant.

2.5 Discussion

In Study 1, we showed that the presence of the left pimfs-v was associated with better reasoning performance in a developmental cohort (6-18 years old). This finding contributes to mounting evidence that the presence or absence of sulci relates to complex cognitive skills (Fornito et al. 2004, 2006; Whittle et al. 2009; Huster et al. 2009, 2011; Buda et al. 2011; Cachia et al. 2014; Borst et al. 2014; Amiez et al. 2018). Crucially, this relationship was not observed for processing speed or working memory, which are theorized to support this high-level cognitive skill (Fry and Hale 2000; Ferrer et al. 2013). Relatedly, we have recently found that the depth of numerous PFC sulci in the left hemisphere – but not the pimfs – is related to working memory manipulation (Yao et al. 2022). Thus, this brain-behavior relationship does not generalize to another challenging cognitive task. It should also be noted that this result was observed across a large developmental age range (6-18 years old). Future work should seek to determine whether this effect holds longitudinally and into adulthood (Huster et al. 2009, 2011; Borst et al. 2014), or if it is specific to the time period when higher-level cognitive skills are being acquired.

Study 2 builds on these results by suggesting that these two sulcal components may be not only behaviorally, but also functionally, dissociable and potentially exhibit distinct patterns of functional connectivity. Furthermore, we show that these patterns vary with reasoning skill.

While these results are preliminary they are in line with previous work. The pimfs-v appears to co-localize with a functionally defined region named rostrolateral PFC, a region that has been implicated in reasoning (e.g. Christoff et al. 2001; Vendetti and Bunge 2014; Urbanski et al. 2016; Hartogsveld et al. 2018; Assem et al. 2020). As children develop, there appears to be specialization of the fronto-parietal network that facilitates reasoning performance. According to previous studies, younger children showed increased bilateral activation in the DLPFC but no significant changes in parietal activation during performance of a relational reasoning task. In contrast, PFC activation in older children was more localized to the left rostrolateral prefrontal cortex and also showed increased left hemisphere LPC activity during a reasoning task (Wendelken et al., 2011). Our findings are consistent with these observations and we extend these findings by providing precise anatomical localization at the individual participant level.

Anatomically, cortical function preferentially related to reasoning has previously been reported to lie along the borders of Brodmann Areas (BA) 10/46 and/or 10/47, although until now, precise localization has been impeded by normalization and group-averaging of fMRI activation, as well as the emergence of newer anatomical parcellation schemes that subdivide anterior PFC in other ways (e.g. Bludau et al. 2014). Given that the pimfs shows pronounced individual variability, is related to reasoning, and is tentatively located around the border of BA 10/46 (Appendix Figure 2.1.5), the presence or absence of this indentation could be a novel factor that helps to explain individual variability in the site of functional and/or cytoarchitectural boundaries.

The sulcal metrics examined here showed significant effects for left pimfs on reasoning skills, with trend-level effects in the right hemisphere. Conversely, we previously showed that sulcal depth of right but not left pimfs (averaged across dorsal and ventral components) was related to reasoning (Voorhies et al. 2021). Both hemispheres have been implicated in reasoning, although there is evidence for functional dissociations between them (Bunge et al. 2009; Vendetti et al. 2015; Goel 2019). The reason for this hemispheric double-dissociation is not yet clear; perhaps it relates to differential developmental trajectories of, and dynamic relations between, the two hemispheres (Toga and Thompson 2003), which can be further explored in future research. Another possibility is that the right hemisphere may be related to visuospatial skills,

which contribute to matrix reasoning performance, whereas the left hemisphere may be more involved in relational integration (REFS).

Mechanistically, differences in sulcal patterning are hypothesized to be related to the underlying white matter connectivity, and broadly speaking, cortical folding patterns are generally optimized with regard to efficiency of communication between brain regions (Van Essen 1997, 2020; White et al. 2010; Zilles et al. 2013). In line with this, previous research has shown that increased fronto-parietal structural connectivity is associated with increased functional connectivity during a reasoning task and improved behavioral reasoning skills (Wendelken et al., 2017). Although our sample size prevented us from effectively characterizing variability in functional connectivity for those with and without a pimfs component, our findings suggest that strong left hemisphere pimfs-v-parietal functional connectivity may support reasoning. This, combined with the behavioral findings from Study 1, suggests that the presence and absence of the pimf-v may be associated with underlying structural and/or functional connectivity differences.

Additionally or alternatively, relationships among tertiary sulci, brain function, and behavior could relate to alterations of local cytoarchitecture (Amiez et al. 2021). Individual differences in the presence and prominence of tertiary sulci in association cortices may reflect variability in the rates of growth of adjacent cytoarchitectural regions (e.g. Fernández et al. 2016). Thus, the presence or absence of the pimfs could also reflect differences in local architecture, which could in turn represent differences in local computations that support reasoning — a multiscale, mechanistic relationship that can be explored in future research.

In conclusion, we have uncovered that the presence of a specific sulcus in LPFC may be indicative of functional or structural variations that contribute to the development of reasoning. While this offers valuable insight into structure-function-behavior relationships, it is important to highlight that these findings do not imply a deterministic relationship. Reasoning involves a large network of regions, and multiple structural variations in all of these regions could contribute to reasoning skill. Other neuroanatomical features in LPFC and elsewhere have also been linked to reasoning during development, including sulcal depth (Voorhies et al. 2021), white matter microstructure (Wendelken et al. 2017), and, in some samples, cortical thickness (e.g., Leonard et al. 2019). Thus, a goal of future research is to work toward developing a comprehensive, unifying model that integrates these and any other neuroanatomical features, yet to be identified, that contribute to the development of reasoning. Finally, it is important to underscore that both reasoning and brain circuitry show experience-dependent plasticity across development (e.g. Mackey et al., 2013). Nonetheless, the present findings underscore the behavioral and functional relevance of cortical folding patterns, providing novel insights into one particular LPFC sulcus that exhibits prominent individual differences that are related to individual differences in cognition and functional network properties.

2.6 References

Allen M, Poggiali D, Whitaker K, et al (2021) Raincloud plots: a multi-platform tool for robust data visualization. Wellcome Open Res 4:63

Amiez C, Neveu R, Warrot D, et al (2013) The location of feedback-related activity in the midcingulate cortex is predicted by local morphology. J Neurosci 33:2217–2228

Amiez C, Petrides M (2007) Selective involvement of the mid-dorsolateral prefrontal cortex in the coding of the serial order of visual stimuli in working memory. Proc Natl Acad Sci U S A 104:13786–13791

Amiez C, Petrides M (2014) Neuroimaging evidence of the anatomo-functional organization of the human cingulate motor areas. Cereb Cortex 24:563–578

Amiez C, Sallet J, Hopkins WD, et al (2019) Sulcal organization in the medial frontal cortex provides insights into primate brain evolution. Nat Commun 10:1–14

Amiez C, Sallet J, Novek J, et al (2021) Chimpanzee histology and functional brain imaging show that the paracingulate sulcus is not human-specific. Commun Biol 4:54

Amiez C, Wilson CRE, Procyk E (2018) Variations of cingulate sulcal organization and link with cognitive performance. Sci Rep 8:1–13

Assem M, Glasser MF, Van Essen DC, Duncan J (2020) A Domain-General Cognitive Core Defined in Multimodally Parcellated Human Cortex. Cereb Cortex 30:4361–4380

Bludau S, Eickhoff SB, Mohlberg H, et al (2014) Cytoarchitecture, probability maps and functions of the human frontal pole. Neuroimage 93 Pt 2:260–275

Borne L, Rivière D, Mancip M, Mangin J-F (2020) Automatic labeling of cortical sulci using patch- or CNN-based segmentation techniques combined with bottom-up geometric constraints. Med Image Anal 62:101651

Borst G, Cachia A, Vidal J, et al (2014) Folding of the anterior cingulate cortex partially explains inhibitory control during childhood: a longitudinal study. Dev Cogn Neurosci 9:126–135

Brown TT, Kuperman JM, Chung Y, et al (2012) Neuroanatomical assessment of biological maturity. Curr Biol 22:1693–1698

Buda M, Fornito A, Bergström ZM, Simons JS (2011) A specific brain structural basis for individual differences in reality monitoring. J Neurosci 31:14308–14313

Bunge SA, Helskog EH, Wendelken C (2009) Left, but not right, rostrolateral prefrontal cortex meets a stringent test of the relational integration hypothesis. Neuroimage 46:338–342

Cachia A, Borst G, Vidal J, et al (2014) The shape of the ACC contributes to cognitive control efficiency in preschoolers. J Cogn Neurosci 26:96–106

Cachia A, Roell M, Mangin J-F, et al (2018) How interindividual differences in brain anatomy shape reading accuracy. Brain Struct Funct 223:701–712

Chiavaras MM, Petrides M (2000) Orbitofrontal sulci of the human and macaque monkey brain. J Comp Neurol 422:35–54

Christoff K, Prabhakaran V, Dorfman J, et al (2001) Rostrolateral prefrontal cortex involvement in relational integration during reasoning. Neuroimage 14:1136–1149

Dale AM, Fischl B, Sereno MI (1999) Cortical surface-based analysis. I. Segmentation and surface reconstruction. Neuroimage 9:179–194

Edlow BL, Mareyam A, Horn A, et al (2019) 7 Tesla MRI of the ex vivo human brain at 100 micron resolution. Sci Data 6:244

Fernández V, Llinares-Benadero C, Borrell V (2016) Cerebral cortex expansion and folding: what have we learned? EMBO J 35:1021–1044

Ferrer E, Whitaker KJ, Steele JS, et al (2013) White matter maturation supports the development of reasoning ability through its influence on processing speed. Dev Sci 16:941–951

Fischl B, Dale AM (2000) Measuring the thickness of the human cerebral cortex from magnetic resonance images. Proc Natl Acad Sci U S A 97:11050–11055

Fornito A, Yücel M, Wood S, et al (2004) Individual differences in anterior cingulate/paracingulate morphology are related to executive functions in healthy males. Cereb Cortex 14:424–431

Fornito A, Yücel M, Wood SJ, et al (2006) Morphology of the paracingulate sulcus and executive cognition in schizophrenia. Schizophr Res 88:192–197

Fry AF, Hale S (2000) Relationships among processing speed, working memory, and fluid intelligence in children. Biol Psychol 54:1–34

Goel V (2019) Hemispheric asymmetry in the prefrontal cortex for complex cognition. Handb Clin Neurol 163:179–196

Harper L, Lindberg O, Bocchetta M, et al (2022) Prenatal Gyrification Pattern Affects Age at Onset in Frontotemporal Dementia. Cereb Cortex. https://doi.org/10.1093/cercor/bhab457

Hartogsveld B, Bramson B, Vijayakumar S, et al (2018) Lateral frontal pole and relational processing: Activation patterns and connectivity profile. Behav Brain Res 355:2–11

Huster RJ, Westerhausen R, Herrmann CS (2011) Sex differences in cognitive control are associated with midcingulate and callosal morphology. Brain Struct Funct 215:225–235

Huster RJ, Wolters C, Wollbrink A, et al (2009) Effects of anterior cingulate fissurization on cognitive control during stroop interference. Hum Brain Mapp 30:1279–1289

James G, Witten D, Hastie T, Tibshirani R (2014) An Introduction to Statistical Learning: with Applications in R. Springer New York

Kail RV, Ferrer E (2007) Processing speed in childhood and adolescence: longitudinal models for examining developmental change. Child Dev 78:1760–1770

Leonard JA, Romeo RR, Park AT, et al (2019) Associations between cortical thickness and reasoning differ by socioeconomic status in development. Dev Cogn Neurosci 36:100641

Le Provost J-B, Bartres-Faz D, Paillere-Martinot M-L, et al (2003) Paracingulate sulcus morphology in men with early-onset schizophrenia. Br J Psychiatry 182:228–232

Lopez-Persem A, Verhagen L, Amiez C, et al (2019) The Human Ventromedial Prefrontal Cortex: Sulcal Morphology and Its Influence on Functional Organization. J Neurosci 39:3627–3639

Lüsebrink F, Sciarra A, Mattern H, et al (2017) T1-weighted in vivo human whole brain MRI dataset with an ultrahigh isotropic resolution of 250 μm. Sci Data 4:170032

Mackey AP, Miller Singley AT, Bunge SA (2013) Intensive reasoning training alters patterns of brain connectivity at rest. J Neurosci 33:4796–4803

McBride-Chang C, Kail RV (2002) Cross-Cultural Similarities in the Predictors of Reading Acquisition. Child Development 73:1392–1407

Miller JA, D'Esposito M, Weiner KS (2021a) Using Tertiary Sulci to Map the "Cognitive Globe" of Prefrontal Cortex. J Cogn Neurosci 1–18

Miller JA, Voorhies WI, Lurie DJ, et al (2021b) Overlooked Tertiary Sulci Serve as a Meso-Scale Link between Microstructural and Functional Properties of Human Lateral Prefrontal Cortex. J Neurosci 41:2229–2244

Ming K, Rosenbaum PR (2000) Substantial gains in bias reduction from matching with a variable number of controls. Biometrics 56:118–124

Nakamura M, Nestor PG, Shenton ME (2020) Orbitofrontal Sulcogyral Pattern as a Transdiagnostic Trait Marker of Early Neurodevelopment in the Social Brain. Clin EEG Neurosci 51:275–284

Petrides M (2019) Atlas of the Morphology of the Human Cerebral Cortex on the Average MNI Brain. Academic Press

Petrides M (2013) Neuroanatomy of Language Regions of the Human Brain. Academic Press

Shim G, Jung WH, Choi J-S, et al (2009) Reduced cortical folding of the anterior cingulate cortex in obsessive-compulsive disorder. J Psychiatry Neurosci 34:443–449

Toga AW, Thompson PM (2003) Mapping brain asymmetry. Nat Rev Neurosci 4:37–48

Urbanski M, Bréchemier M-L, Garcin B, et al (2016) Reasoning by analogy requires the left frontal pole: lesion-deficit mapping and clinical implications. Brain 139:1783–1799

Van Essen DC (2020) A 2020 view of tension-based cortical morphogenesis. Proc Natl Acad Sci U S A. https://doi.org/10.1073/pnas.2016830117

Van Essen DC (1997) A tension-based theory of morphogenesis and compact wiring in the central nervous system. Nature 385:313–318

Vendetti MS, Bunge SA (2014) Evolutionary and developmental changes in the lateral frontoparietal network: a little goes a long way for higher-level cognition. Neuron 84:906–917

Vendetti MS, Johnson EL, Lemos CJ, Bunge SA (2015) Hemispheric differences in relational reasoning: novel insights based on an old technique. Front Hum Neurosci 9:55

Voorhies WI, Miller JA, Yao JK, et al (2021) Cognitive insights from tertiary sulci in prefrontal cortex. Nat Commun 12:5122

Wandell BA, Chial S, Backus BT (2000) Visualization and measurement of the cortical surface. J Cogn Neurosci 12:739–752

Wechsler D (1999) Wechsler abbreviated scale of intelligence--

Wechsler D (1949) Wechsler Intelligence Scale for Children; manual. 113:

Weiner KS (2019) The Mid-Fusiform Sulcus (sulcus sagittalis gyri fusiformis). Anat Rec 302:1491–1503

Weiner KS, Natu VS, Grill-Spector K (2018) On object selectivity and the anatomy of the human fusiform gyrus. Neuroimage 173:604–609

Wendelken C, Ferrer E, Ghetti S, et al (2017) Frontoparietal Structural Connectivity in Childhood Predicts Development of Functional Connectivity and Reasoning Ability: A Large-Scale Longitudinal Investigation. J Neurosci 37:8549–8558

Wendelken C, Ferrer E, Whitaker KJ, Bunge SA (2016) Fronto-Parietal Network Reconfiguration Supports the Development of Reasoning Ability. Cereb Cortex 26:2178–2190

Wendelken C, O'Hare ED, Whitaker KJ, et al (2011) Increased functional selectivity over development in rostrolateral prefrontal cortex. J Neurosci 31:17260–17268

White T, Su S, Schmidt M, et al (2010) The development of gyrification in childhood and adolescence. Brain Cogn 72:36–45

Whittle S, Allen NB, Fornito A, et al (2009) Variations in cortical folding patterns are related to individual differences in temperament. Psychiatry Research: Neuroimaging 172:68–74

Willbrand EH, Parker BJ, Voorhies WI, et al (2021) A new tripartite landmark in posterior cingulate cortex. bioRxiv 2021.10.30.466521

Woodcock RW, McGrew KS, Mather N, Others (2001) Woodcock-Johnson III tests of achievement

Yao JK, Voorhies WI, Miller JA, et al (2022) Sulcal depth in prefrontal cortex: a novel predictor of working memory performance. Cereb Cortex bhac173

Yücel M, Stuart GW, Maruff P, et al (2002) Paracingulate morphologic differences in males with established schizophrenia: a magnetic resonance imaging morphometric study. Biol Psychiatry 52:15–23

Yücel M, Wood SJ, Phillips LJ, et al (2003) Morphology of the anterior cingulate cortex in young men at ultra-high risk of developing a psychotic illness. Br J Psychiatry 182:518–524

Zilles K, Palomero-Gallagher N, Amunts K (2013) Development of cortical folding during evolution and ontogeny. Trends Neurosci 36:275–284

Esteban O, Markiewicz CJ, Blair RW, Moodie CA, Isik AI, Erramuzpe A, Kent JD, Goncalves M, DuPre E, Snyder M, Oya H, Ghosh SS, Wright J, Durnez J, Poldrack RA, Gorgolewski KJ. fMRIPrep: a robust preprocessing pipeline for functional MRI. Nat Meth. 2018; doi:10.1038/s41592-018-0235-4

fMRIPrep Available from: 10.5281/zenodo.852659.

Gorgolewski K, Burns CD, Madison C, Clark D, Halchenko YO, Waskom ML, Ghosh SS. Nipype: a flexible, lightweight and extensible neuroimaging data processing framework in python. Front Neuroinform. 2011 Aug 22;5(August):13. doi:10.3389/fninf.2011.00013.

Gorgolewski KJ, Esteban O, Ellis DG, Notter MP, Ziegler E, Johnson H, Hamalainen C, Yvernault B, Burns C, Manhães-Savio A, Jarecka D, Markiewicz CJ, Salo T, Clark D, Waskom M, Wong J, Modat M, Dewey BE, Clark MG, Dayan M, Loney F, Madison C, Gramfort A, Keshavan A, Berleant S, Pinsard B, Goncalves M, Clark D, Cipollini B, Varoquaux G, Wassermann D, Rokem A, Halchenko YO, Forbes J, Moloney B, Malone IB, Hanke M, Mordom D, Buchanan C, Pauli WM, Huntenburg JM, Horea C, Schwartz Y, Tungaraza R, Iqbal S, Kleesiek J, Sikka S, Frohlich C, Kent J, Perez-Guevara M, Watanabe A, Welch D, Cumba C, Ginsburg D, Eshaghi A, Kastman E, Bougacha S, Blair R, Acland B, Gillman A, Schaefer A, Nichols BN, Giavasis S, Erickson D, Correa C, Ghayoor A, Küttner R, Haselgrove C, Zhou D, Craddock RC, Haehn D, Lampe L, Millman J, Lai J, Renfro M, Liu S, Stadler J, Glatard T, Kahn AE, Kong X-Z, Triplett W, Park A, McDermottroe C, Hallquist M, Poldrack R, Perkins LN, Noel M, Gerhard S, Salvatore J, Mertz F, Broderick W, Inati S, Hinds O, Brett M, Durnez J, Tambini A, Rothmei S, Andberg SK, Cooper G, Marina A, Mattfeld A, Urchs S, Sharp P, Matsubara K, Geisler D, Cheung B, Floren A, Nickson T, Pannetier N, Weinstein A, Dubois M, Arias J, Tarbert C, Schlamp K, Jordan K, Liem F, Saase V, Harms R, Khanuja R, Podranski K, Flandin G, Papadopoulos Orfanos D, Schwabacher I, McNamee D, Falkiewicz M, Pellman J,

Tustison NJ, Avants BB, Cook PA, Zheng Y, Egan A, Yushkevich PA, Gee JC. N4ITK: improved N3 bias correction. IEEE Trans Med Imaging. 2010 Jun;29(6):1310–20. doi:10.1109/TMI.2010.2046908.

Dale A, Fischl B, Sereno MI. Cortical Surface-Based Analysis: I. Segmentation and Surface Reconstruction. Neuroimage. 1999;9(2):179–94. doi:10.1006/nimg.1998.0395.

Fonov VS, Evans AC, McKinstry RC, Almli CR, Collins DL. Unbiased nonlinear average age-appropriate brain templates from birth to adulthood. NeuroImage; Amsterdam. 2009 Jul 1;47:S102. doi:10.1016/S1053-8119(09)70884-5.

Avants BB, Epstein CL, Grossman M, Gee JC. Symmetric diffeomorphic image registration with cross-correlation: evaluating automated labeling of elderly and neurodegenerative brain. Med Image Anal. 2008 Feb;12(1):26–41. doi:10.1016/j.media.2007.06.004.

Jenkinson M, Bannister P, Brady M, Smith S. Improved optimization for the robust and accurate linear registration and motion correction of brain images. Neuroimage. 2002 Oct;17(2):825–41. doi:10.1006/nimg.2002.1132.

Jenkinson M. Fast, automated, N-dimensional phase-unwrapping algorithm. Magn Reson Med. 2003 Jan;49(1):193–7. doi:10.1002/mrm.10354.

Greve DN, Fischl B. Accurate and robust brain image alignment using boundary-based registration. Neuroimage. 2009 Oct;48(1):63–72. doi:10.1016/j.neuroimage.2009.06.060.

Zhang Y, Brady M, Smith S. Segmentation of brain MR images through a hidden Markov random field model and the expectation-maximization algorithm. IEEE Trans Med Imaging. 2001 Jan;20(1):45–57. doi:10.1109/42.906424.

Behzadi Y, Restom K, Liau J, Liu TT. A component based noise correction method (CompCor) for BOLD and perfusion based fMRI. Neuroimage. 2007 Aug 1;37(1):90–101. doi:10.1016/j.neuroimage.2007.04.042.

Klein A, Ghosh SS, Bao FS, Giard J, Häme Y, Stavsky E, et al. Mindboggling morphometry of human brains. PLoS Comput Biol 13(2): e1005350. 2017. doi:10.1371/journal.pcbi.1005350.

Behzadi, Y., Restom, K., Liau, J., & Liu, T. T. (2007). A component based noise correction method (CompCor) for BOLD and perfusion based fMRI. NeuroImage, 37(1), 90–101. https://doi.org/10.1016/j.neuroimage.2007.04.042

Buckner, R. L., Sepulcre, J., Talukdar, T., Krienen, F. M., Liu, H., Hedden, T., Andrews-Hanna, J. R., Sperling, R. A., & Johnson, K. A. (2009). Cortical Hubs Revealed by Intrinsic Functional

Connectivity: Mapping, Assessment of Stability, and Relation to Alzheimer's Disease. Journal of Neuroscience, 29(6), 1860–1873. https://doi.org/10.1523/JNEUROSCI.5062-08.2009

Friston, K. J., Williams, S., Howard, R., Frackowiak, R. S. J., & Turner, R. (1996). Movement-Related effects in fMRI time-series: Movement Artifacts in fMRI. Magnetic Resonance in Medicine, 35(3), 346–355. https://doi.org/10.1002/mrm.1910350312

Gratton, C., Laumann, T. O., Nielsen, A. N., Greene, D. J., Gordon, E. M., Gilmore, A. W., Nelson, S. M., Coalson, R. S., Snyder, A. Z., Schlaggar, B. L., Dosenbach, N. U. F., & Petersen, S. E. (2018). Functional Brain Networks Are Dominated by Stable Group and Individual Factors, Not Cognitive or Daily Variation. Neuron, 98(2), 439-452.e5. https://doi.org/10.1016/j.neuron.2018.03.035

Hermosillo, R. J. M., Moore, L. A., Fezcko, E., Dworetsky, A., Pines, A., Conan, G., Mooney, M. A., Randolph, A., Adeyemo, B., Earl, E., Perrone, A., Carrasco, C. M., Uriarte-Lopez, J., Snider, K., Doyle, O., Cordova, M., Nagel, B. J., Feldstein Ewing, S. W., Satterthwaite, T., … Fair, D. A. (2022). A Precision Functional Atlas of Network Probabilities and Individual-Specific Network Topography [Preprint]. Neuroscience. https://doi.org/10.1101/2022.01.12.475422

Sun, L., Zhao, T., Liang, X., Duan, D., Liu, J., Chen, Y., Wang, X., Liao, X., Xia, M., & He, Y. (2022). Structural insight into the individual variability architecture of the functional brain connectome [Preprint]. Neuroscience. https://doi.org/10.1101/2022.02.16.480803

Pinheiro JC, Bates DM (2000). Mixed-Effects Models in S and S-PLUS. Springer, New York. doi:10.1007/b98882.

Chapter 3 Defining tertiary sulci in lateral prefrontal cortex in chimpanzees using human predictions.

In the previous chapters, I link tertiary sulcal morphology in lateral prefrontal cortex (LPFC) with functional representations and cognition in humans. I show that variations in the presence, prominence, and depth of these structures can provide insights across development. In this chapter, I take an evolutionary lens and ask whether tertiary sulci are identifiable in non-human primates and if they vary along these morphological dimensions. I show that these structures can be identified in chimpanzees. However, in stark contrast to the consistency of the components in humans, we could only identify components in tertiary sulci in a subset of chimpanzees. LPFC tertiary sulci were relatively smaller and shallower in chimpanzees compared to humans.This work expands our understanding of tertiary sulci and the role they play in cognition and evolution.

With permission, this chapter contains previously published material from the following work:
Hathaway CB.*, Voorhies WI.*, Sathishkumar N., Mittal C., Yao JK., Miller JA.,Parker BJ., Weiner KS. *Defining tertiary sulci in lateral prefrontal cortex in chimpanzees using human predictions.* **In Press** (2023).
* co-first author

3.2 Introduction

Similarities and differences in brain structure and function across species is of major interest in systems neuroscience and comparative biology. Recently, increased emphasis has been placed on tertiary sulci, which are shallow indentations of the cerebral cortex that appear late in gestation, continue to develop after birth, and are related to the organization of cortical networks (Connolly 1950; Welker 1990; Armstrong et al. 1995; Weiner 2019; Lopez-Persem et al. 2019; Miller et al. 2020; Miller et al. 2021a, 2021b). Additionally, the morphology of some tertiary sulci is related to cognition and behavior (Amiez et al. 2018; Voorhies et al. 2021) with translational and clinical applications (Garrison et al. 2015; Ammons et al. 2021). Tertiary sulci are present in hominoid brains, but not other widely studied animals in neuroscience research such as mice, marmosets, and macaques (Amiez et al.; Lopez-Persem et al. 2019; Miller et al. 2020; Voorhies et al. 2021; Miller et al. 2020; Miller et al. 2021a, 2021b).

Intriguingly, some tertiary sulci are human-specific, while other tertiary sulci are only present in some, but not all human brains. For example, the mid-fusiform sulcus in ventral temporal cortex and the inframarginal sulcus in posterior cingulate cortex are present in every human brain (Miller et al. 2020; Willbrand et al. 2021), while the paracingulate sulcus in medial frontal cortex (Paus et al. 1996; Fornito et al. 2004, 2006, 2008; Amiez et al. 2018) and the paraintermediate frontal sulcus in lateral prefrontal cortex (Amiez and Petrides 2007; Voorhies et al. 2021) are not. The former three sulci also have been studied in non-human hominoid brains such as chimpanzees (Amiez et al., 2019; Amiez et al. 2021; Miller et al. 2020; Willbrand et al. 2021), while the latter has not. To fill this gap in knowledge, we focus on tertiary sulci in lateral prefrontal cortex (LPFC) in the present study and ask two main questions: 1) Can LPFC tertiary sulci be defined in chimpanzee cortical surfaces from human predictions? and 2) As surface area and depth are defining features differentiating tertiary sulci from primary and secondary sulci (Connolly 1950; Welker 1990; Armstrong et al. 1995; Weiner 2019; Lopez-Persem et al. 2019; Miller et al. 2020; Miller et al. 2021a, 2021b), do LPFC tertiary sulci in chimpanzees differ in the relative surface area and relative depth compared to LPFC tertiary sulci identified in humans?

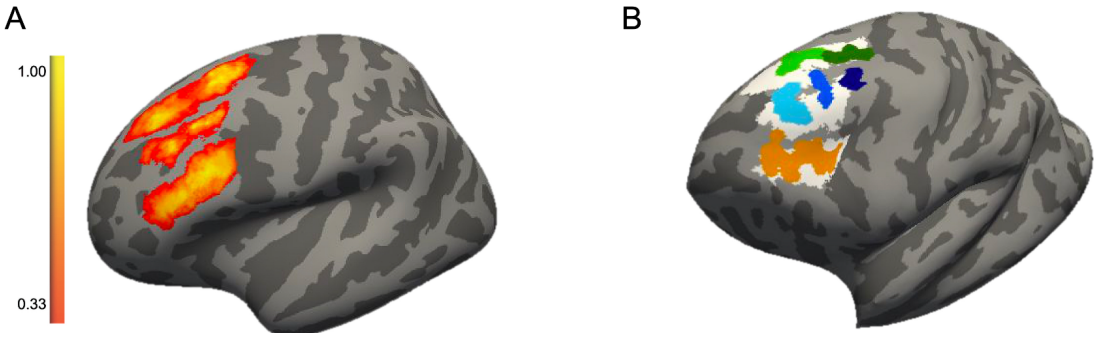

Figure 3.1. Manual labeling protocol of LPFC tertiary sulci in chimpanzees guided by human predictions. **A.***fsaverage* surface showing maximum sulcal probability maps of LPFC sulci from previous work (Miller et al., 2021a). Binarized maps were used to guide labeling on chimpanzee cortical surfaces. Sulcal maps were thresholded at 33% to minimize overlap for visualization purposes. **B.** Example chimpanzee inflated cortical surface illustrating manual labeling procedure. Binarized maximum probability maps in humans were projected to individual chimpanzee cortical surfaces (*white*). These projections were used to guide manual sulcal labeling (colors) for the ifs (orange), sfs-p (dark green), sfs-a (light green), pmfs-p (dark blue), pmfs-i (blue), and pmfs-a (light blue) in individual chimpanzee hemispheres.

3.3 Methods

Participants

Humans: 30 human participants (19 female; 11 male; ages between 22 and 36) randomly selected from the database provided by the Human Connectome Project (HCP): https ://www.human connectome.org/study /hcp-young -adult. This sample has been used previously in studies of LPFC sulcal morphology (Miller et al., 2021a,b). HCP consortium data were previously acquired using protocols approved by the Washington University Institutional Review Board. As our previous morphological analyses of LPFC sulci did not show any sex differences across a range of participant ages (from 6–36; Miller et al., 2021a, Voorhies et al., 2021), we did not specifically balance sex when selecting participants. Additionally, the chimpanzee sample also contains a similar ratio of female to male participants.

Chimpanzees: Anatomical T1 scans were previously acquired using MRI in 60 chimpanzees (38 female; 22 male; ages between 9 and 54), and no new data were collected for the present study. 30 chimpanzees were used to create a species-specific average template and were not included in any other analyses. Of the remaining chimpanzees, 29 are included in the manual labeling and morphological analyses. 1 chimpanzee was excluded for substantial errors in the cortical surface reconstruction. These participants have also been used in a previous study of sulcal morphology in ventral temporal cortex (Miller et al., 2020). The chimpanzees were all members of the colony housed at the Yerkes National Primate Research Center (YNPRC) of Emory University. All methods were carried out in accordance with YNPRC and Emory University's Institutional Animal Care and Use Committee (IACUC) guidelines. Institutional approval was obtained prior to the onset of data collection. Chimpanzee MRIs were obtained from a data archive of scans collected prior to the 2015 implementation of U.S. Fish and Wildlife Service and National Institutes of Health regulations governing research with chimpanzees. These scans were made available through the National Chimpanzee Brain Resource (https://www.chimpanzeebrain.org; supported by NIH grant NS092988).

Data Acquisition

Humans: Anatomical T1-weighted MRI scans (0.8 mm voxel resolution) were obtained in native space from the HCP database, along with outputs from the HCP modified FreeSurfer pipeline.

Chimpanzees: Detailed descriptions of the scanning parameters have been described in Keller et al. 2009, but we also describe the methods briefly here. Specifically, T1-weighted magnetization-prepared rapid-acquisition gradient echo (MPRAGE) MR images were obtained using a Siemens 3 T Trio MR system (TR = 2300 ms, TE = 4.4 ms, TI = 1100 ms, flip angle = 8, FOV = 200 mm) at YNPRC in Atlanta, Georgia. Before reconstructing the cortical surface, the T1 of each chimpanzee was scaled to the size of the human brain. As described in Hopkins et al. 2017, within FSL, the BET function was used to automatically strip away the skull, (2) the FAST function was used to correct for intensity variations due to magnetic susceptibility artifacts and radio frequency field inhomogeneities (i.e., bias field correction), and (3) the FLIRT function was used to normalize the isolated brain to the MNI152 template brain using a 7 degree of freedom transformation (i.e., three translations, three rotations, and one uniform scaling), which preserved the shape of individual brains. Next, each T1 was segmented using FreeSurfer. The fact that the brains are already isolated, both bias-field correction and size-normalization, greatly

assisted in segmenting the chimpanzee brain in FreeSurfer. Furthermore, the initial use of FSL also has the specific benefit, as mentioned above, of enabling the individual brains to be spatially normalized with preserved brain shape, and the values of this transformation matrix and the scaling factor were saved for later use.

Manual sulcal labeling

Each T1-weighted image was segmented to separate gray and white matter. The resulting boundary was used to reconstruct the cortical surface. The automatically generated .sulc and .curv maps allow automatic detection of sulcal and gyral features based on the concavity of the surface (Destrieux, 2010). Sulcal features were calculated from the native meshes generated during the FreeSurfer cortical reconstruction process.

Humans: We first manually defined the LPFC sulci within each individual hemisphere in tksurfer (Miller et al., 2021a). Manual lines were drawn on the inflated cortical surface to define sulci based on the most recent schematics of sulcal patterning in LPFC by Petrides (2019), as well as by the pial and smoothwm surfaces of each individual (Miller et al., 2021a, 2021b). In some cases, the precise start or end point of a sulcus can be difficult to determine on a surface (Borne et al., 2020). Thus, using the inflated, pial, and smoothwm surfaces of each individual to inform our labeling allowed us to form a consensus across surfaces and clearly determine each sulcal boundary. For each hemisphere, the location of LPFC sulci was confirmed by trained independent raters (C.B.H., W.I.V., J.A.M.) and finalized by a neuroanatomist (K.S.W.).

Chimpanzees: Probability maps generated from the human sulcal labels (Miller et al., 2021a) were used to guide sulcal labeling in chimpanzees (Figure 3.1A). Binarized maps for posterior middle frontal tertiary sulci (pmfs-p, pmfs-i, pmfs-a) were projected into individual chimpanzee hemispheres as a combined label with freesurfer's *mris_label2label function.* Additionally, three dorsal and ventral bounding sulci were included in the analysis: The posterior and anterior components of the superior frontal sulcus (sfs_p, sfs_a) and the inferior frontal sulcus (ifs). These human predictions were used to inform the manual identification of these sulci in chimpanzees (Figure 3.1B). For each hemisphere, we identified between one and three pmfs components. These sulci were labeled posterior, intermediate, or anterior based on their position relative to the bounding sulci as in our previous work (Miller et al., 2021a; Petrides 2019). Tertiary sulci that fell outside of the human pmfs prediction and anterior to the bounding sulci were defined as components of the paraintermediate frontal sulcus (pimfs; Voorhies et al., 2021; Petrides 2019). The pimfs was only present in one chimpanzee (c19). As with humans, for each hemisphere, the location of LPFC sulci was confirmed by trained independent raters (C.B.H., W.I.V., N.S., J.K.Y., C.M.) and finalized by a neuroanatomist (K.S.W.). We emphasize that while human predictions were used to guide the labeling, all labeling was performed at the individual surface level. The spatial relation criteria that we implemented in our previous studies in humans (Miller et al., 2021; Voorhies et al., 2021; Yao et al., 2022) was implemented in chimpanzees as in our previous work in ventral temporal cortex (Miller et al., 2020). In this way, our definitions are not dependent on the alignment to fsaverage. Additionally, the chimpanzee brains were scaled to the fsaverage surface before performing any analyses (Miller et al., 2020). This scaling procedure allowed us to use built-in FreeSurfer functions on the chimpanzee hemispheres, including accurate projections of labels between human and chimpanzee surfaces (Appendix Figure 3.4).

We emphasize that while human predictions were used to guide the labeling, all labeling was performed at the individual surface level. We ensured that all sulcal definitions met the same spatial relation criteria in chimpanzees that we used in humans. In this way our definitions are not completely dependent on the alignment to fsaverage. Additionally, the chimpanzee brains were scaled before performing any analyses (Miller et al., 2020). This scaling allowed us to use built in freesurfer functions on the chimpanzee hemispheres, including accurate projections of labels between human and chimpanzee surfaces (Appendix Figure 3.4).

Characterization of sulcal patterning

The criteria for sulcal identification is as follows: All sulci are defined on both the pial and inflated surfaces. Primary Large and deep sulci (sfs and ifs) weare identified first, followed by smaller sulci which are labeled sequentially from posterior to anterior based on their position relative to the larger primary sulci. The same labeling process was used for chimpanzees with the additional criterion that sulcal labeling in chimpanzees was guided by human predictions. Images of post-mortem chimpanzee brains from Retzius (1906) further guided the labeling process to assure that the smaller tertiary sulci are also identifiable in ground truth anatomical data (Appendix Figure 3.5) as in our previous work in ventral temporal cortex (Miller et al., 2020) and medial parietal cortex (Willbrand et al., 2022). For all hemispheres, intersecting components are split based on the junction between the pseudo fold visible on the pial surface. This criterion has been previously verified in volume space (Weiner et al., 2014).

The same labeling process was used for chimpanzees however human predictions were used to guide the labeling process, in addition to considering the human positions we also ensured that the labels had the same relative positioning as in humans. For all hemispheres, intersecting components are split based on the junction between the pseudo fold visible on the pial surface. This criteria has been previously verified in volume space

We characterized the frequency of occurrence of each sulcus separately for left and right hemispheres. We compared the frequency of occurrence of the tertiary sulcal components between hemispheres and species with chi-square tests. For each sulcus, we also characterized sulcal patterns, or types, based on intersections with surrounding sulci. For each sulcal pair, we report the number of intersections relative to the total frequency of occurrence of that sulcus in the hemisphere (Figure 3.2C). We report Pearson correlation coefficients between left and right hemispheres in each sample, as well as the correlation between species.

Sulcal morphology

Depth: Depth of each sulcus was calculated in millimeters from each native cortical surface reconstruction. Raw values for sulcal depth were calculated from the sulcal fundus to the smoothed outer pial surface using a modified version of a recent algorithm for robust morphological statistics which builds on the Freesurfer pipeline. The original algorithm samples the 100 deepest vertices to determine the fundal depth. To address differences in sulcal size across species and sulci, particularly in the small tertiary sulci, we modified the algorithm to sample the deepest 10% of vertices in a given sulcus. Results are consistent when titrating the percentage of the deepest vertices included in the analyses (Appendix Figure 3.2). As the chimpanzee surfaces were scaled prior to reconstruction, we also report relative depth values for the sulci of interest. For these metrics, within each species, depth was calculated relative to the deepest point in the inferior frontal sulcus.

Surface area: Surface area (in square millimeters) was generated for each sulcus from the *mris_anatomical_stats* function in FreeSurfer (Dale et al., 1999; Fischl et al., 1999a). Again, to address scaling concerns between species, we report surface area relative to the surface area of the central sulcus to account for scaling effects as well as raw surface area.

Morphological comparisons

All comparisons were conducted using mixed effects linear models implemented in the nlme R package. For both depth and surface area analyses, model predictors included sulcus, hemisphere, and species, as well as their interaction terms. Species, hemisphere, and sulcus were considered fixed effects. Sulcus was nested within hemisphere which was nested within subjects. Post-hoc analyses were computed with the *emmeans* function.

Asymmetry analyses

For each label, hemispheric asymmetry was computed with the following calculation:

$$(rh - lh)/(rh + lh) * 2$$

Asymmetry values were computed for each species separately. A linear mixed effects model was used to assess the sulcus by species interaction.

Probability maps

Sulcal probability maps were calculated to summarize those vertices that had the highest and lowest correspondence across individual chimpanzees, respectively. To generate these maps, each sulcal label was transformed from the individual to a chimpanzee template surface from a held-out population of 30 chimpanzee brains that was made with the FreeSurfer *make_average_subject* function (Miller et al., 2020). Once transformed to this common template space, for each vertex, we calculated the proportion of chimpanzees for whom the vertex is labeled as the given sulcus. In the case of multiple labels, we employed a greedy, "winner-take-all" approach such that the sulcus with the highest overlap across participants was assigned to a given vertex. Consistent with previous studies (Miller et al., 2020; Voorhies et al., 2021) in addition to providing unthresholded maps, we also constrain these maps to maximum probability maps (MPMs) with 20% participant overlap. MPMs help to avoid overlapping sulci and increase interpretability (Figure 3.5A).

3.4 Results

To answer these questions, we leveraged two freely available multimodal datasets: The National Chimpanzee Brain Resource (https://www.chimpanzeebrain.org/) and The Human Connectome Project (http://www.humanconnectomeproject.org/). Briefly, cortical surface reconstructions were generated for both species from T1 images using FreeSurfer (https://www.freesurfer.net). Leveraging our previously published pipeline that accurately projects probabilistic definitions of sulci defined in the human cerebral cortex to individual chimpanzee hemispheres (Miller et al., 2020), we tested if LPFC tertiary sulci could be defined in chimpanzee cortical surfaces from human predictions (Figure 3.1). Importantly If possible, we then used our previously published morphological pipeline to statistically test if relative surface area and relative depth of LPFC tertiary sulci differed between humans and chimpanzees. For comparison, we also included surrounding sulci, though the main focus was on tertiary sulci. We report five main findings.

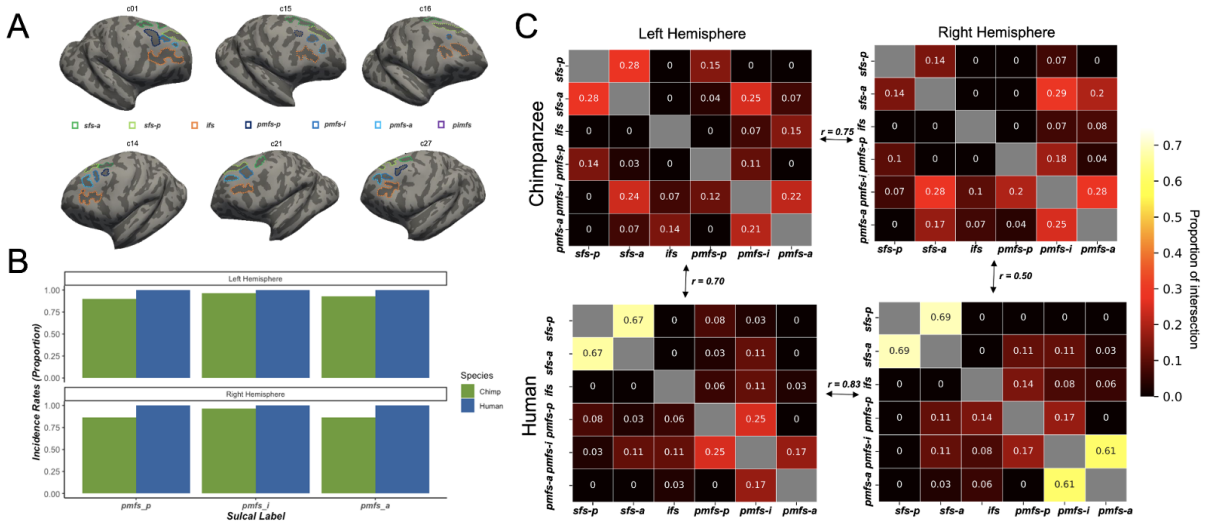

Figure 3.2. Tertiary sulci in lateral prefrontal cortex are identifiable in chimpanzees using human sulcal predictions. **A.** Example right *(top)* and left *(bottom)* sulcal labels for 6 chimpanzees. Chimpanzees had between 1 and 4 identifiable tertiary sulci in a given hemisphere. **B**.Comparison of tertiary sulcal incidence rates (pmfs components) for chimpanzees and humans. Incidence rates of pmfs components in chimpanzees were significantly less than in humans (lh: $\chi^2 = 5.54$, $p = 0.01$; rh: $\chi^2 = 11.7$, $p < 0.001$). C**.**For each sulcus, we report the proportion of intersection (frequency of occurrence/total number of observations in the hemisphere) with every other LPFC sulcus included in the present study (see colorbar for reference; empty white cells in the matrix reflect the fact that a sulcus cannot intersect with itself). ifs: inferior frontal sulcus; pimfs: paraintermediate frontal sulcus; pmfs-a, pmfs-i, pmfs-p: anterior, intermediate, and posterior components of the posterior middle frontal sulcus; sfs-a, sfs-p: anterior and posterior components of the superior frontal sulcus. Similarity between hemispheres and species are reported as Pearson's r correlation coefficients.

Tertiary pmfs components were identifiable in a majority, but not all, chimpanzee hemispheres (lh: 83%; rh: 79%; Figure 3.2B; Appendix Figure 2A). Interestingly, the incidence rates of pmfs components in chimpanzees were significantly less than in humans (lh: $\chi^2 = 5.54$, $p = 0.01$; rh: $\chi^2 = 11.7$, $p < 0.001$), as humans consistently had three identifiable pmfs components in every hemisphere, but chimpanzees did not. Additionally, while at least one pimfs component was identifiable nearly 100% of the time in the human brain, a pimfs component was only identifiable in 2 of the 60 chimpanzee hemispheres measured (Figure 3.2A, Appendix Figure

3.1). Based on this variability in the presence and absence of pmfs components, we identified three main types and subsequent subtypes (Appendix Figure 3.3). Due to the consistent identification of the pmfs components in chimpanzees, and the consistent absence of the pimfs components in chimpanzees, we focus our cross-species morphological analyses on the pmfs components. We emphasize for the reader that though previous studies have identified a middle frontal sulcus in the brains and endocasts of chimpanzees (Bailey et al. 1950; Connolly 1950; Sherwood et al. 2003; Schenker et al. 2010; Falk et al. 2018), these sulcal definitions are often distinct from tertiary pmfs definitions as discussed previously (Miller et al., 2021a, 2021b). Additionally, we refer to these sulci as tertiary because they emerge late in gestation as reviewed previously (Miller et al, 2021b), as well as are small in surface area and shallow in depth – three main features that are commonly used to define tertiary sulci (Armstrong et al., 1995; Welker, 1990; Connolly, 1950; Miller et al., 2021b). Nevertheless, we recognize there is contention regarding which sulci are primary, secondary, or tertiary; thus, the reader can broadly think of our results as identifying small and shallow sulci in the Middle Frontal Gyrus in chimpanzees using human predictions.

Second, quantifying tertiary sulcal variability by examining the prevalence of sulcal types (Figure 3.2C) based on their rate of intersection with neighboring sulci (Materials and Methods) reveals similar rates of intersections between left and right hemispheres in chimpanzees (Pearson's r = 0.75) and humans (Pearson's r = 0.83). In general, humans and chimpanzees showed similar patterns of sulcal intersections (Figure 3.2C) with higher similarity in the left compared to the right hemisphere (lh: Pearson's r = 0.70; rh: Pearson's r = 0.50). In the left hemisphere, the posterior and anterior portions of the sfs showed higher rates of intersection in humans (Figure 3.2C), while in the right hemisphere, humans showed higher rates of intersection between intermediate and anterior pmfs components (Figure 3.2C).

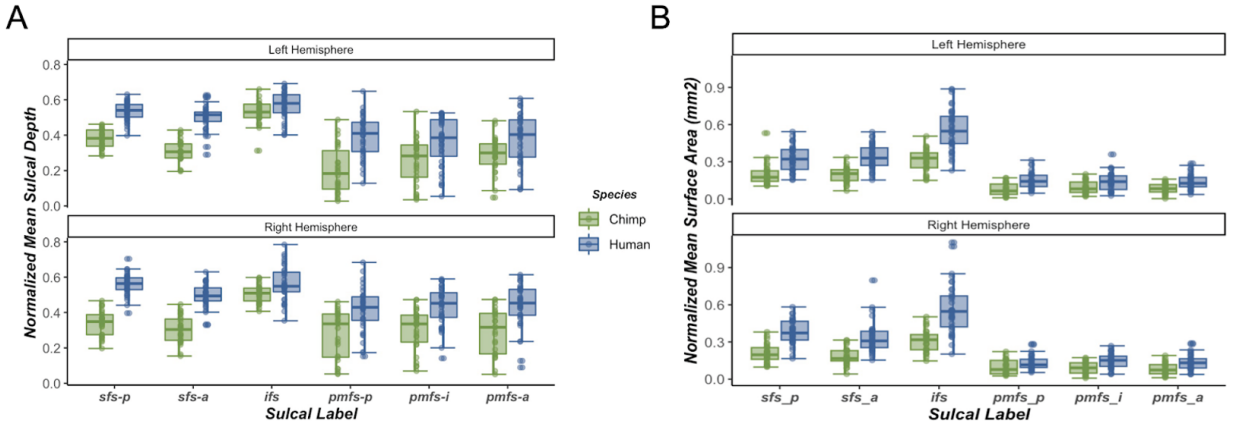

Figure 3.3 ***LPFC sulci are relatively smaller and shallower in chimpanzees compared to humans.*** **A** Normalized mean sulcal depth (mm) for each sulcus in chimpanzees (*green*) and humans (*blue*) for the left and right hemispheres. Sulci were consistently shallower in chimpanzees. Normed sulcal depth is calculated as a proportion relative to the deepest point in the hemisphere. **B.** The same as a) but for relative mean surface area (mm^2). Sulci were relatively larger in humans than chimpanzees. Horizontal lines represent median values, boxes represent interquartile range, and whisker lines represent the 1st and 3rd quartiles.

Third, for sulcal depth, a mixed effects linear model with sulcus, hemisphere, and species as factors showed that (i) sulci were shallower in chimpanzees relative to humans ($F(1,63)$ =

199.32, p < 0.0001, Figure 3.3A), (ii) depth varied by sulcus (F(5,615) = 86.50, p < 0.0001), and (iii) in both species, the pmfs components were shallower (*Mean(sd)*: pmfs-p = 10.4(4.73), pmfs-i = 10.8(4.39), pmfs-a = 11.2(4.29)) than the surrounding ifs and sfs (*Mean(sd)*: ifs = 17.0(2.39), sfs-p = 14.4(3.28), sfs-a = 12.8(3.44)) components (Figure 3.3A; Appendix Figure 3.2B for raw depth values). There was also a main effect of hemisphere in which sulci in the left hemisphere were shallower than the right hemisphere in both species (F(1,63) = 11.82, p = 0.001; *left:* Chimpanzee mean(sd) = 10.5(4.46), Human mean(sd) = 13.9(4.07); *right*: Chimpanzee mean(sd) =10.9(4.11), Human mean(sd) = 15.0(3.63). Post-hoc analyses revealed that the differences between species were most pronounced for the tertiary sulci and the sfs components (Figure 3.3A; all *p*s < 0.0001).

Fourth, for surface area, a mixed effects linear model with the same three factors showed an expected species effect in which all sulci were less prominent in chimpanzees than in humans (F(1,63) = 220.03, p < 0.0001; *left:* Chimpanzee mean(sd) = 0.16(0.11), Human mean(sd) = 0.28(0.18); *right*: Chimpanzee mean(sd) = 0.17(0.11), Human mean(sd) = 0.28(0.20); Figure 3.3B; Appendix Figure 3.2C for raw surface area). There was also an effect of sulcus (F(5,609) = 288.65, p < 0.0001) in which the pmfs components (*Mean(sd)*: pmfs-p = 0.12(0.06), pmfs-i = 0.12(0.65), pmfs-a = 0.16(0.06)) were smaller than the ifs and sfs *Mean(sd)*: (ifs = 0.46(0.20), sfs-p = 0.29(0.12), sfs-a = 0.27(0.12)) components across species and hemispheres (Figure 3.3B).

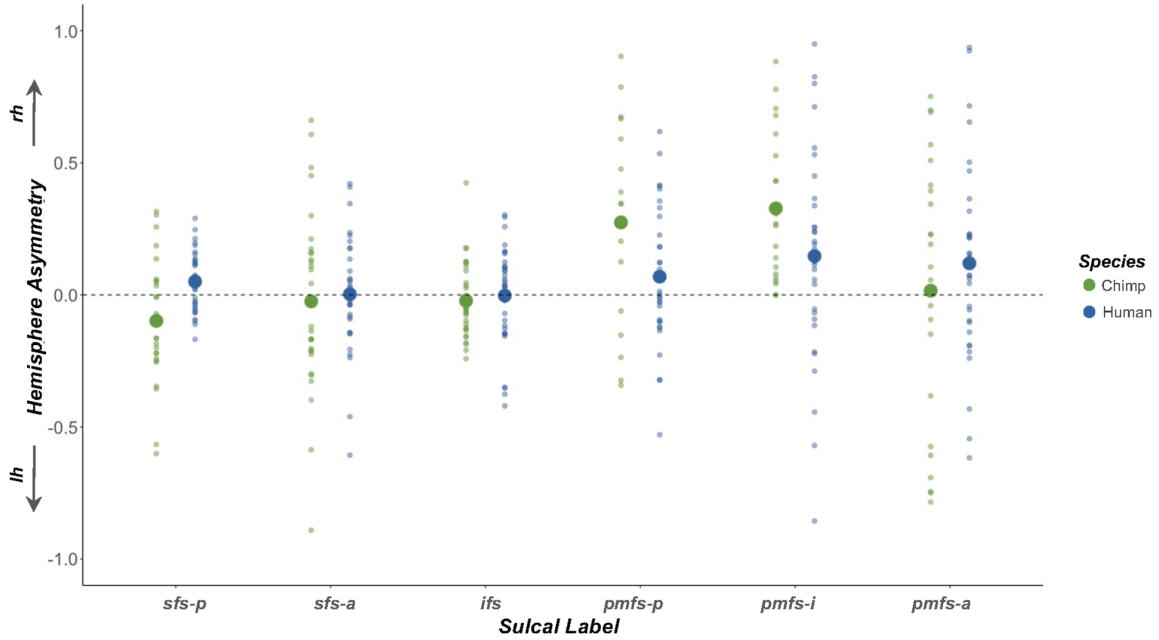

Figure 3.4. Some LPFC tertiary sulci are deeper in the right compared to the left hemisphere in both chimpanzees and humans. Depth asymmetry for each sulcus in chimpanzees *(green)* and humans *(blue)*. Asymmetry was calculated as (RH - LH)/(RH + LH)*2. Large dots represent mean asymmetry values across species. Small dots reflect asymmetry for individual members in each species. Deeper sulci in the right hemisphere are above zero, while deeper sulci in the left hemisphere are below zero.

Fifth, we replicated and extend previous findings showing that the ifs was comparably deep between the two hemispheres in chimpanzees with little asymmetry (Bogart et al. 2012).

We also find that the ifs does not show hemispheric asymmetry in either species and report a comparable asymmetry value in chimpanzees (*chimpanzee:* mean(sd) = -0.02 (0.07); *human*: mean(sd) = -0.0002(0.07)) as previously reported. We also extend these previous results by considering tertiary sulci and show that, in both chimpanzees and humans, the pmfs-i and pmfs-p showed significant rightward asymmetry (*pmfs-p*: mean(sd) = 0.18(0.54); *pmfs-i:* mean(sd) = 0.25 (0.58)); Figure 3.4). Although this effect was present in both species, we did observe a significant species difference in the pmfs-p, in which chimpanzees showed a greater rightward asymmetry than humans (*Mean(sd):* chimpanzee = 0.36(0.72) human = 0.07(0.36); $p = 0.01$).

3.5 Discussion

To our knowledge, the present findings are the first to identify and quantify morphological features of the three shallow components of the posterior middle frontal sulcus (pmfs-a, pmfs-i, and pmfs-p) in LPFC of chimpanzees. In a recent historical analysis and review of the literature (Miller et al., 2021b), the pmfs components were largely overlooked in previous studies due to their variability in both human and non-humanoid primate brains. Nevertheless, previous studies often mentioned the presence and variability of sulcal components within the posterior MFG of chimpanzees (Bailey et al. 1950; Connolly 1950; Sherwood et al. 2003; Schenker et al. 2010; Falk et al. 2018, Appendix Figure 3.5). In direct reference to this variability, Falk and colleagues (2018) write:

"These newly identified configurations for *fm* show that variation in chimpanzee frontal lobes includes more complex midfrontal gyri than previously described [Connolly 1950; Falk 2014]."

Figure 3.5 ***pmfs sulcal probability maps in chimpanzees.*** Maximum probability maps for the three consistently identifiable pmfs sulcal labels (pmfs-p, pmfs-i, pimfs-a). To generate the maps, each label was transformed from each individual to a custom average template created for 30 additional chimpanzees not included in the original analysis. For each vertex we calculated the proportion of chimpanzees for whom that vertex is labeled as the given sulcus (the warmer the color, the higher the overlap in each image). In the case of multiple labels for one vertex the sulcus with the highest overlap across participants was assigned to a given vertex. To reduce spatial overall for visualization purposes, these maps were thresholded to 20% overlap across chimpanzees.

Here, we explicitly quantify that these "newly identified configurations" of the pmfs components are more humanlike in their appearance within the chimpanzee LPFC than previously thought, while the pimfs components in the anterior MFG are rarer in chimpanzees than in humans. Interestingly, the presence or absence of the pimfs has been linked to higher-level aspects of cognition in humans (Willbrand et al., 2022), which begs the question: What is the functional and cognitive role of the pimfs in chimpanzees?

Additionally, the present findings provide novel insight into the morphological asymmetry of LPFC tertiary sulci in chimpanzees for the first time. After replicating previous findings of a lack of asymmetry in the depth of the inferior frontal sulcus in chimpanzees (Bogart

et al. 2012), we further showed that there is a larger rightward depth asymmetry for an LPFC tertiary sulcus (pmfs-p) in chimpanzees compared to humans. Thus, future studies can further explore the functional and cognitive meaning of this asymmetry guided by our shared probabilistic predictions of LPFC sulci (Figure 3.5), as well as further build from the recent foundation showing the similarities and differences in tertiary sulci across the hominoid clade in ventral temporal (Miller et al. 2020), medial prefrontal (Amiez et al., 2019), posterior cingulate (Willbrand et al. 2021), and now lateral prefrontal cortices.

The present study would not have been possible without using freely available multimodal atlases. The fact that some LPFC tertiary sulci are identifiable in both humans and chimpanzees informs a "horizontal translation" of relating neuroanatomical structures between species. Specifically, our findings show that there are morphological precursors to small and shallow sulci within the human MFG. Although more research is needed to establish the ontogeny of these structures in both chimpanzees and humans, these structures show a high spatial correspondence and may serve as a foundation from which to formally compare functional and neuroanatomical features and spatial scales between species. Importantly our methodology is agnostic to sulcal type and our results hold independent of sulcal classifications. Building on the findings from the present study, future studies could consider at least three features. First, an important aspect that is still not well understood is the effect of allometry on cortical folding (Toro et al., 2008), especially while considering tertiary sulci. Previous work has shown that global changes in brain size leads to variability in sulcal patterning (Germanaud 2012, 2014). However, the relationship between allometry and tertiary sulci has not been well explored. As the brains here were scaled as part of our analysis pipeline, we did not directly investigate the relationship between brain size and cortical folding patterns. Future work should consider how the identification, size, and shape of the tertiary sulci identified here scale and change across evolution and development. Second, do certain cytoarchitectonic or functional areas co-localize with these tertiary sulci between species or do they identify transitions in one species, but not another? Third, do these sulci have consistent relationships with underlying short or long-range white matter tracts between species? As resting state data are available for both species (Amiez et al. 2021), these sulci can also serve as seeds in functional connectivity analyses in future studies. Interestingly, previous research indicates that the presence or absence of tertiary sulci in medial PFC affects the organization of functional networks – both in the location of the hub of the default mode network as well as the appearance or absence of new clusters elsewhere in the brain, respectively (Lopez-Persem et al. 2019). Thus, the presence or absence of the pimfs components in the human brain may be reflective of individual differences in functional networks within species, while the absence of the pimfs components in chimpanzees may be reflective of differences in functional connectivity across species, which can be tested in future research. Crucially, this prediction in direct relation to the pimfs would not have been generated without these freely available datasets. Finally, future work can also examine, quantify, and model how elementary entities of the folding pattern (sulcal roots (Regis et al., 2005) or sulcal pits; Lohmann et al., 2008; Im et al., 2010, 2011; Im and Grant, 2019; Auzias et al., 2015; Le Guen et al., 2018; Leroy et al., 2015; Natue et al., 2021) relate to LPFC sulci between species. For example, does the asymmetry of sulcal depth in the pmfs-p extend to sulcal pits? This would be a novel extension of recent work showing that a superior temporal asymmetrical pit (STAP) was specific to the human brain (Leroy et al., 2015).

In conclusion, our study builds on recent studies showing that tertiary sulci are not just a feature of the human cerebral cortex, but also are commonly identifiable in other hominoid

brains although they are less prominent than in humans. Future research will show the generalizability or specificity of the methodological approach implemented here in other cortical expanses and species, as well as functional and cognitive insights that it may provide for understanding the evolution of association cortices, functional representations, and cognition.

3.6 References

Amiez C, Wilson CRE, Procyk E (2018) Variations of cingulate sulcal organization and link with cognitive performance. Sci Reports 2018 81 8:1–13. https://doi.org/10.1038/s41598-018-32088-9

Amiez C, Petrides M (2007) Selective involvement of the mid-dorsolateral prefrontal cortex in the coding of the serial order of visual stimuli in working memory. Proc Natl Acad Sci 104:13786–13791. https://doi.org/10.1073/PNAS.0706220104

Amiez C, Sallet J, Hopkins WD, et al (2019) Sulcal organization in the medial frontal cortex provides insights into primate brain evolution. Nat Comms 10: 3437. https://doi.org/10.1038/s41467-019-11347-x

Amiez C, Sallet J, Novek J, et al (2021) Chimpanzee histology and functional brain imaging show that the paracingulate sulcus is not human-specific. Comms Bio 4:54. https://doi.org/10.1038/s42003-020-01571-3

Ammons CJ, Winslett ME, Bice J, et al (2021) The Mid-Fusiform Sulcus in Autism Spectrum Disorder: Establishing a Novel Anatomical Landmark Related to Face Processing. Autism Res 14:53–64. https://doi.org/10.1002/aur.2425

Armstrong E, Schleicher A, Omran H, et al (1995) The ontogeny of human gyrification. Cereb Cortex 5:56–63

Auzias, Guillaume, et al (2015) "Deep sulcal landmarks: algorithmic and conceptual improvements in the definition and extraction of sulcal pits." Neuroimage 111: 12-25. https://doi.org/10.1016/j.neuroimage.2015.02.008

Bailey P, von Bonin G, McCulloch WS (1950) The isocortex of the chimpanzee. University of Illinois Press, Urbana

Borne, L., Rivière, D., Mancip, M. & Mangin, J. F. (2020) Automatic labeling of cortical sulci using patch- or CNN-based segmentation techniques combined with bottom-up geometric constraints. Med. Image Anal. 62, 101651 https://doi.org/10.1016/j.media.2020.101651

Bogart SL, Mangin J-F, Schapiro SJ, et al (2012) Cortical Sulci Asymmetries in Chimpanzees and Macaques: A New Look at an Old Idea. Neuroimage 61:533–541. https://doi.org/10.1016/j.neuroimage.2012.03.082

Connolly JC (1950) External morphology of the primate brain. C. C. Thomas, Springfield

Falk D, Zollikofer CPE, et al (2018) Identification of in vivo Sulci on the External Surface of Eight Adult Chimpanzee Brains: Implications for Interpreting Early Hominin Endocasts. Brain Behav Evol 91:45–58. https://doi.org/10.1159/000487248

Falk D (2014) Interpreting sulci on hominin endocasts: Old hypotheses and new findings. Front Hum Neurosci 8:134. https://doi.org/10.3389/FNHUM.2014.00134/BIBTEX

Fornito A, Whittle S, Wood SJ, et al (2006) The influence of sulcal variability on morphometry of the human anterior cingulate and paracingulate cortex. Neuroimage 33:843–854. https://doi.org/10.1016/J.NEUROIMAGE.2006.06.061

Fornito A, Wood SJ, Whittle S, et al (2008) Variability of the paracingulate sulcus and morphometry of the medial frontal cortex: associations with cortical thickness, surface area, volume, and sulcal depth. Hum Brain Mapp 29:222–236. https://doi.org/10.1002/HBM.20381

Fornito A, Yücel M, Wood S, et al (2004) Individual differences in anterior cingulate/paracingulate morphology are related to executive functions in healthy males. Cereb Cortex 14:424–431. https://doi.org/10.1093/CERCOR/BHH004

Garrison JR, Fernyhough C, McCarthy-Jones S, et al (2015) Paracingulate sulcus morphology is associated with hallucinations in the human brain. Nat Commun 6:8956. https://doi.org/10.1038/ncomms9956

Germanaud, David, et al (2012) "Larger is twistier: spectral analysis of gyrification (SPANGY) applied to adult brain size polymorphism." Neuroimage 63.3: 1257-1272. https://doi.org/10.1016/j.neuroimage.2012.07.053

Germanaud, David, et al (2014) "Simplified gyral pattern in severe developmental microcephalies? New insights from allometric modeling for spatial and spectral analysis of gyrification." NeuroImage 102: 317-331. https://doi.org/10.1016/j.neuroimage.2014.07.057

Hopkins WD, Li X, Crow T, Roberts N (2017) Vertex- and atlas-based comparisons in measures of cortical thickness, gyrification and white matter volume between humans and chimpanzees. Brain Struct Funct 222: 229–245. https://doi.org/10.1007/s0042 9-016-1213-1.

Im, Kiho, et al (2010) "Spatial distribution of deep sulcal landmarks and hemispherical asymmetry on the cortical surface." Cerebral cortex 20.3: 602-611. https://doi.org/10.1093/cercor/bhp127

Im, Kiho, and P. Ellen Grant (2019) "Sulcal pits and patterns in developing human brains." Neuroimage 185: 881-890. https://doi.org/10.1016/j.neuroimage.2018.03.057

Keller SS, Roberts N, Hopkins W (2009) A comparative magnetic resonance imaging study of the anatomy, variability, and asymmetry of Broca's area in the human and chimpanzee brain. J Neurosci 29: 14607–14616. https://doi.org/10.1523/JNEUROSCI.2892- 09.2009

Leroy F, et al (2015) New human-specific brain landmark: the depth asymmetry of superior temporal sulcus. Proc Natl Acad Sci. 112:1208–1213. https://doi.org/10.1073/pnas.1412389112

Le Guen, Yann, et al (2018) "Genetic influence on the sulcal pits: on the origin of the first cortical folds." Cerebral Cortex 28.6: 1922-1933. https://doi.org/10.1093/cercor/bhx098

Lohmann, Gabriele, D. Yves Von Cramon, and Alan CF Colchester (2008) "Deep sulcal landmarks provide an organizing framework for human cortical folding." Cerebral Cortex 18.6: 1415-1420. https://doi.org/10.1093/cercor/bhm174

Lopez-Persem A, Verhagen L, Amiez C, et al (2019) The human ventromedial prefrontal cortex: Sulcal morphology and its influence on functional organization. J Neurosci 39:3627–3639. https://doi.org/10.1523/JNEUROSCI.2060-18.2019

Miller JA, Voorhies WI, Li X, Raghuram I, Palomero-Gallagher N, Zilles K, Sherwood CC, Hopkins WD, Weiner KS (2020) Unique sulcal morphology of ventral temporal cortex is shared between humans and other hominoids. Sci Rep 10:17132.

Miller JA, Voorhies WI, Lurie DJ, et al (2021a) Overlooked Tertiary Sulci Serve as a Meso-Scale Link between Microstructural and Functional Properties of Human Lateral Prefrontal Cortex. J Neurosci 41:2229–2244. https://doi.org/10.1523/JNEUROSCI.2362-20.2021

Miller JA, D'Esposito M, Weiner KS (2021b) Using Tertiary Sulci to Map the "Cognitive Globe" of Prefrontal Cortex. J Cogn Neurosci 33:1698–1715. https://doi.org/10.1162/JOCN_A_01696

Natu VS, et al (2021) Sulcal Depth in the Medial Ventral Temporal Cortex Predicts the Location of a Place-Selective Region in Macaques, Children, and Adults. Cereb Cortex 31: 48–61, https://doi.org/10.1093/cercor/bhaa203

Paus T, Tomaiuolo F, Otaky N, et al (1996) Human cingulate and paracingulate sulci: pattern, variability, asymmetry, and probabilistic map. Cereb Cortex 6:207–214. https://doi.org/10.1093/CERCOR/6.2.207

Petrides M (2019) Atlas of the morphology of the human cerebral cortex on the average MNI brain, Ed 1. London, UK: Elsevier.

Régis, Jean, et al (2005) ""Sulcal root" generic model: a hypothesis to overcome the variability of the human cortex folding patterns." Neurologia medico-chirurgica 45.1: 1-17. https://doi.org/10.2176/nmc.45.1

Schenker NM, Hopkins WD, Spocter MA, et al (2010) Broca's Area Homologue in Chimpanzees (Pan troglodytes): Probabilistic Mapping, Asymmetry, and Comparison to Humans. Cereb Cortex 20:730–742. https://doi.org/10.1093/cercor/bhp138

Sherwood CC, Broadfield DC, Holloway RL, et al (2003) Variability of Broca's Area Homologue in African Great Apes: Implications for Language Evolution. Anat. Rec. 71A:276 –285. https://doi.org/10.1002/ar.a.10046

Toro, Roberto, et al (2008). "Brain size and folding of the human cerebral cortex." Cerebral cortex 18.10 (2008): 2352-2357. https://doi.org/10.1093/cercor/bhm261

Vickery S, Hopkins WD, Sherwood CC, et al (2020) Chimpanzee brain morphometry utilizing standardized MRI preprocessing and macroanatomical annotations. Elife 9:e60136. https://doi.org/10.7554/eLife.60136

Voorhies WI, Miller JA, Yao JK, Bunge SA WK (2021) Cognitive insights from tertiary sulci in prefrontal cortex. Nat Commun 12(1):5122.

Weiner KS (2019) The Mid-Fusiform Sulcus (sulcus sagittalis gyri fusiformis). Anat. Rec. 302:1491–1503

Welker W (1990) Why Does Cerebral Cortex Fissure and Fold? In *Cerebral Cortex,* eds. E.G. Jones et al. pp. 3–136. Springer: New York. https://doi.org/10.1007/978-1-4615-3824-0_1

Willbrand EH, Parker BJ, Voorhies WI, et al (2021) A new tripartite landmark in posterior cingulate cortex. bioRxiv 2021.10.30.466521. https://doi.org/10.1101/2021.10.30.466521

Conclusion

These studies take an individualized anatomical approach and combine classic neuroanatomy with modern techniques to reveal that cortical sulci have relevance for cognition.

Across the chapters, I show that small, late-developing tertiary sulci can be used as loci of comparison across individuals, development, and evolution to gain new insight into structure-function-behavior relationships in the LPFC. By considering individual anatomy, I extend current knowledge around the acquisition of reasoning skills and provide a fine-grained link between cortical structure and behavior. Throughout this work, I emphasize the importance of considering individual-level anatomy in cognitive neuroscience research and provide a method for doing so.

In Chapter 1, I tested the classic hypothesis that tertiary sulci in the LPFC are relevant for cognition. Using a novel, data-driven analysis pipeline, I show that a subset of tertiary sulci in the LPFC reliably predicts reasoning performance in a developmental sample. Notably, the depths of these sulci explain variance in reasoning not accounted for by age. After establishing that tertiary sulci are relevant for cognition, in Chapter 2, I further explore variability in these structures. I show that variable tertiary sulcal components have distinct functional connectivity profiles and that the presence and prominence of these structures is linked to reasoning behavior. Paralleling behavioral results, preliminary analyses suggest that the functional connectivity of these sulci interact with reasoning skills. Finally, in Chapter 3, I take an evolutionary lens and show that while these structures can be identified in the prefrontal cortex of chimpanzees, they are less present, smaller, and shallower compared to humans. As reasoning is largely believed to be a human-specific skill (Vendetti & Bunge, 2014), this dovetails with the developmental findings that the presence, prominence, and depth of these structures are associated with the acquisition of cognitive skills.

In this work, we present new methods to identify tertiary sulci and link them to cognition. While we focus our investigation on one cortical area and cognitive process, the methods we provide can be extended to other regions and cognitive processes. Already, we have successfully applied these methods to study working memory (Yao et al., 2023) and face processing (Parker et al., 2022). Work is ongoing to apply these methods in the parietal cortex to explore both development and evolution.

Performing a complex cognitive task requires networks of cortical regions. While there is a growing body of work suggesting that tertiary sulci are functionally relevant (Lopez-Persem et al., 2019; Weiner & Zilles, 2016; Willbrand et al., 2021), the role of sulci in functional networks remains unclear. Although it seems likely that tertiary sulci could serve as landmarks for functional networks, further research is needed. Relatedly, it is important that future studies unpack the underlying mechanism for this relationship. Tertiary sulci are a promising mesoscale link between cortical microstructure and cognitive function (Miller et al., 2021B). However, it will be important to investigate how microstructural properties relate to variability in sulcal morphology.

It is crucial to emphasize that while these results give us valuable insights into how the structure and organization of the brain support cognition, none of these findings suggest that there is an optimal type of sulcal morphology. In fact, we observed a striking amount of variability in cortical anatomy and function (Appendix Figures 1.1, 2.1.1, 2.2.1, 3.1). While the presence and depth of a subset of sulci were associated with better performance on a reasoning task, these features did not relate to other cognitive processes (Appendix Figure 1.6). In fact, in

some situations, shallower structures have been associated with better cognitive performance (Yao et al., 2023). Ultimately the brain is a complex, dynamic system that varies across evolution, development, and experience to best meet the needs of our environment. By studying how structure and cognition co-vary, we can advance our understanding of the system. However, it is important to remember that what is considered an adaptive pattern of cortical function varies with context and experience (Ellwood-Lowe et al., 2021) and we should be cautious when making large generalizations about brain-behavior relationships.

References

Donahue, C. J., Glasser, M. F., Preuss, T. M., Rilling, J. K. & Van Essen, D. C. Quantitative assessment of prefrontal cortex in humans relative to nonhuman primates. *Proc. Natl. Acad. Sci. U. S. A.* 115, E5183–E5192 (2018).

Miller, E. K. & Cohen, J. D. An Integrative Theory of Prefrontal Cortex Function. *Annu. Rev. Neurosci.* 24, 167–202 (2001).

Stuss, D. T. & Knight, R. T. *Principles of Frontal Lobe Function*. (Oxford University Press, 2002). doi:10.1093/acprof:oso/9780195134971.001.0001.

Stuss, D. T. Functions of the frontal lobes: relation to executive functions. *J. Int. Neuropsychol. Soc.* 17, 759–765 (2011).

Stuss, D. T. & Alexander, M. P. Executive functions and the frontal lobes: a conceptual view. *Psychol. Res.* 63, 289–298 (2000).

Fuster, J. M. Proceedings of the Human Cerebral Cortex : From Gene to Structure and Function Prefrontal neurons in networks of executive memory. *Brain Res. Bull.* 52, 331–336 (2000).

Gogtay, N. *et al.* Dynamic mapping of human cortical development during childhood through early adulthood. *Proc. Natl. Acad. Sci. U. S. A.* 101, 8174–8179 (2004).

Fry, A. F. & Hale, S. Relationships among processing speed, working memory, and fluid intelligence in children. *Biol. Psychol.* 54, 1–34 (2000).

Mcardle, J. J., Ferrer-Caja, E., Hamagami, F. & Woodcock, R. W. Comparative Longitudinal Structural Analyses of the Growth and Decline of Multiple Intellectual Abilities Over the Life Span. (2002) doi:10.1037/0012-1649.38.1.115.

He, W. & Seymour, R. A. Commentary: Frontoparietal structural connectivity in childhood predicts development of functional connectivity and reasoning ability: A large-scale longitudinal investigation. *Frontiers in Psychology* (2018) doi:10.3389/fpsyg.2018.00265.

Wendelken, C., O'Hare, E. D., Whitaker, K. J., Ferrer, E. & Bunge, S. A. Increased functional selectivity over development in rostrolateral prefrontal cortex. *J. Neurosci.* 31, (2011).

Wendelken, C. *et al.* Frontoparietal structural connectivity in childhood predicts development of functional connectivity and reasoning ability: A large-scale longitudinal investigation. *J. Neurosci.* 37, 8549–8558 (2017).

Amiez, C., Kostopoulos, P., Champod, A. S. & Petrides, M. Local morphology predicts functional organization of the dorsal premotor region in the human brain. *J. Neurosci.* 26, 2724–2731 (2006).

Amiez, C. & Petrides, M. Anatomical organization of the eye fields in the human and non-human primate frontal cortex. *Prog. Neurobiol.* 89, 220–230 (2009).

Croxson, P. L., Forkel, S. J., Cerliani, L. & Thiebaut De Schotten, M. Structural Variability Across the Primate Brain: A Cross-Species Comparison. *Cereb. Cortex* 28, 3829–3841 (2018).

Neubert, F. X., Mars, R. B., Sallet, J. & Rushworth, M. F. S. Connectivity reveals relationship of brain areas for reward-guided learning and decision making in human and monkey frontal cortex. *Proc. Natl. Acad. Sci. U. S. A.* 112, E2695–E2704 (2015).

Petrides, M. Lateral prefrontal cortex: Architectonic and functional organization. *Philos. Trans. R. Soc. B Biol. Sci.* 360, 781–795 (2005).

Petrides, M., Tomaiuolo, F., Yeterian, E. H. & Pandya, D. N. The prefrontal cortex: Comparative architectonic organization in the human and the macaque monkey brains. *Cortex* 48, 46–57 (2012).

Eickhoff, S. B., Yeo, B. T. T. & Genon, S. Imaging-based parcellations of the human brain. *Nat. Rev. Neurosci.* 19, 672–686 (2018).

Glasser, M. F. *et al.* A multi-modal parcellation of human cerebral cortex. *Nature* 536, 171–178 (2016).

Goulas, A., Uylings, H. B. M. & Stiers, P. Unravelling the intrinsic functional organization of the human lateral frontal cortex: a parcellation scheme based on resting state fMRI. *J. Neurosci.* 32, 10238–10252 (2012).

Szczepanski, S. M. & Knight, R. T. Insights into Human Behavior from Lesions to the Prefrontal Cortex. *Neuron* vol. 83 1002–1018 (2014).

Rajkowska, G. & Goldman-Rakic, P. S. Cytoarchitectonic definition of prefrontal areas in the normal human cortex: II. Variability in locations of areas 9 and 46 and relationship to the Talairach coordinate system. *Cereb. Cortex* 5, 323–337 (1995).

Petrides, M. & Pandya, D. N. Dorsolateral prefrontal cortex: comparative cytoarchitectonic analysis in the human and the macaque brain and corticocortical connection patterns. *Eur. J. Neurosci.* 11, 1011–1036 (1999).

Catani, M. *et al.* Short frontal lobe connections of the human brain. *Cortex* 48, 273–291 (2012).

Sallet, J. *et al.* The organization of dorsal frontal cortex in humans and macaques. *J. Neurosci.* 33, 12255–74 (2013).

Miller, J. A. D'esposito, M. Weiner, K.S. Using tertiary sulci to map the 'cognitive globe' of prefrontal cortex. *J. Cogn. Neurosci* (2021).

Miller, J. A., Voorhies, W. I., Lurie, D. J., D'Esposito, M. & Weiner, K. S. Overlooked tertiary sulci serve as a meso-scale link between microstructural and functional properties of human lateral prefrontal cortex. *J. Neurosci.* JN-RM-2362-20 (2021) doi:10.1523/jneurosci.2362-20.2021.

Voorhies, W. I., Miller, J. A., Yao, J. K., Bunge, S. A. & Weiner, K. S. Cognitive insights from tertiary sulci in prefrontal cortex. *Nat. Commun. 2021 121* 12, 1–14 (2021).

Van Essen, D. C. & Dierker, D. L. Surface-Based and Probabilistic Atlases of Primate Cerebral Cortex. *Neuron* 56, 209–225 (2007).

Zilles, K., Palomero-Gallagher, N. & Amunts, K. Development of cortical folding during evolution and ontogeny. *Trends Neurosci* 36, 275–284 (2013).

Weiner, K. S. The Mid-Fusiform Sulcus (sulcus sagittalis gyri fusiformis). (2018) doi:10.1002/ar.24041.

Sanides, F. Structure and function of the human frontal lobe. *Neuropsychologia* 2, 209–219 (1964).

Weiner, K. S., Natu, V. S. & Grill-Spector, K. On object selectivity and the anatomy of the human fusiform gyrus. (2018) doi:10.1016/j.neuroimage.2018.02.040.

Garrison, J. R. *et al.* Paracingulate sulcus morphology is associated with hallucinations in the human brain. *Nat. Commun.* 6, 1–6 (2015).

Lopez-Persem, A., Verhagen, L., Amiez, C., Petrides, M. & Sallet, J. The human ventromedial prefrontal cortex: Sulcal morphology and its influence on functional organization. *J. Neurosci.* 39, 3627–3639 (2019).

Ferrer, E. *et al.* White matter maturation supports the development of reasoning ability through its influence on processing speed. *Dev. Sci.* 16, 941–951 (2013).

Blair, C. How similar are fluid cognition and general intelligence? A developmental neuroscience perspective on fluid cognition as an aspect of human cognitive ability. (2006).

Cattell, R. B. Intelligence : its structure, growth, and action. (North-Holland, 1987).

Goswami, U. Analogical reasoning in children. (Lawrence Erlbaum Associates, Inc, 1992).

Vendetti, M. S. & Bunge, S. A. Evolutionary and Developmental Changes in the Lateral Frontoparietal Network: A Little Goes a Long Way for Higher-Level Cognition. *Neuron* 84, 906–917 (2014).

Yao, J. K., Voorhies, W. I., Miller, J. A., Bunge, S. A. & Weiner, K. S. Sulcal depth in prefrontal cortex: a novel predictor of working memory performance. *Cereb. Cortex* 33, 1799–1813 (2023).

Parker, B. J. *et al.* Hominoid-specific sulcal variability is related to face perception ability. *bioRxiv* 2022.02.28.482330 (2022) doi:10.1101/2022.02.28.482330.

Willbrand, E. H. *et al.* A new tripartite landmark in posterior cingulate cortex. *bioRxiv* 2021.10.30.466521 (2021) doi:10.1101/2021.10.30.466521.

Weiner, K. S. & Zilles, K. The anatomical and functional specialization of the fusiform gyrus. *Neuropsychologia* (2016) doi:10.1016/j.neuropsychologia.2015.06.033.

Ellwood-Lowe, M. E., Whitfield-Gabrieli, S. & Bunge, S. A. Brain network coupling associated with cognitive performance varies as a function of a child's environment in the ABCD study. *Nat. Commun. 2021 121* 12, 1–14 (2021).

Appendices

Appendix - Chapter 1

No differences in cortical thickness among primary and tertiary sulci in LPFC

As discussed throughout this paper, sulcal depth is the main morphological feature differentiating tertiary from primary and secondary sulci (Chi et al., 1977; Miller et al., 2021a; Petrides, 2019; Sanides, 1964; Weiner, 2018; Weiner et al., 2018; Welker, 1990; Zilles et al., 1988). Nevertheless, previous developmental work on structural variability in PFC has frequently focused on cortical thickness (Brown et al., 2012; Gogtay et al., 2004; Tamnes et al., 2013; Vijayakumar et al., 2016). Thus, we also investigated variability in cortical thickness in both the *Discovery* and *Replication* samples as a function of sulcal type (*tertiary* vs. *primary*) and hemisphere (*left* vs. *right*). There were no significant differences in cortical thickness between primary and tertiary sulci in the *Discovery* ($F(1,27) = 2.44$, $p = 0.13$; Mean(sd))Tertiary = 2.41(0.36); Mean(sd)Primary = 2.37 (0.26); Appendix Fig. 1.3a) or *Replication* ($F(1,26) = 2.31$, $p = 0.14$; Mean(sd))Tertiary = 2.31(0.41), Mean(sd)Primary = 2.38(0.30); Appendix Fig. 1.3a) samples. Interestingly, the rm-ANOVA revealed a main effect of hemisphere in both samples in which right hemisphere sulci were cortically thinner than left hemisphere sulci (*Discovery:* ($F(1,27) = 123.1$, $p<10^{-3}$, $\eta^2G = 0.09$; Mean(sd)RH; = 2.30 (0.28); Mean(sd)LH = 2.47(0.27); *Replication:* ($F(1, 26) = 42.91$, $p<10^{-3,}$ $\eta^2G= 0.06$; Mean(sd)RH = 2.20(0.36), Mean(sd)LH =2.41(0.29); Appendix Fig. 1.3). Thus, while previous developmental work on structural variability in PFC has focused on cortical thickness (Brown et al., 2012; Gogtay et al., 2004; Tamnes et al., 2013; Vijayakumar et al., 2016), when considering tertiary sulci, the present analyses emphasize the utility of sulcal depth, not cortical thickness, for differentiating tertiary from primary sulci.

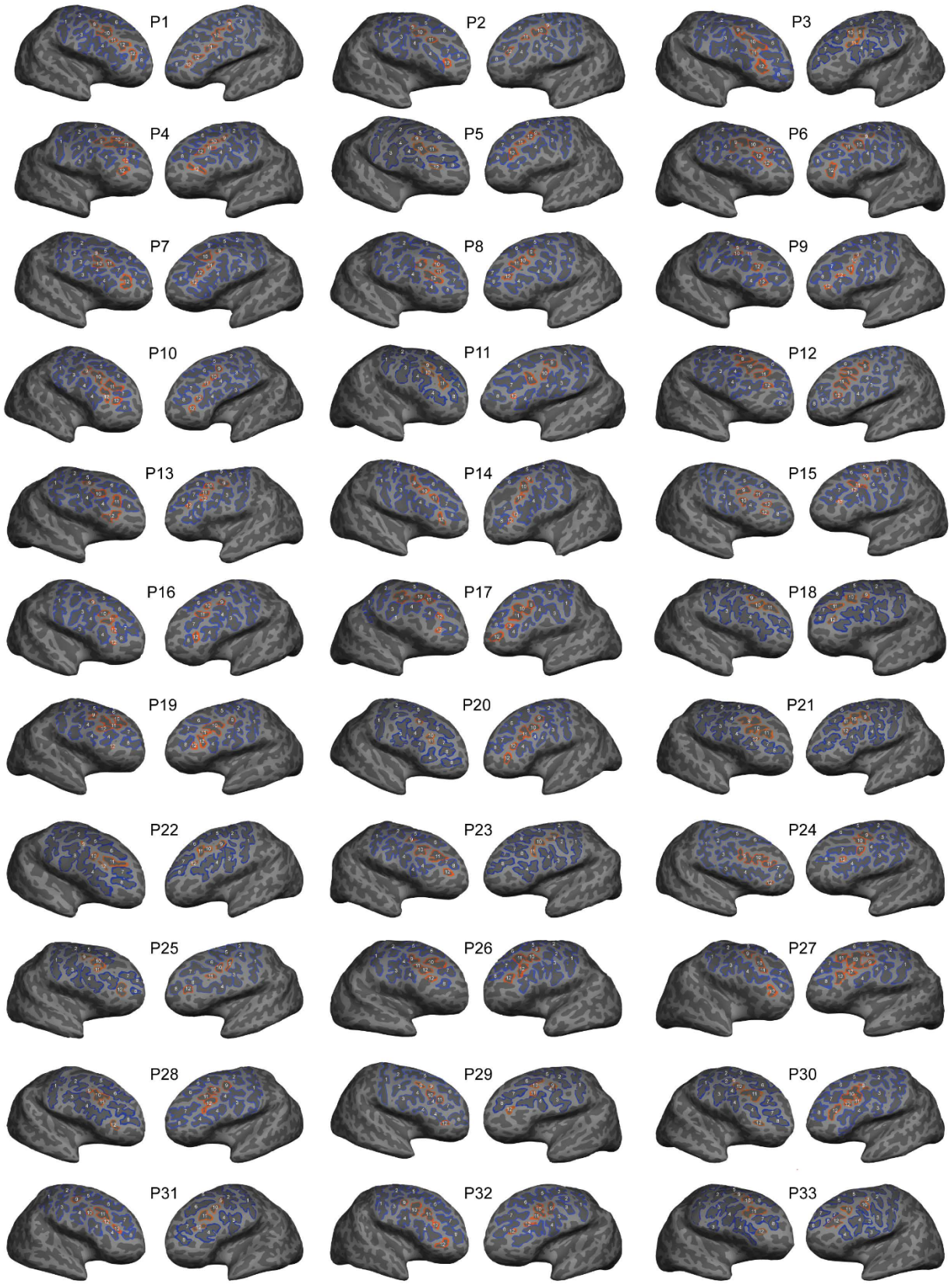
P1
P2
P3
P4
P5
P6
P7
P8
P9
P10
P11
P12
P13
P14
P15
P16
P17
P18
P19
P20
P21
P22
P23
P24
P25
P26
P27
P28
P29
P30
P31
P32
P33

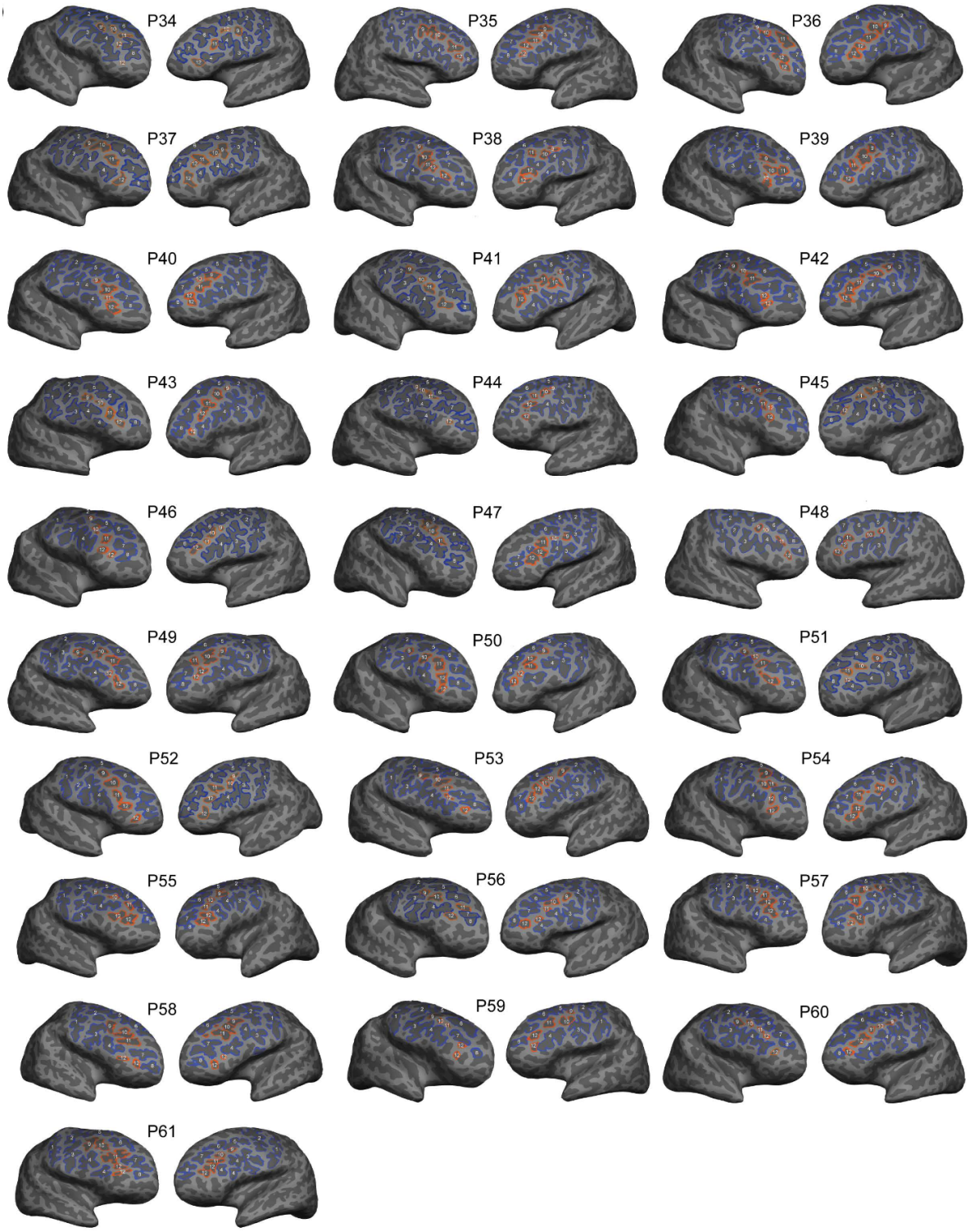

Appendix Fig. 1.1 Manual labels in the left and right hemispheres of every participant displayed on the inflated cortical surface in FreeSurfer 6.0.0. Manually labeled sulci on the inflated cortical surface in the left and right hemisphere for every participant in the *Discovery* Sample (1-33) and *Replication* sample (33-60). Tertiary *(orange)* and primary *(blue)* sulci are identifiable in every participant. The *pimfs* (*) can contain two components, one component, or can be absent altogether in a given hemisphere (Appendix Table 1.1). Sulci are labeled according to the numbering system in Fig. 1.2A.

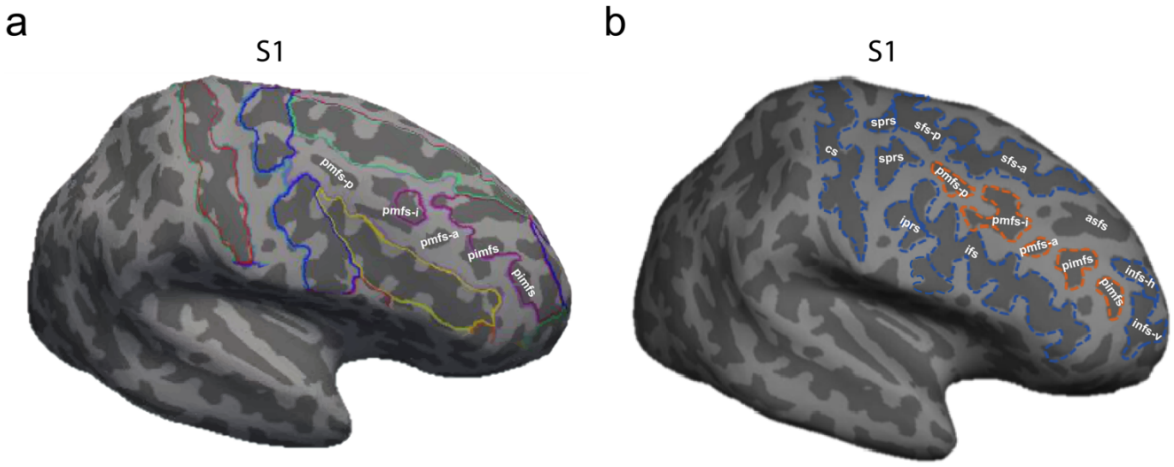

Appendix Fig. 1.2. ***LPFC tertiary sulci are often omitted in commonly used atlases.*** A**.** Example inflated cortical surface reconstruction of a right hemisphere. Colors indicate sulcal and gyral definitions provided by automated methods. The omitted tertiary sulci explored in the present study are labeled by the white acronyms. While the automated approach is useful for many studies, we manually defined sulci for our study as present approaches do not yet include tertiary sulci (labeled in white: *pmfs-p, pmfs-i, pmfs-a, pimfs*), and automated methods often include gyral components in the sulcal definitions. Red: central sulcus. Blue: pre-central sulcus. Yellow: inferior frontal sulcus. Turquoise: superior frontal sulcus. Magenta: fronto-marginal sulcus (which includes the horizontal and ventral components of the intermediate frontal sulcus, as well as portions of the *pmfs-i,* and what Petrides[26] refers to as the *accessory superior frontal sulcus* (*asfs*; not examined in the present study). B. Example of manual sulcal definitions in the same participant as in A. Manual definitions capture both tertiary (*orange*) and primary (*blue*) sulci.

	Discovery (n = 33)		Replication (n = 28)	
Components	***left***	***right***	***left***	***right***
0	2/33	3/33	1/28	0/28
1	15/33	18/33	3/28	9/28
2	16/33	12/33	24/28	19/28

Appendix Table 1.1 ***Variability in the number of pimfs components across individuals.***
Participants had 0, 1, or 2 *pimfs* components in each hemisphere. As a majority of participants in both samples had at least one *pimfs* component, our inclusion criteria was to include participants who had at least one *pimfs* component in each hemisphere (*Discovery*: 28/33, *Replication*: 27/28), which assures that all repeated measures statistics are balanced for effects of sulcus and hemisphere.

Annual Household Income	Count
$16,000 to $24,999	2
$50,000 to $74,999	5
$75,000 to $99,999	7
Over $100,000	8
Over $200,000	3
Unknown/Not Reported	14
Highest Degree Earned by Parent/Guardian	
High School/ GED	7
Associate degree	6
Bachelor's degree	12
Master's degree	14
Doctorate	3
Professional	1
Other	2
None of the above (less than high school)	1
Ethnic Categories	
Hispanic or Latino	6
Not Hispanic or Latino	24
Unknown/ Not Reported	25
Racial Categories	
American Indian/Alaska Native	0
Asian	1
Native Hawaiian or Other Pacific Islander	0
Black or African American	3
White	31
More Than One Race	12
Unknown/Not Reported	8

Appendix Table 1.2. ***Summary of sample demographics.*** Parent/Guardian reported Race, Ethnicity, Family income, and Education are summarized across the Discovery and Replication samples for all participants included in the behavioral portion of the present study (N = 55).

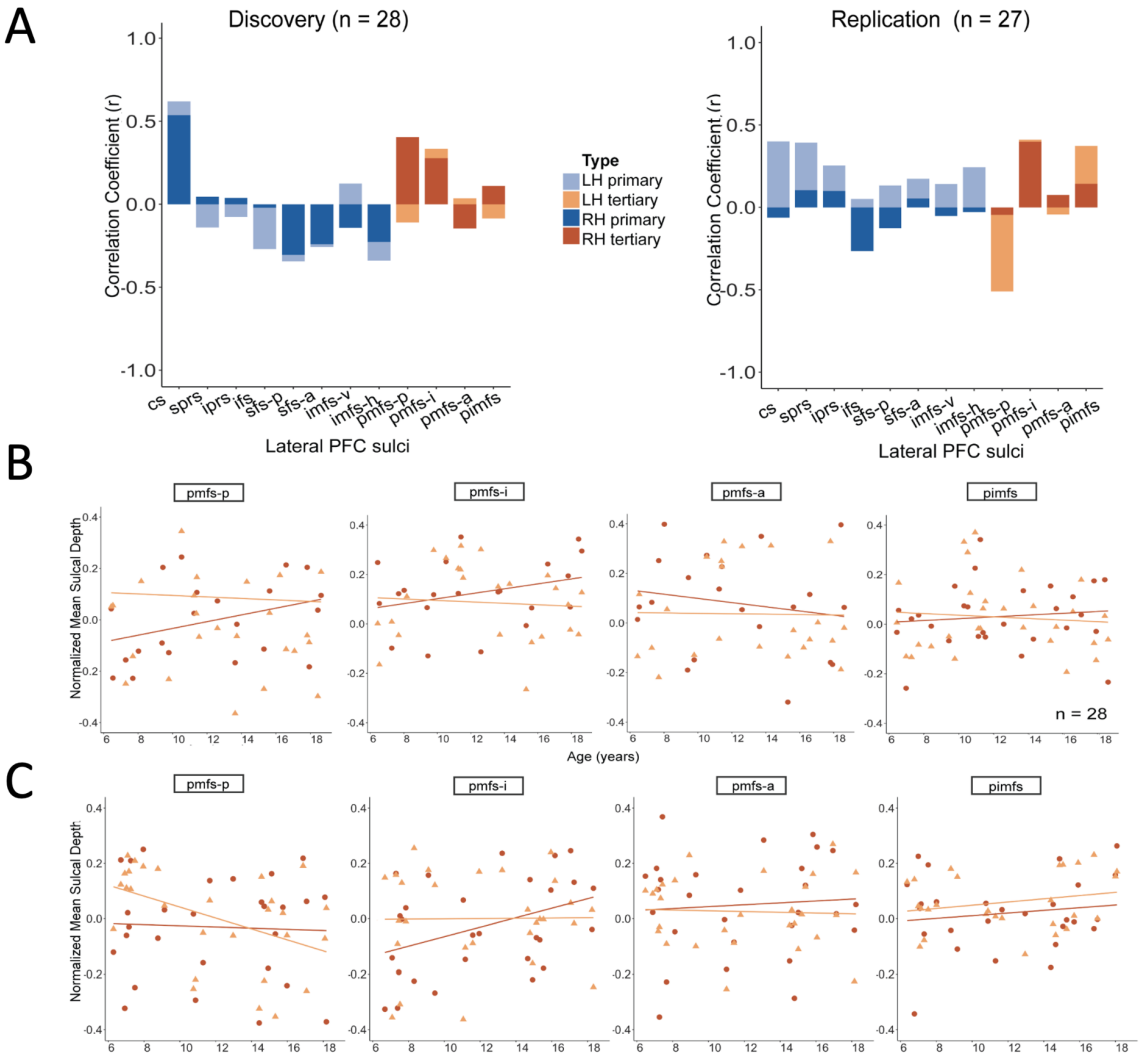

Appendix Fig. 1.3. ***Morphological and behavioral associations with age in both Discovery and Replication samples.*** A. Correlation between age and sulcal depth in the Discovery (left) and Replication (right) samples. Each bar represents the correlation coefficient (Pearson's r) between sulcal depth and age for each sulcus (orange: tertiary; blue: primary) in the left (lighter shades) and right (darker shades) hemispheres. There is not a clear relationship between sulcal depth and age that is generalizable among LPFC sulci. B-C. Scatterplots showing the association between age and sulcal depth for each of the 4 tertiary sulci explored in the present study in each hemisphere (left: lighter triangles; right: darker circles) for individual participants in the Discovery (B) and Replication (C) samples. Age does not account well for individual variability in LPFC tertiary sulcal depth.

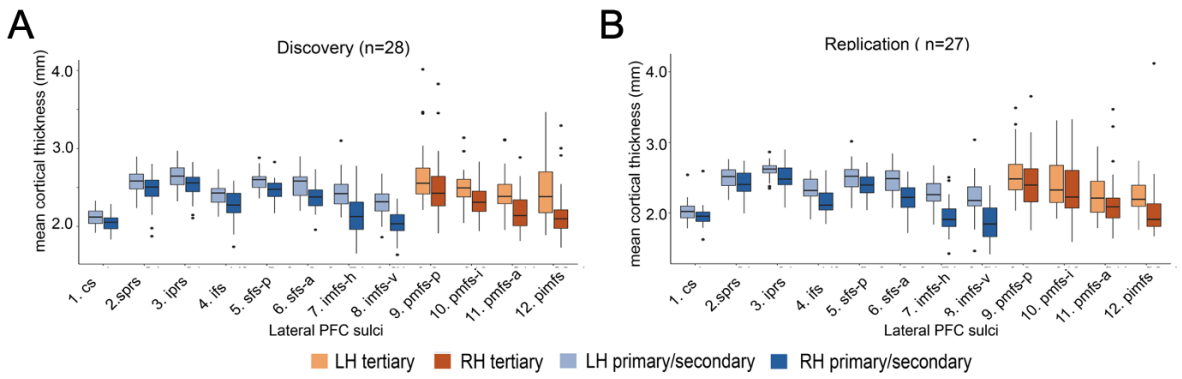

Appendix Fig. 1.4. ***No difference in cortical thickness between tertiary and primary sulci in lateral prefrontal cortex.*** A. Mean cortical thickness for each of the 12 lateral prefrontal (LPFC) sulci in the Discovery sample (n = 28 participants). B. Mean cortical thickness for each of the 12 LPFC sulci in the Replication sample (n = 27 participants). Tertiary sulci (orange) and primary sulci (blue) do not significantly differ in cortical thickness in either sample. Light colors indicate left hemisphere (LH) sulci and dark colors indicate right hemisphere (RH) sulci respectively.Horizontal lines represent median values and whisker lines represent the 1st and 3rd quartiles. Values falling outside of this range are represented as black dots.

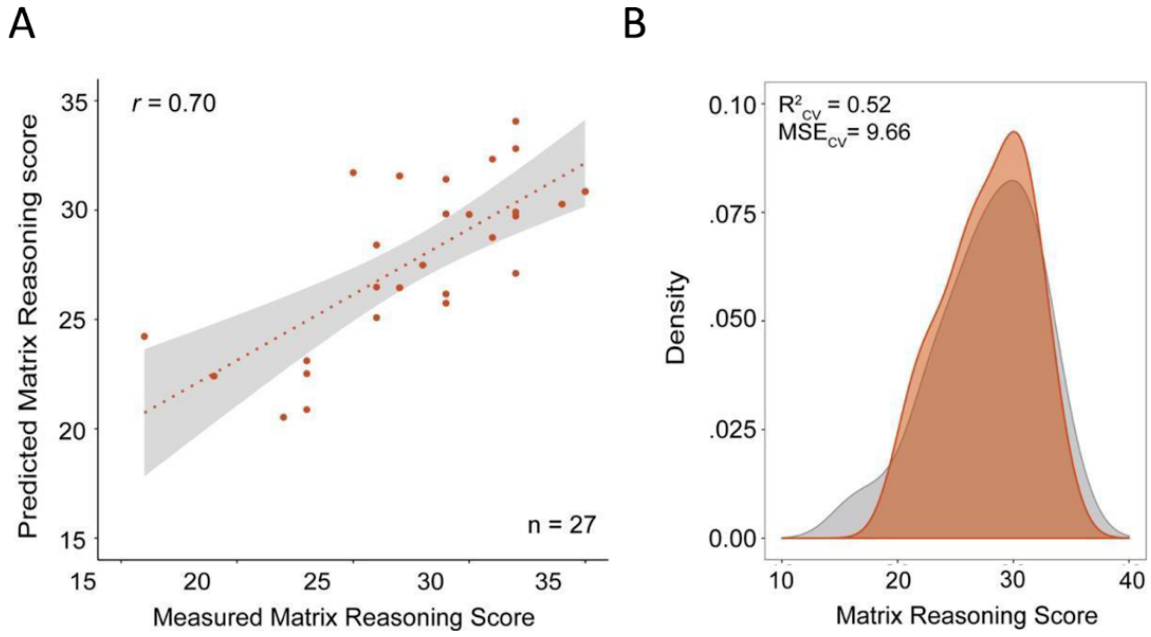

Appendix Fig. 1.5. ***Predicted matrix reasoning score in the Replication sample from three tertiary sulci (pmfs-i, pmfs-a, pimfs).*** A. Spearman's correlation (r) between measured and predicted Matrix reasoning scores in the Replication sample for the model including all three tertiary sulci identified in the Discovery sample (pmfs-iRH, pmfs- aRH, pimfsRH). Gray bar represents the 95% confidence interval for the linear model. B. Density plot showing model fit indexed by cross-validated mean-squared error (MSECV) and model fit (R2CV). orange: The distribution of predicted scores from this model. gray: the distribution of measured Matrix reasoning scores.

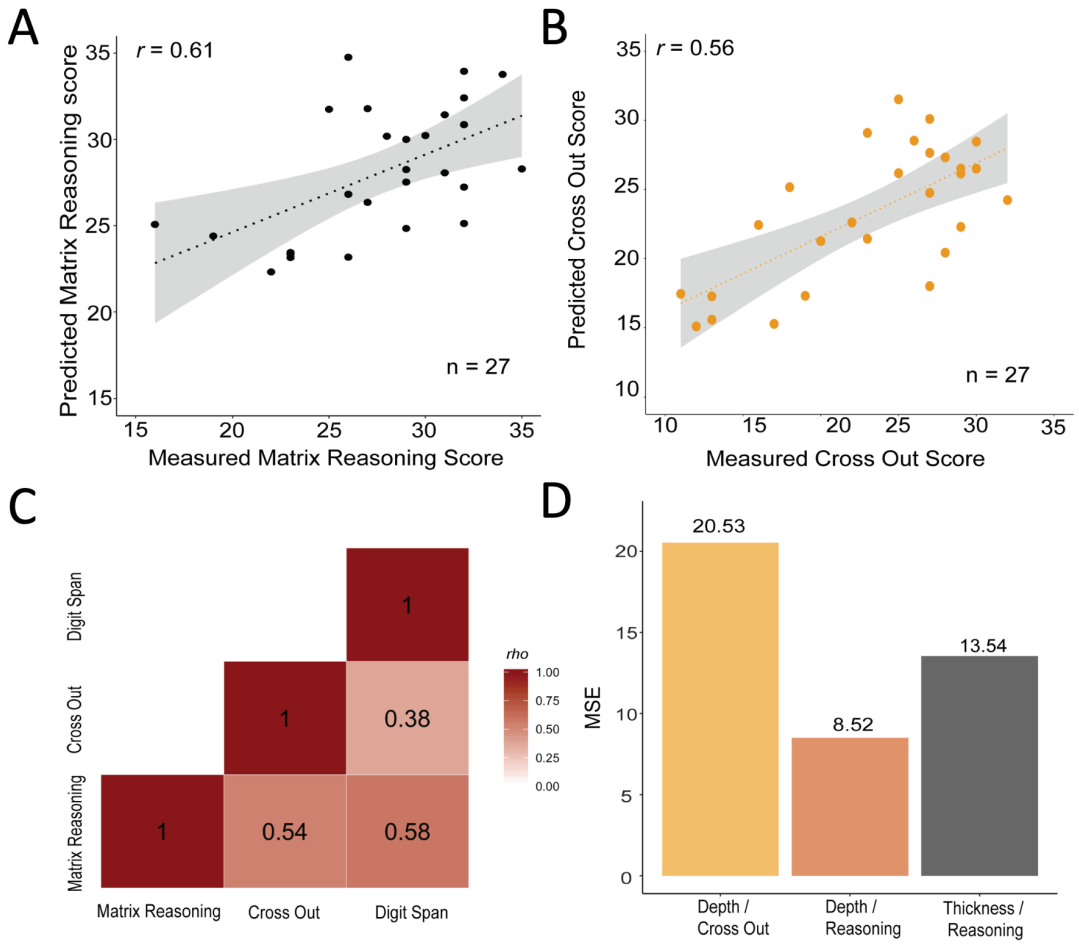

Appendix Fig. 1.6. ***Tertiary sulcal depth more strongly relates to reasoning than cortical thickness and this relationship shows behavioral preference over other cognitive measures.*** A. Thickness was used in place of depth to predict Matrix reasoning in the Replication sample. The model was fit with looCV. Spearman's correlation (r) between measured and predicted Matrix reasoning scores in the Replication sample for the best model (pmfs-iRH + pimfsRH. + age). Gray bar represents the 95% confidence interval for the linear model. B. The same depth model was used to predict Cross Out score instead of Matrix reasoning in the Replication sample. Spearman's correlation between measured and predicted Cross Out scores in the Replication sample using the best performing depth model (pmfs-iRH + pimfsRH + age). C. Correlation (Spearman's rho) between Matrix reasoning, Cross Out (Processing speed), and Digit Span (Working memory). Digit Span was included as an additional comparison measure in the Replication sample; it was not predicted by the depth model (R2 cv = 0.10) and was not explored further. D. MSEcv for the thickness and Cross Out score models compared to the analogous depth model. Tertiary sulcal depth offered substantially better predictions than cortical thickness. The depth model did not generalize to processing speed.

Appendix - Chapter 2

Pimfs surface area explains marginally more variance than age alone

Pimfs morphology was also behaviorally relevant when examined with a continuous metric (total surface area of the sulcus), albeit to a lesser degree than the discrete metric of presence/absence of a pimfs component. Specifically, a linear regression (with age included as a covariate), revealed that the total surface area of the left pimfs (ß = 0.01, t = 2.35, p = .022) was positively associated with reasoning (Appendix Fig. 2.1.4); this relationship was marginal (ß = 0.01, t = 1.85, p = .068) in the right hemisphere. Whereas the discrete models examining sulcal components explained *significantly* more variance in reasoning than age alone, this model only explained *marginally* more variance than age alone (pimfs: R^2_{adj} = 0.49, p < .001; age: R^2_{adj} = 0.46, p < .001; model comparison: p = .071). A repeated K-fold (5-fold, 10 repeats) and leave-one-out cross-validation (looCV) confirmed that the predictiveness of the total pimfs surface area model (*5-fold*: R^2 = 0.51, RMSE = 4.33; *looCV*: R^2 = 0.45, RMSE = 4.45) was only slightly better than age alone (*5-fold*: R^2 = 0.49, RMSE = 4.40; *looCV*: R^2 = 0.43, RMSE = 4.50). Further, when normalizing left pimfs surface area by the total surface area of the PFC, the relationship was marginal (p = .075). Thus, from our analyses, the presence or absence of pimfs-v was more directly linked to reasoning than total pimfs surface area, which was related to PFC surface area more broadly.

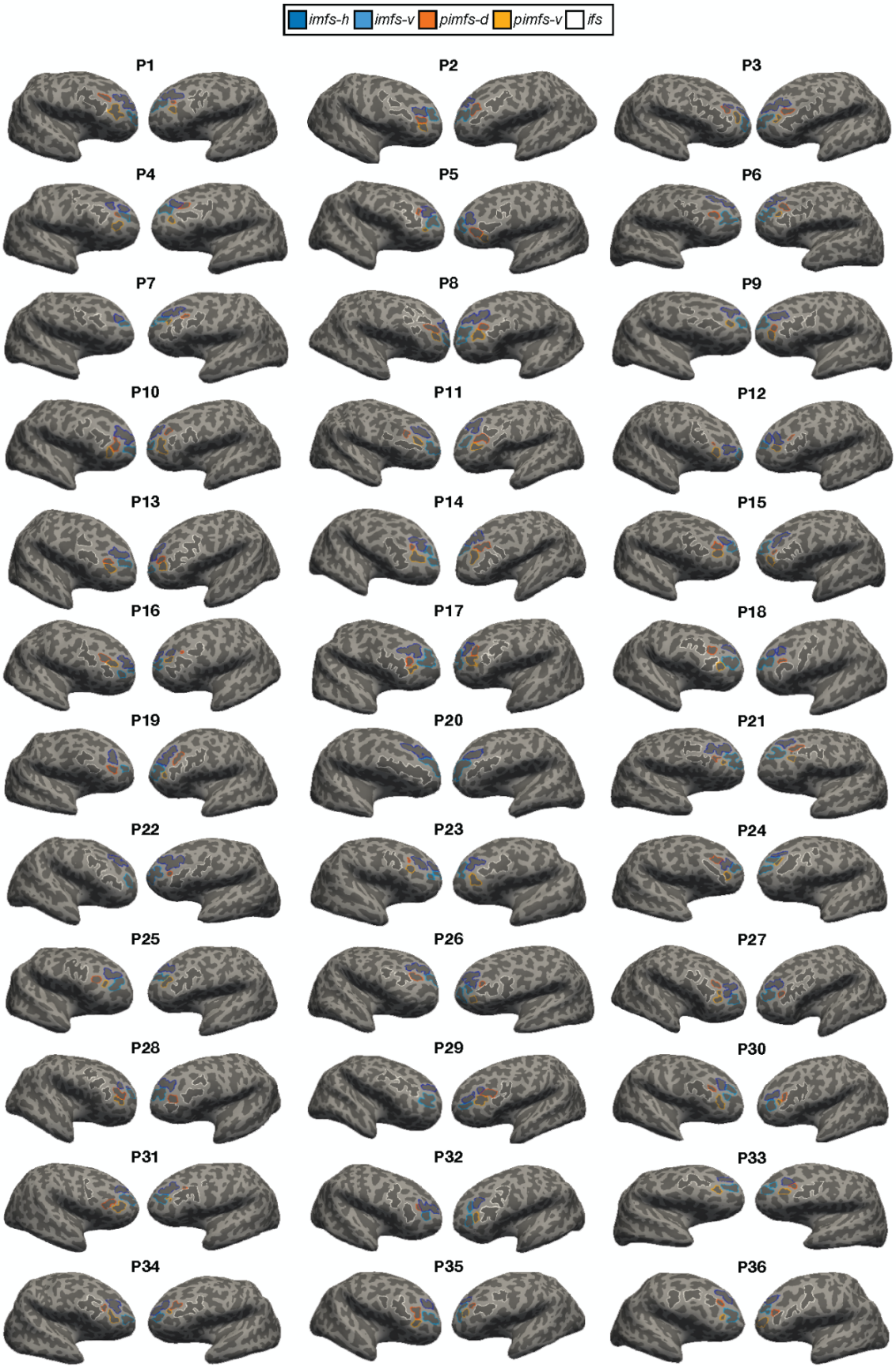
imfs-h
imfs-v
pimfs-d
pimfs-v
ifs
P1
P2
P3
P4
P5
P6
P7
P8
P9
P10
P11
P12
P13
P14
P15
P16
P17
P18
P19
P20
P21
P22
P23
P24
P25
P26
P27
P28
P29
P30
P31
P32
P33
P34
P35
P36

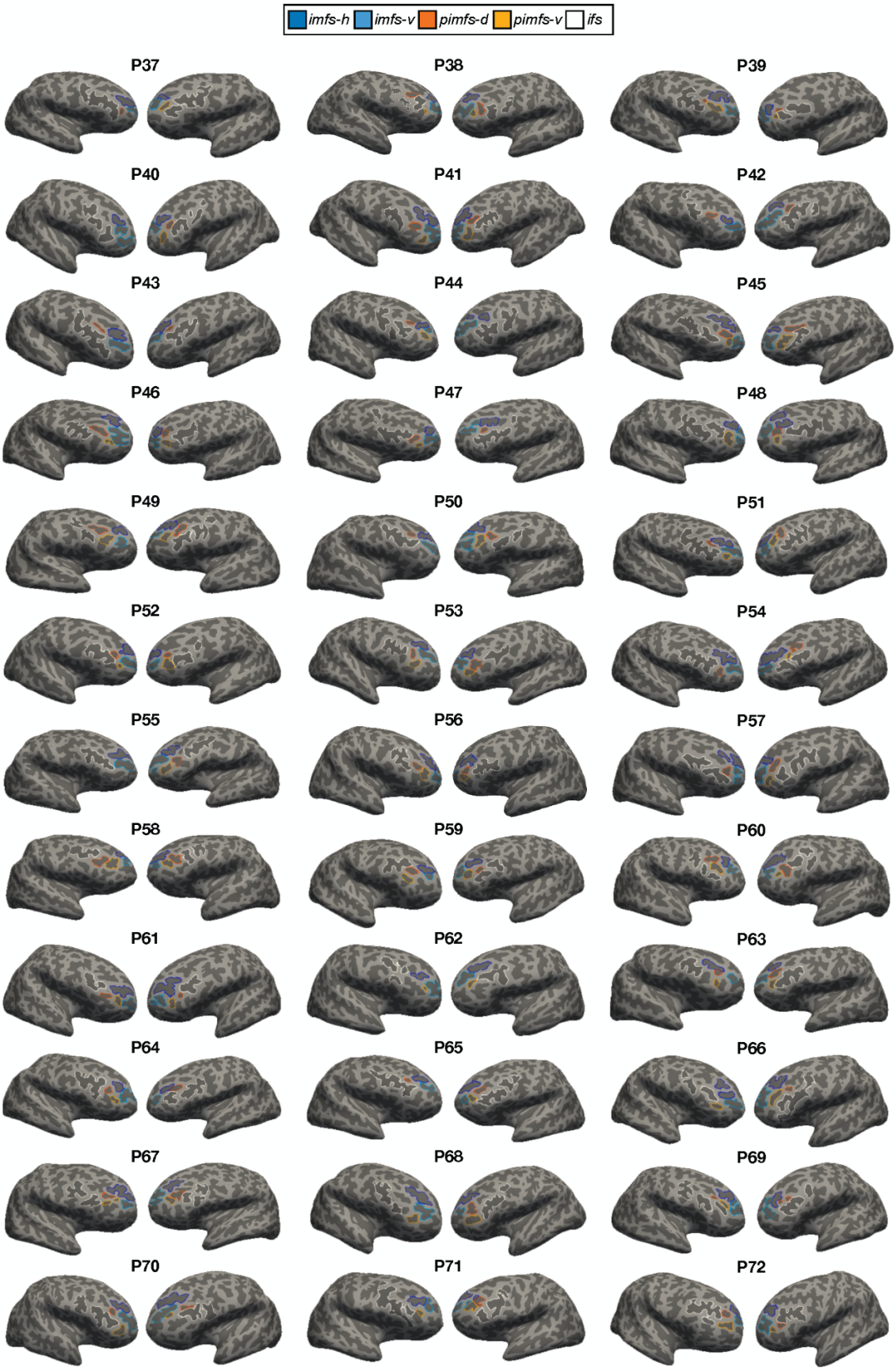
imfs-h
imfs-v
pimfs-d
pimfs-v
ifs
P37
P38
P39
P40
P41
P42
P43
P44
P45
P46
P47
P48
P49
P50
P51
P52
P53
P54
P55
P56
P57
P58
P59
P60
P61
P62
P63
P64
P65
P66
P67
P68
P69
P70
P71
P72

Appendix Fig. 2.1.1. ***Manual sulcal labels in the left and right hemispheres of each participant (N=72).*** As in Figure 1A, each sulcus is displayed on the inflated cortical surface (surfaces are not to scale) in FreeSurfer 6.0.0 and is colored according to the key at the top. Sulci were defined according to the most recent atlas and criteria by Petrides (2013, 2019; Materials and Methods). All hemispheres have the horizontal (imfs-h; dark blue) and ventral (imfs-v; light blue) intermediate frontal sulci and inferior frontal sulcus (ifs; white). The para-intermediate frontal sulcus (pimfs; orange) is more variable: participants can have zero, one (dorsal (dark) or ventral (light)), or two components (dorsal and ventral).

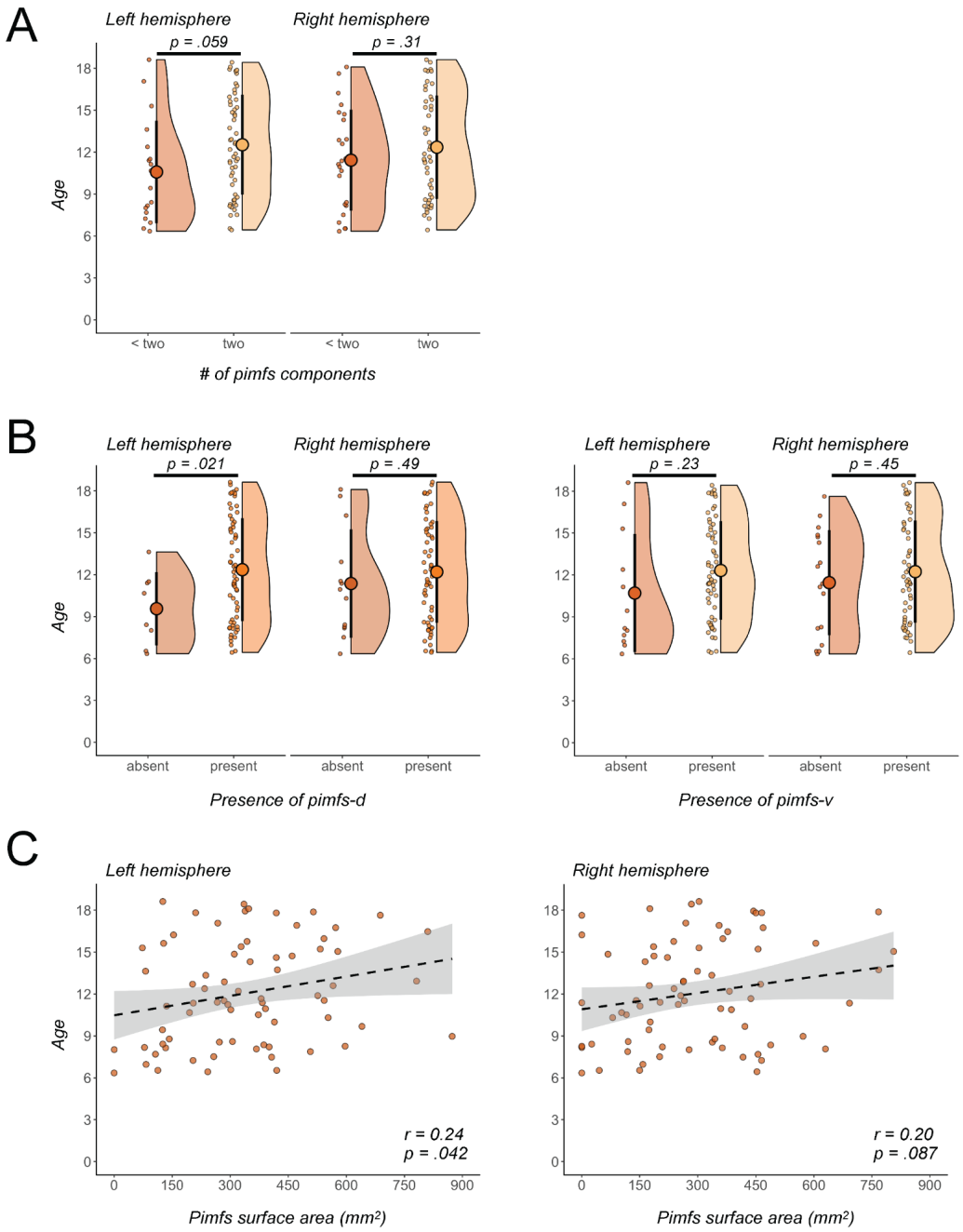

Appendix Fig. 2.1.2. ***Relationship between age and para-intermediate frontal sulcus morphological metrics.*** A. Raincloud plot (Allen et al. 2021) depicting age as a function of the number of para-intermediate frontal sulcus (pimfs) components in the left and right hemispheres using the whole sample (N = 72). The large dots and error bars represent the mean±std reasoning score and the violin shows the kernel density estimate. The smaller dots indicate individual participants. These features are colored (dark and light orange) to distinguish between the two groups. B. Same format as A, except for the presence/absence of the pimfs-d (Left) and pimfs-v (Right). C. Scatterplot visualizing age as a function of left and right pimfs surface area (mm2). The best fit line, ±95% confidence interval, and correlation coefficient (r) are included. The smaller dots represent individual participants (N = 72). Despite there being correlations between age and some pimfs features, these collinearities did not affect the model results (see Materials and Methods)

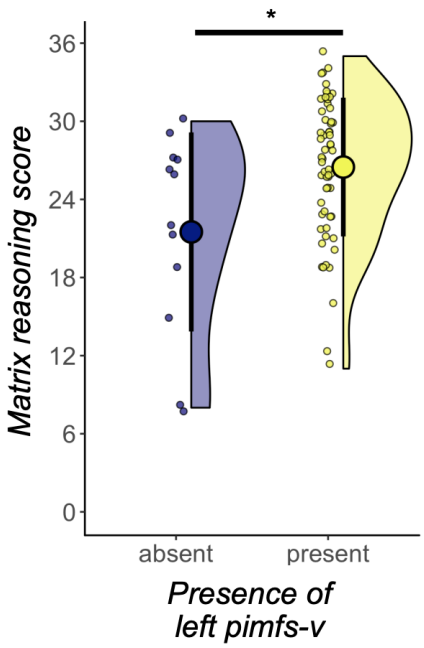

Appendix Fig. 2.1.3. ***The presence of the ventral para-intermediate frontal sulcus is related to reasoning (whole sample).*** Raincloud plot (Allen et al. 2021) depicting reasoning score as a function of the presence of the ventral para-intermediate frontal sulcus (pimfs-v) component in the left hemisphere using the whole sample (N = 72). The large dots and error bars represent the mean±std reasoning score and the violin shows the kernel density estimate. The smaller dots indicate individual participants. These features are colored (blue and yellow) to distinguish between the two groups. After controlling for age, those with the pimfs-v in the left hemisphere (*p = .027) had better reasoning scores than those without.

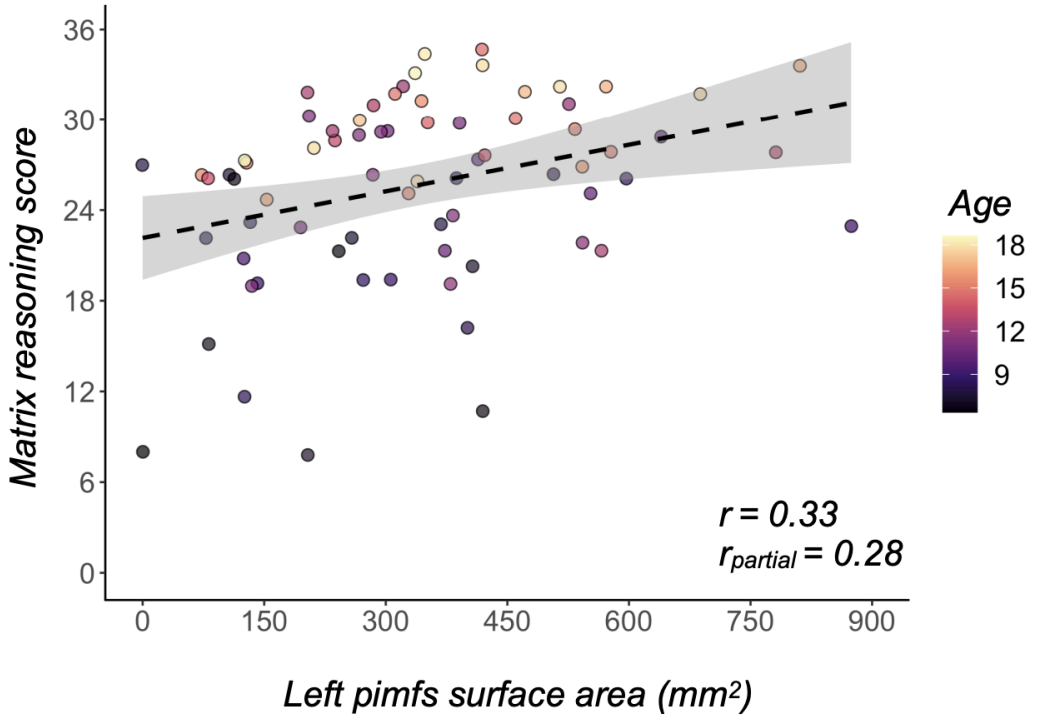

Appendix Fig. 2.1.4. ***Pimfs surface area explains marginally more variance than age alone.*** Scatterplot visualizing reasoning scores as a function of left para-intermediate frontal sulcus (pimfs) surface area (raw, in mm2), controlling for age. The best fit line, ±95% confidence interval, correlation coefficient (r), and rpartial from the regression are included. The smaller dots represent individual participants, colored by age (darker = younger; lighter = older). In the left hemisphere, the surface area of the pimfs is positively associated with reasoning (p = .022), even after controlling for age. Nevertheless, whereas the discrete models examining sulcal components explained significantly more variance in reasoning than age alone, a linear model explained marginally more variance than age alone (pimfs: R^2adj = 0.49, p < .001; age: R^2_{adj} = 0.46, p < .001; model comparison: p = .071; Appendix).

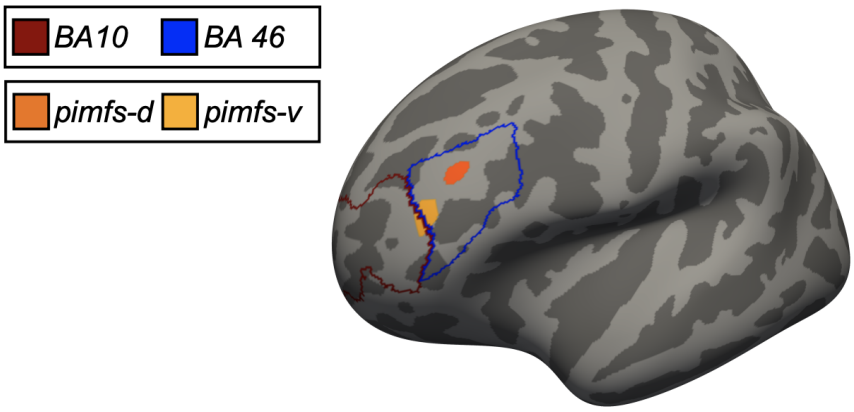

Appendix Fig. 2.1.5. ***The para-intermediate frontal sulcus relative to Brodmann Areas in LPFC associated with reasoning.*** Left hemisphere inflated fsaverage surface with putative paraintermediate frontal sulcus (pimfs) components and Brodmann Areas (BA) overlayed onto the surface. BAs and pimfs components are color-coded according to the key. Here, the pimfs-v (light orange) likely serves as a transition zone (border) between BA 46 (blue) and BA 10 (maroon). Notably, BA 10/46 overlaps with functionally-defined rostrolateral prefrontal cortex, a sub-region of LPFC implicated in reasoning abilities (for review see Vendetti and Bunge 2014).

	Count
Racial categories	
American Indian/Alaskan Native	0
Asian/Native Hawaiian/Other Pacific Islander	5
Black or African American	4
White	47
More Than One Race	14
Unknown or Not Reported	2
Ethnic categories	
Hispanic or Latino	11
Not Hispanic or Latino	59
Unknown or Not Reported	2
Highest degree earned by parent/guardian	
High School/GED	8
Vocational	1
Associate degree	6
Bachelor's degree	18
Master's degree	15
Doctorate	4
Professional	3
Other	3
None of the above (less than high school)	1
Unknown or Not Reported	13
Total household income	
$16,000-$24,999	2
$25,000-$34,999	3
$50,000-$74,999	6
$75,000-$99,999	8
$100,000-$199,999	27
Over $200,000	5
Unknown or Not Reported	21

Appendix Table. 2.1.1. ***Demographic and socioeconomic information of the child/adolescent sample (N = 72).*** All information is parent/guardian reported.

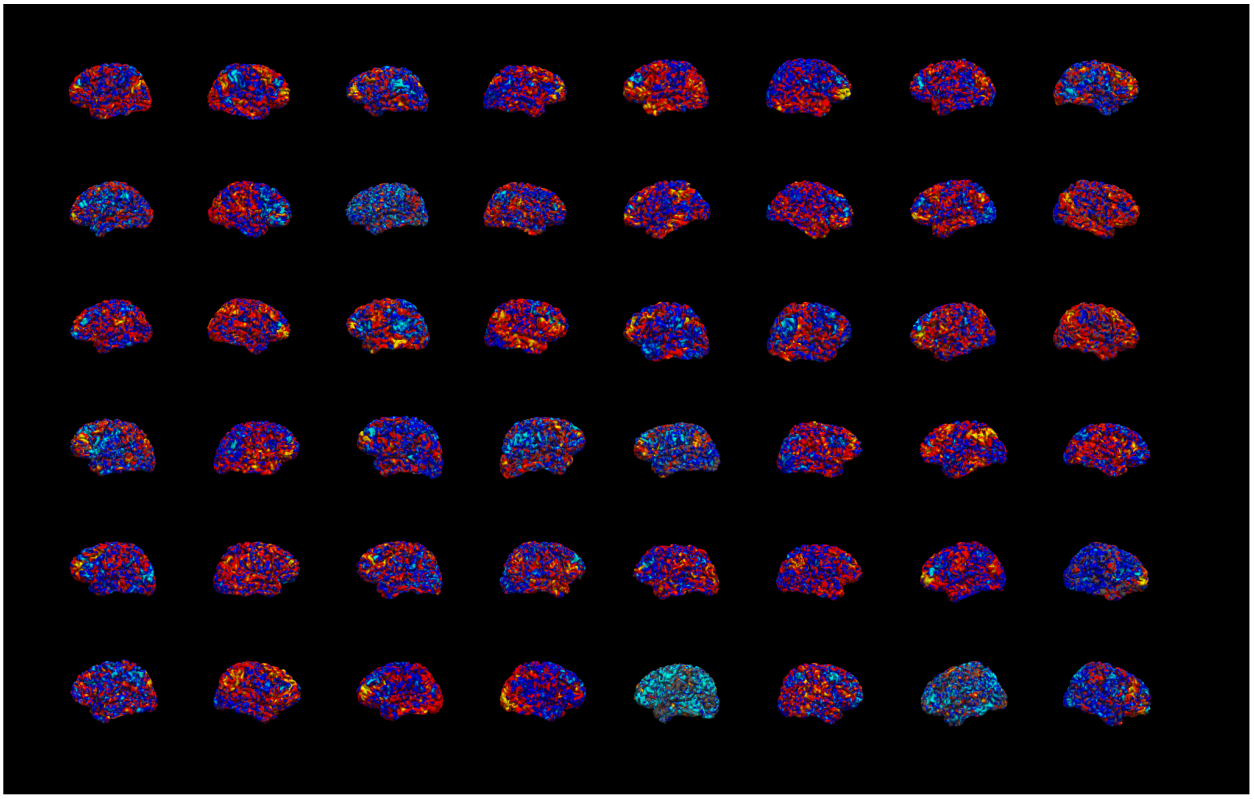

Appendix Fig. 2.2.1. ***Individual differences in functional connectivity between pimfs-v and pimfs-d components.*** Maps represent differences in pimfs component seed-to-whole brain functional connectivity in each hemisphere for all participants with both pimfs components (N = 24). After calculating seed-to-whole brain connectivity (Methods) differences were calculated as a simple, vertex-wise subtraction (*pimfs-v* - *pimfs-d*) for visualization purposes. Warmer colors represent stronger *pimfs-v* connectivity and cooler colors represent stronger *pimfs-d* connectivity. Maps reveal notable inter-participant differences.

Appendix - Chapter 3

Appendix Fig. 3.1 ***Manual labeling protocol of LPFC tertiary in chimpanzees guided by human predictions.*** We defined sulci on the inflated and pial cortical surfaces of each hemisphere for each chimpanzee. The ifs (orange), sfs-p (dark green), sfs-a (light green), pmfs-p (dark blue), pmfs-i (blue), and pmfs-a (light blue) are consistently identifiable across hemispheres. The pimfs (purple) is only present for one chimpanzee (c19) in the left and right hemisphere.

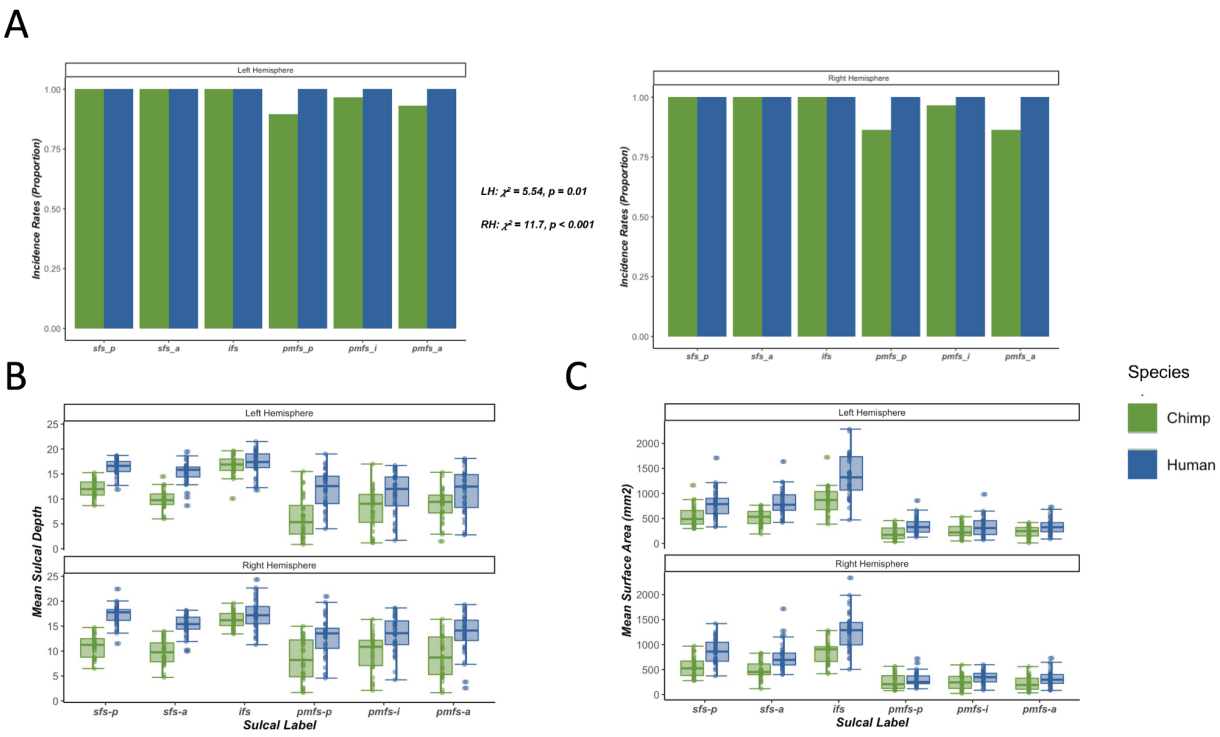

Appendix Fig. 3.2 ***Chimp-Human sulcal comparisons.*** A. Comparison of tertiary sulcal incidence rates (pmfs components) for chimpanzees and humans. B. Raw mean sulcal depth values. Overall sulci are more shallow in chimpanzees **c.** Total mean surface area values. Overall sulci are shallower in chimpanzees than humans.

KEY	
T3 (1 tertiary sulci)	
T3.a	just pmfs-a
T3.b	just pmfs-p
T3.c	just pmfs-i
T2 (2 tertiary sulci)	
T2.a	pmfs-a & pmfs-i
T2.b	pmfs-a & pmfs-p
T2.c	pmfs-i & pmfs-p
T1 (all 3 tertiary sulci)	

TOTAL	
T3	LH: 2 RH: 2
T3.a	LH: 2 RH: 0
T3.b	LH: 0 RH: 1
T3.c	LH: 0 RH: 1
T2	LH: 5 RH: 4
T2.a	LH: 3 RH: 2
T2.b	LH: 0 RH: 1
T2.c	LH: 2 RH: 1
T1	LH: 22 RH: 23

Appendix Fig. 3.3 Sulcal Types. *left.* A key showing the three types and subsequent subtypes based on the presence and absence of certain tertiary sulci in each chimpanzee hemisphere. *right.* The number of chimp hemispheres with each type and subsequent subtype. One chimpanzee had a 4th tertiary sulcus that showed spatial correspondence with the human paraintermediate frontal sulcus. All humans were Type 1.

Appendix Fig. 3.4. ***Human and chimpanzee surfaces show good cortical alignment, allowing accurate projection of sulcal labels.*** *Left:* A maximum probability map for the central sulcus created from human sulcal definitions shown on the *fsaverage* surface. *Right:* Human probability map is accurately projected onto an individual chimpanzee cortical surface (white). The projected human label (white) and actual sulcal label (blue) show a high level of overlap (dice coefficient = 0.86) indicating the spatial mapping between the two surfaces is highly accurate.

Annual Household Income	Count
$16,000 to $24,999	2
$50,000 to $74,999	5
$75,000 to $99,999	7
Over $100,000	8
Over $200,000	3
Unknown/Not Reported	14
Highest Degree Earned by Parent/Guardian	
High School/ GED	7
Associate degree	6
Bachelor's degree	12
Master's degree	14
Doctorate	3
Professional	1
Other	2
None of the above (less than high school)	1
Ethnic Categories	
Hispanic or Latino	6
Not Hispanic or Latino	24
Unknown/ Not Reported	25
Racial Categories	
American Indian/Alaska Native	0
Asian	1
Native Hawaiian or Other Pacific Islander	0
Black or African American	3
White	31
More Than One Race	12
Unknown/Not Reported	8

Appendix Table 3.1. ***Summary of sample demographics***. Parent/Guardian reported Race, Ethnicity, Family income, and Education are summarized across the *Discovery* and *Replication* samples for all participants included in the behavioral portion of the present study (N = 55).